Effects of Thermomechanical Refining on Douglas fir Wood

Mohammad Tasooji

Dissertation submitted to the faculty of the Virginia Polytechnic Institute and State

University in partial fulfillment of the requirements for the degree of

Doctor of Philosophy

In

Macromolecular Science and Engineering

Charles E. Frazier, Chairman

Kevin Edgar

Justin Barone

Johan Foster

Maren Roman

April 25th, 2018

Blacksburg, VA

Keywords: Thermomechanical refining, Medium density fiberboard, Fiber quality, Wood fiber characterization.

Effects of Thermomechanical Refining on Douglas fir Wood

Mohammad Tasooji

Abstract (academic)

Medium density fiberboard (MDF) production uses thermomechanically refined fiber processed under shear with high pressure steam. The industry evaluates fiber quality with visual and tactile inspection, emphasizing fiber dimensions, morphology, and bulk density. Considering wood reactivity, the hypothesis is that a variety of chemical and physical changes must occur that are not apparent in visual/tactile inspection. An industry/university cooperation, this work studies effects of refining energy (adjusted by refiner-plate gap) on fiber: size, porosity, surface area, surface and bulk chemistry, fiber crystallinity and rheology, and fiber interaction with amino resins. The intention is to reveal novel aspects of fiber quality that might impact MDF properties or process control efficiency, specific to a single industrial facility.

In cooperation with a North American MDF Douglas fir plant, two refining energies were used to produce resin and additive-free fibers. Refining reduced fiber dimensions and increased bulk density, more so at the highest energy. Thermoporosimetry showed increases in sub-micron scale porosity, greatest at the highest energy. Mercury intrusion porosimetry (MIP) revealed porosity changes on a higher dimensional scale. Brunauer-Emmett-Teller gas adsorption and MIP showed that refining increased specific surface area, more so at the highest energy. Inverse gas chromatography showed that the lowest refining energy produced surfaces dominated by lignin and/or extractives. The highest energy produced more fiber damage, revealing higher energy active sites. A novel rheological method was devised to study fiber compaction and densification; it did not distinguish fiber types, but valuable aspects of mechano-sorption and densification were observed.

Refining caused substantial polysaccharide degradation, and other degradative effects that sometimes correlated with higher refining energy. Lignin acidolysis was detected using nitrobenzene oxidation, conductometric titration of free phenols, and formaldehyde determination. Formaldehyde was generated via the C2 lignin acidolysis pathway, but C3

cleavage was the dominant lignin reaction. Observations suggested that in-line formaldehyde monitoring might be useful for process control during biomass processing. According to rheological and thermogravimetric analysis, lignin acidolysis was not accompanied by repolymerization and crosslinking. Lignin repolymerization must have been prevented by the reaction of benzyl cations with non-lignin nucleophiles. This raises consideration of additives that compete for lignin benzyl cations, perhaps to promote lignin crosslinking and/or augment the lignin network with structures that impart useful properties.

Fiber/amino resin interactions were studied with differential scanning calorimetry (DSC) and X-ray diffraction (XRD). All fiber types, refined and unrefined, caused only a slight increase in melamine-urea-formaldehyde (MUF) resin reactivity. Generally, all fiber types decreased the enthalpy of MUF cure, suggesting fiber absorption of small reactive species. But DSC did not reveal any dependency on fiber refining energy. According to XRD, all fiber types reduced crystallinity in cured MUF, more so with refined fiber, but independent of refining energy. The crystallinity in cured urea-formaldehyde resin was studied with one fiber type (highest refining energy); it caused a crystallinity decrease that was cure temperature dependent. This suggests that resin crystallinity could vary through the thickness of an MDF panel.

Effects of Thermomechanical Refining on Douglas fir Wood

Mohammad Tasooji

Abstract (general audience)

Medium density fiberboard (MDF) is a wood-based composite which is widely used for making kitchen cabinets and furniture. In the process of making MDF, wood particles are softened under steam pressure and under high temperature and pressure, inside a refiner, mechanically cut into wood fibers. Wood fibers are then mixed with adhesive and additives then hot-pressed and form the final board. In the MDF industry, wood fiber quality has significant effect on final board properties and is evaluated based on visual and tactile inspections. The research hypothesis is that, during the refining, a variety of chemical and physical changes must occur that are not apparent in visual/tactile inspection. An industry/university cooperation, this work studies effects of refining energy (adjusted by refiner-plate gap) on fiber: size, porosity, surface area, surface and bulk chemistry, fiber crystallinity and rheology, and fiber interaction with adhesive. The intention is to reveal novel aspects of fiber quality that might impact MDF properties or process control efficiency, specific to a single industrial facility.

It was found that refining had significant effect on wood fiber properties: increased surface area, porosity, and changed the surface energy; and also on wood fiber chemistry: significant degradation in wood fiber main chemical components: poly saccharides and lignin. These changes also had effect on fiber/adhesive interaction. Therefore the hypothesis was confirmed that MDF fiber quality must involve more than a simple visual/tactile evaluation and the effect of refining can be detected on other fiber quality aspects. However more research needs to be conducted to test and find feasible new methods for fiber quality evaluation.

Acknowledgment

Foremost I would like to thank my advisor Prof. Charles E. Frazier for his continuous support, enthusiasm, patience, and motivation throughout this study. He is the best teacher that I have ever had.

I would also like to thank my committee members Prof. Kevin Edgar, Prof. Johan Foster, Prof. Justine Barone and Prof. Maren Roman for their support and insightful comments.

The friendship, kindness and support of my friends: Christa Stables, Guigui Wan and Kyle definitely helped me a lot throughout these years. This thesis would not have been done without the help of our industrial sponsors especially Arauco, Hexion and Araclin. I also want to thank David Kruse, Dan Kelley, and Randy Polson from Arauco for teaching me a lot about medium density fiberboard manufacturing. I would also like to thanks Dr. Zink-Sharp for her tremendous knowledge, support and patience regarding using different microscopes. I want to thank Doctor Ann Norris for all her supports and help with running crystallinity and compositional analysis samples. I also want to thank Debbie Garnand for reimbursing all the money that I spent on conferences and lab supplies!

Without the endless love, care and support of my dear wife and best friend Sarah this work would not be possible. I also like to thank my dear family for their all-time support, kindness, and love.

Table of Contents

Abstract (academic) ii

Abstract (general audience) iv

Acknowledgment iv

Chapter 1 Introduction 1

1.1. Motivation 1

1.2. Literature Review 1

1.2.1. Medium density fiberboard 1

1.2.2. Thermomechanical refining 3

1.2.3. Effect of refining on wood fiber characteristics 6

1.2.3.1. Dimensions and bulk density 6

1.2.3.2. Porosity 8

1.2.3.3. Specific surface area 11

1.2.3.4. Surface energy 13

1.2.3.5. Compositional analysis 19

1.2.3.6. Lignin chemistry 22

1.2.3.7. Rheology 28

1.2.3.8. Resin cure 31

1.2.3.9. Resin crystallinity 32

1.3. References 33

Chapter 2 Physical, surface, and rheological characterization of thermomechanical wood fiber 45

2.1. Abstract 45

2.2. Introduction 46

2.3. Experimental 47

2.4. Results and discussion 51

2.5. Summary and conclusions 61

2.6. References 62

Chapter 3 Lignin acidolysis without repolymerization during thermomechanical refining of Douglas fir wood 67

3.1. Abstract 67

3.2. Introduction 68

3.3. Experimental 69
3.4. Results and discussion 73
3.5. Summary and conclusions 84
3.6. References 86
Chapter 4 Thermosetting resin/fiber interactions impacted by thermomechanical refining energy 91
4.1. Abstract 91
4.2. Introduction 91
4.3. Experimental 92
4.4. Results and discussion 95
4.5. Summary and conclusions 101
4.6. References 103
Chapter 5 Conclusions and future work 105
Appendix A Thermoporosimetry 107
Appendix B BET gas adsorption 108
Appendix C Conductometric titration 112
Appendix D Nitrobenzene oxidation reaction 113
Appendix E 2DNMR HSQC 114
Appendix F MUF kinetic study (activation energy) 121
Appendix G Aging effect on MDF fibers 123
Appendix H Biogenic formaldehyde: Content and heat generation in the wood of three tree species 127

Chapter 1 Introduction

1.1. Motivation

In the medium density fiberboard (MDF) industry, wood fiber quality has a significant effect on final board properties. There are several production factors that have effect on wood fiber quality such as: digester retention time, digester pressure, refining pressure, refining energy, refining retention time, speed of the refiner plates, and raw material. Among all these factors refining energy is the most important one which is controlled by changing the gap between the refiner plates. Fiber quality determination in the MDF industry is mostly based on visual and tactile evaluation. Fiber size and the amount of fiber bundles are the main indicators in visual and tactile fiber quality determination. For example high refining energy produces fibers with good quality because they are shorter in size and include less fiber bundles. On the other hand, lower refining energy causes poor fiber quality with high amounts of fiber bundles. But the effect of refining on fiber properties should be more than just a simple fiber size shortening. Fiber physical and chemical characteristics can undergo changes inside the refiner. It is important to study these characteristics that are affected by refining in order to develop new fiber quality measurements instead of using simple visual fiber quality evaluation. This study focuses on the effect of refining on various physical and chemical fiber characteristics and also determines if the change in fiber characteristics has impact on fiber/resin interactions which probably have effect on MDF panel properties.

1.2. Literature Review

1.2.1. Medium density fiberboard

Fiberboard is a category of wood based composites which is distinct from solid wood since they are composed of wooden elements of different sizes (with dimensions of the same order of magnitude as those of the wood cells, roughly about 3000 x 30 microns) bonded together with an adhesive. The wooden elements used in making fiberboards are called “fibers” which applies to any wood element with the dimensions about 3000 x 30 microns regardless of its origin[1]. This term is different than the term “fiber” used in wood anatomy which is reserved for a specific cell type in hardwoods[2]. There are different types of fiberboards which are

classified by density including: insulation board (0.2-0.4 g/cm^3), medium density fiber board (MDF, 0.65-0.8 g/cm^3), and hardboard (0.9-1.1 g/cm^3). Except for the insulation board which can be produced only by the wet process, the rest can be produced by both the wet and dry processes[1]. This research only focuses on MDF produced by the dry process.

MDF is a wood based composite used indoors. Its good mechanical and physical properties as well as better machinability compared to solid wood, molding ability, insensitivity to the quality of raw material, smooth surface suitable for finishing, and screw holding ability make it an excellent candidate in interior furniture and decoration markets[3-4]. For manufacturing MDF, typically debarked wood (chips, shavings and sawdust) is softened in a digester (vessel with steam pressure about 0.77 MPa, retention time about 3.5 min), refined in a pressurized thermomechanical refiner (almost the same pressure as the digester), blended with resin, wax and urea, then dried, formed into a mat, cold pressed, hot pressed, cooled, finished and cut, Figure 1.

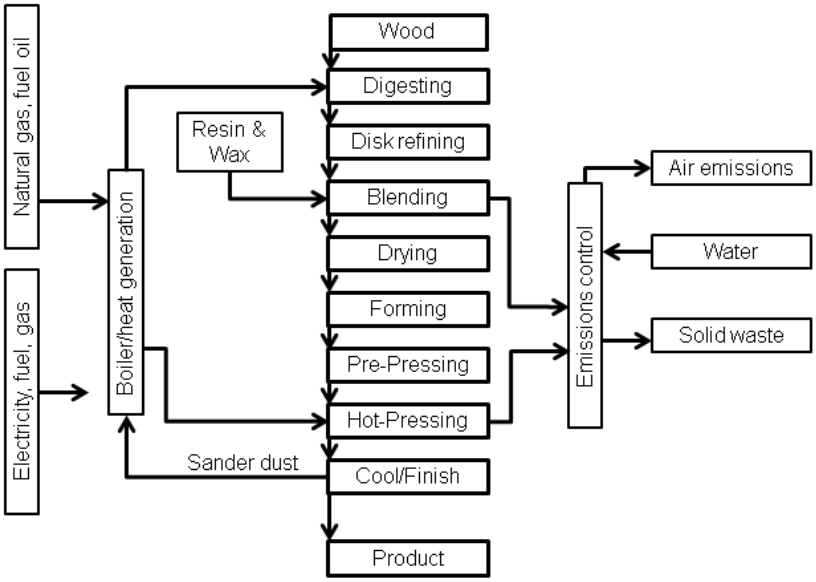

Figure 1-1. MDF manufacturing process

MDF production is a complicated process and fiber quality is one of the crucial factors affecting the final board properties[5]. There are different methods for determining MDF fiber quality such as: various sieving methods, optical evaluation by instrument, Pulmac shive analyzer, bulk density after mat forming, and visual and tactile evaluation by the operator[5].

Visual and tactile evaluation by the operator is the most common method for fiber quality determination in the MDF industry[6]. In this method the average fiber size and the occurrence of fiber bundles (shives) are the crucial indicators of fiber quality. There are several production factors having effect on fiber quality including: tree species[3, 7-9], digester and refining pressure[8, 10-18] and retention time[15, 18-19], refining temperature[19], rotational speed of the refiner plates, age of the refiner plates, and the gap between the refiner plates[20]. The most important production variable is perhaps the refining energy (kW•h/ton of fiber)[5], which is controlled by the refiner-plate gap. Therefore this research focuses on the effect of refining energy on MDF fiber quality and having a good understanding of MDF refining (thermomechanical refining) is necessary.

1.2.2. Thermomechanical refining

Thermomechanical refining involves processing the wood (chips, shavings, and sawdust) under high temperature steam and mechanical shearing, cutting, squeezing, and abrading inside a refiner. Refiner consists of two disks and there are two different disk settings known as single-disk and double-disk refiners. In the single-disk refiner only one disk moves (rotor) and the other is stationary (stator); however in double-disk both disks revolve at the same speed and in opposite directions[1]. In MDF industry most of the refiners are single-disk refiners. Each disk is equipped with a plate which consists of wear and corrosion-resistant alloyed steel castings bolted to the disk. Plates have different patterns and produce different types of fibers for different applications[1]. The infeed and outfeed of the pressurized thermomechanical refiner are sealed. The infeed is connected to the digester where the wood is steamed and softened and it is continuously fed into the refiner and discharged to atmospheric pressure after it is resinated. Additives (wax and urea) can be added inside or right before the refiner. When the wood enters the refiner in stage A wood fibers are picked up, make contact with the bars (edge to edge) of the refiner plates, and are accumulated and trapped between the edges of bars and compressed. In stage B, they are compressed between the surfaces of the stator and rotor bars. In the stage C, they hit the bars on the surface to edge and again edge to edge, Figure 2. Tensile, compression and shear forces are imparted to the wood fibers during the bars crossing.

These forces act on the wood fibers due to the contact between fibers and bars and also the contact between wood fibers themselves [21-23].

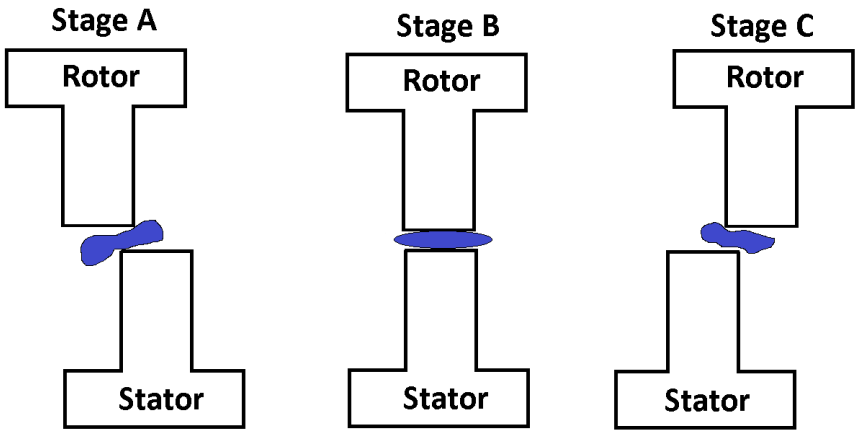

Figure 1-2. Refining mechanism

Refining theories

Specific edge load (SEL)

SEL (J/m) is the amount of effective energy spent per unit edge length of bar crossing and it is the most reliable theory in the pulp and paper industry [24-28]. SEL can be calculated as follows:

$$SEL = \frac{P_{net}}{CEL}$$

$$P_{net} = P_{tot} - P_{noload}$$

P_{tot} is the total power consumed, P_{net} is the net power consumed to change the fiber properties, and P_{noload} is the initial power which is the power of rotating the refiner plates (no noticeable change occurs to fiber properties due to P_{noload}). CEL which is cutting edge length can be calculated as shown below.

$$CEL = BEL \times \omega$$

BEL is bar edge length and ω is rotational speed.

Different plate designs are characterized by BEL and BEL/CEL. In pulp and paper industry, when softwoods and hardwoods are used, SEL of 1.5-3 J/m and 0.2-1.0 J/m are respectively recommended [22]. Although this theory is frequently used in pulp and paper industry, it only considers the length of the bar edges and not the width.

Specific surface load (SSL)

SSL theory is a modification to SEL theory and it considers the width of the bars as well [29-30].

$$SSL = \frac{SEL}{IL}$$

IL which refers to the impact length of the bars can be calculated as follows:

$$IL = \frac{W_r + W_{st}}{2} \times \frac{1}{\cos(\propto/2)}$$

W_r and W_{st} are width of rotor and stator bars respectively. $\propto$ is the average intersecting angle of the rotor and stator bars. SSL (J/m^2) works well in the case of having narrow bars.

Specific refining energy (SRE)

SRE (kWh/t) theory[21-22] is about the energy that is given from the refiner to the fibers and can be calculated as follows:

$$SRE = \frac{P_{net}}{\dot{m}}$$

P_{net} is described above and is the net power that applied to the fibers that can change their properties, and $\dot{m}$ which is the mass of the fibers through the refiner (t/h). The specific refining energies recommended for producing softwood and hardwood fibers in pulp and paper industry are 120-160 and 80-120 respectively. Specific refining energy theory is commonly used in the MDF industry.

Force base

All the previous mentioned theories were energy-based, however it has been reported that force and not energy is responsible for changing the fiber properties. Researchers [26, 31-32] have been working on this theory and more studies are needed to develop this concept [23].

It should be noted that thermomechanical refining is used in both MDF and pulp and paper industries, however the refining temperatures are different. In the paper making industry refining must be conducted at temperature below 140°C to make sure fibers are separated at the secondary layer of the cell wall[33] which contains cellulose hydroxyl groups which are necessary in paper making. However in MDF industry since adhesive is used, not only it is not

necessary to conduct the refining at temperature below 140°C but also it is better to increase the refining temperature to about 170°C. At this temperature (which is over glass transition temperature of lignin) lignin softens and fibers are separated more easily at the middle lamella[1, 34] which results in less refining energy consumption[1, 4].

1.2.3. Effect of refining on wood fiber characteristics

1.2.3.1. Dimensions and bulk density

Wood fiber size distribution and bulk density are important fiber characteristics which affect the performance of MDF[3, 35-37] and are controlled mostly via visual and tactile evaluation in the MDF industry[1]. A survey which targeted 29 different MDF plants worldwide showed that the amount of very short fibers (fines) has negative effect on the internal bonding, thickness swelling and density profile of the final board[35]. The same survey showed that fiber size also has effect on the MDF production process; for example fines have negative effects on production speed, heat transfer, blister formation, energy consumption. Groom et al. also reported that fines in the fiber furnish decreased the stiffness, strength, and internal bonding of MDF[36]. Fines also consume a higher amount of adhesives[1] compared to regular fibers. Besides fines, fiber bundles or shives (collection of two or more fibers) are also not desirable[6]. Regarding the effect of fiber bulk density it is stated that increasing fiber bulk density increased internal bonding, modulus of rapture (MOR) and modulus of elasticity (MOE) of MDF[38].

The effect of refining on fiber size distribution and bulk density has been studied. Short and Lyon showed that increasing refining energy by decreasing the gap between the refiner plates resulted in fibers with higher bulk density and shorter size[20]. Xing et al. found that refining pressure between 0.2 and 0.4 MPa caused no obvious damage to the cell wall while at 0.6-1.2 and 1.4-1.8 MPa nano-cracks and micro-cracks in fibers were observed respectively[16]. The same study reported that low refining pressure generated more fiber bundles as opposed to individual fibers. Krug and Kehr reported that increasing refining pressure resulted in shorter fibers and decreased fiberboard strength[11].

In MDF industry, besides the tactile and visual determination method, fiber dimensions are measured using sieving methods, Pulmac shive analyzer and optical evaluation (Fibercam

and FiberCube). Fiber bulk density can be measured using sieving methods[38]. Mercury intrusion[39] and gas pycnometry[40] methods can also be used, but last two are not practical in industry. In the MDF industry bulk density is measured after fiber mat formation. In this study Fibercam and mercury intrusion porosimetry methods were used for measuring fiber size distribution and bulk density respectively.

Fibercam

IMAL Fibercam 100 machine is shown in Figure 1-3. Fibers pass a small filter which is located on top of the conveying system and pass a high speed camera which is connected to software that plots the distribution of fiber length and width. It also reports the number of individual fibers that were tested. After the test is done the vibrator moves and all the remaining fibers were sucked via vacuum and transferred into the waste container. The software is able to detect and eliminate data for the fibers that are too tangled or overlapped.

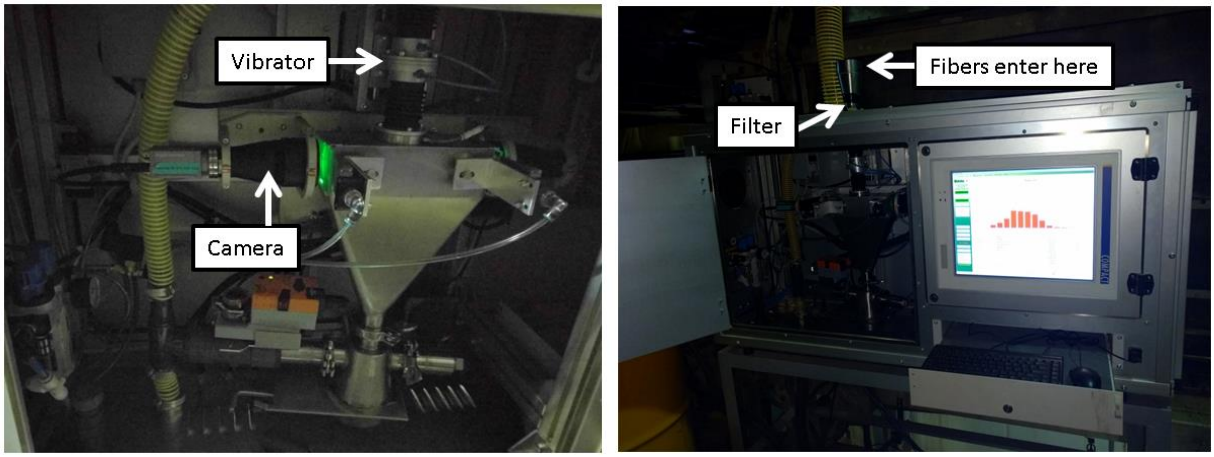

Figure 1-3. IMAL fibercam. Left: inside and Right: outside the machine

Mercury intrusion porosimetry (for bulk density)

Mercury intrusion porosimetry is capable of measuring not only fiber bulk density and skeletal density but also fiber pore size distribution, surface area and porosity (will be discussed in porosity section). Bulk density is defined as the mass of the sample divided by the sample bulk volume (including sample pores). For measuring bulk density the sample is loaded into a

penetrometer (sample cell). The volume of the penetrometer is accurately known. The mass of the sample can be calculated by subtracting the mass of the penetrometer containing the sample from the empty penetrometer. The penetrometer which contains the sample is then filled with mercury. Since mercury is a non-wetting liquid, it will not sorb by the sample hence without applying pressure no mercury should penetrate into the sample pores. The volume of mercury in the penetrometer can be determined from weight and density. The sample bulk volume can be simply calculated by subtracting the mercury volume from the penetrometer volume. By having the sample mass and bulk volume, bulk density can be calculated.

1.2.3.2. Porosity

The effect of refining on porosity has been studied in the field of pulp and paper. It has been reported that thermomechanical refining opens cell wall pores by disrupting surface polysaccharides[41-42] which makes thermomechanical fibers more porous than unrefined wood [41]. Refining can also produce fines which have larger volume of small pores than the parent fibers [41-42].

The porosity of wood fibers can be measured in the wet state using solute exclusion [43], nuclear magnetic resonance cryoporometry[44-45], polymer adsorption[46], and thermoporosimetry[47] [41] and in dry state using gas adsorption[48-49] and mercury intrusion porosimetry[39]. In this research thermoporosimetry and mercury intrusion methods were used.

Thermoporosimetry

When wood fibers are saturated with water, the water can be categorized as non-freezing bound water, freezing bound water, and unbound (bulk) water[50-52]. Non-freezing water is the first 1-3 layers of water adjacent to the sample surface and does not freeze since the motion of water is extremely restricted by the association with the surface[53]. Freezing bound water is the water located in small capillaries and is thermodynamically different than unbound water[54]. Freezing bound water can be used for calculating the wood fibers porosity since it has a depressed melting point temperature due to the lower pressure at a curved interface in

cavities. According to the Gibbs-Thomson equation (equation 1) there is a relationship between pore diameter and the depressed melting point temperature of freezing bound water[54]:

1) $D = \frac{-4T_0\gamma_{ls}\cos\theta}{(T_0 - T_m)\rho H_f}$

Where D is the average pore diameter (nm), T_0 is the melting temperature of bulk water (273.15 K), T_m is the freezing bound water depressed melting point temperature (K), θ is the contact angle between ice and pore wall (assume to be 180°), γ_{ls} is the surface energy of ice/water interface (12.1 mJ/m^2) , ρ is the water density (1000 kg/m^3) , and H_f is the specific melting enthalpy of water (333.5 J/g).

For thermoporosimetry analysis, an isothermal step scan procedure is conducted using a differential scanning calorimeter (DSC) [47, 54]. In this procedure wet sample (2.47±0.64 g H_2O/g dry sample or generally values higher than 1[41]) was cooled down to -30°C and maintained for 5 min to make sure the water was completely frozen. The temperature was then increased to -20°C at 1°C/min and this step (-30 to -20 °C) was used for measuring the sensible heat of the wet sample (it was assumed that no melting occurred at this step). Next heating steps (-15, -10, -6, -4, -2, -1.5, -1.1, -0.8, -0.5, -0.2, and -0.1°C) were performed at 1°C/min and for each step, which corresponds to a specific depressed melting point temperature or specific pore diameter (Table 1-1), melting enthalpy was calculated as follows[54]:

2) $H_m = H_t - H_s$

Where H_m is the melting enthalpy (J), H_t is the total enthalpy (J), and H_s is the sensible heat (J). Sensible heat must be subtracted from the total enthalpy of each step because it is the amount of heat that is consumed for increasing the temperature of the sample and not for melting. Sensible heat as mentioned before is calculated from the first step (-30 to -20°C) of the isothermal step scan (equation 3):

3) $H_s = C \times \Delta T$

4) $C = \frac{q}{\Delta T*}$

Where C is the specific heat, ΔT is the temperature difference for each step, and ΔT* is the temperature difference for first step (-30° to -20°C).

Table 1-1. Relationship between the freezing bound water depressed melting point temperature (Tm) and the pore diameter (D) according to the Gibbs-Thomson equation (equation 1)[54]

T_m (°C)	D (nm)
-15	2.6
-10	4.0
-6	6.6
-4	9.9
-2	19.8
-1.5	26.4
-1.1	36.0
-0.8	49.5
-0.5	79.2
-0.2	198
-0.1	396

Finally total melting enthalpies were (except first step: -30 to -20°C) used for calculating the total amount of freezing bound water which corresponds to the sample porosity. An example of isothermal step scan data is shown in Appendix A. Thermoporosimetry has been used for studying pore size distribution of cellulosic materials [41, 47, 54-55] . However this method has some drawbacks: pores are assumed to be cylindrical which is not always the case in wood[56]; water soluble substances in wood such as organic and inorganic extractives can reduce the specific melting enthalpy of water and cause error.

Mercury intrusion porosimetry (pore size distribution)

Mercury intrusion porosimetry is a method used for exploring pore structures larger than about 3.5 nm. This method can determine both pore volume and pore diameter of wood fibers by the forced intrusion of a non-wetting liquid (mercury). This involves degassing the

sample at room temperature and then evacuating the sample in a sample cell (penetrometer) and filling the penetrometer with mercury so as to completely surround the sample with mercury, applying pressure to the filled sample cell by 1) compressed air (up to 0.3 MPa maximum) and 2) hydraulic pressure generator (up to 400 MPa maximum). Intruded volume is measured by change in capacitance as mercury moves from outside the sample into its pores under the influence of external pressure gradient. The corresponding pore size diameter at which intrusion takes place is calculated directly from the Washburn equation (equation 5):

5) $D=\frac{-4\gamma COS\theta}{P}$

Where D is pore diameter (µm), γ is the surface tension of liquid mercury (0.52 N/m), θ is the contact angle between mercury and the sample's surface (assumed to be 140°) and P is the applied pressure (Pa).

The equation 5 can be reduced to equation 6:

6) $D=\frac{1.52\times10^{6}}{P}$

The plot of intruded volume of mercury versus applied pressure is obtained from the analysis and the pressures are converted to pore sizes based on equation 6. One of the major drawbacks of this method (as for thermoporosimetry) is that it assumes the pores have cylindrical geometry, which is not always the case in wood. Another drawback is that the pores with wide inner body and narrow opening, intrusion will not occur until sufficient pressure is applied to push the mercury into the narrow opening [57]. This is called the ink-bottle effect which has been reported for wood samples [39]. In this case, for wood samples, mercury can enter the lumen through the pits; hence the volume intruded will be assigned to the pit diameter and not the lumen diameter[39]. However mercury intrusion has been used for studying the pore size distribution of solid wood [58-60] and pulp/paper [39, 61-62].

1.2.3.3. Specific surface area

Specific surface area which is defined as the surface area divided by the mass of the sample can be affected by refining. It has been shown that refining can result in fibrillation and formation of fines which both increase the surface area [63]. Fibrillation can be internal and

external; in internal, the breakage of inner bonds between poly saccharides and poly saccharides and lignin makes the cell wall pore structure to expand and swell [41] . External fibrillation associates with pilling off the fibrils from the fiber surface which can increase specific surface area and roughness. External fibrillation can also produce fines which have high specific surface area. The increase in fiber surface area by increasing specific refining energy and refining time is also reported [1, 63]. Increase in porosity due to refining (discussed in porosity section[41-42]) might also lead to increase in surface area.

There are many different methods available for measuring the specific surface area including geometrical measurements (using optical microscopes), sedimentation, conductance-measuring, kinetic, adsorption, and gas permeability methods. Methods based on physical-chemical interactions between the same and liquids, such as adsorption heat, heat of wetting, sorption of dyes, etc. are less common. Raiochemical, X-ray, and mercury intrusion porosimetry can also be used. Among all these methods the gas adsorption and gas-permeability methods provide the best accuracy. In this study Brunauer-Emmett-Teller (BET) gas adsorption and mercury intrusion porosimetry methods were used for measuring the specific surface area of wood fibers. In mercury intrusion porosimetry method analysis was conducted as described in porosity section above and specific surface area was calculated from the area above the cumulative intrusion volume vs pressure graph. Below the BET gas adsorption method is discussed.

Brunauer-Emmett-Teller (BET) gas adsorption

The surface molecules of any solid material are bonded on one side only, therefore the other side is ready to adsorb gas, vapor, or liquid molecules by van der Waals forces (physical adsorption)[64]. In gas adsorption method sample (with known mass) is placed in a glass cell (with known mass) and loaded into the equipment (Auto-sorb). In order to remove all the contaminations and moisture from the surface of the sample, loaded sample cell is outgassed (vacuumed) normally at elevated temperature for couple of hours. Then the mass of the sample is recorded and analysis initiated. During the analysis, loaded sample cell is immersed in liquid nitrogen and adsorbate gas molecules are injected and adsorbed by the surface of the sample.

An adsorption isotherm plot is then obtained by measuring the amount of gas adsorbed across a range of relative pressures (0.05-0.3 P/P_0). In this narrow range of relative pressures adsorbed gas molecules form a monomolecular layer on the surface of the sample. Specific surface area can then be calculated by knowing the volume of the adsorbed monomolecular layer and the cross-sectional area of the adsorbate gas using the BET equation[65] (Appendix B). Different adsorbate gas molecules can be used; for example for measuring materials with high specific surface area, N_2 gas is a good option while for materials with low surface area (0.5-1 m^2/g) Kr gas is suggested. The reason is that for materials with low surface areas the number of unadsorbed N_2 molecules in the void volume of the sample cell are more than the number of adsorbed molecules; this results in large measurement uncertainty. This can be fixed by increasing the sample mass, but due to the size limitation of the sample cell, it is sometimes not practical. When Kr is used, due to its lower vapor pressure compared to N_2, the number of unadsorbed Kr gas in the void volume of sample cell is low and results in more sensitive measurement. It has been shown that sample preparation (drying) has effect on the specific surface area[66]. It is found that different drying methods such as vacuum drying, freeze drying and solvent exchange drying have effect on the sample specific surface area (Chapter 2 and Appendix B).

1.2.3.4. Surface energy

There are two main methods for measuring the surface energy of powder or fibrous shape materials such as wood fibers which are Wicking column[67] and inverse gas chromatography (IGC). There are few studies focusing on the effect of refining on wood fiber surface energy. Ormondroyd et al. (2017) studied the effect of refining pressure on spruce fiber surface energy using IGC; they found that upon increasing the refining pressure from 0.4 to 0.8 MPa dispersive surface energy increased [68]. The effect of thermal modification on surface energy of spruce wood was also studied using IGC and the results showed that thermally modified wood had more heterogeneous nature in terms of the dispersive surface energy compare to unmodified wood; also thermally modified wood had higher dispersive surface energy at the higher surface active sites compare to unmodified wood [69]. The effect of beating

on the surface energy of bleached pulp was studied using IGC and results showed that beating increased the dispersive surface energy[70-71]. In another study on kraft pulp Aquino et al. (2002) reported that high cooking temperature strongly decreased the fiber surface energy, and that the delignification stage prior to bleaching enhances the Lewis acidic character of the fibers[72]. Carvalho et al. (2005) also found that extended cooking decreased dispersive surface energy of Eucalyptus globulus kraft fibers[73]. Peterlin et al. (2010) found that delignification increased the dispersive surface energy of thermomechanical spruce fiber[74]. Additionally, surface energy of cellulose, extractives and lignin has been extensively studied. It has been reported that extractives generally have low dispersive surface energy and their removal from wood/pulp resulted increased the dispersive surface energy[75-78]. However different results have been reported regarding cellulose and lignin surface energies[79]. Although it was stated in some reports that *in situ* lignin had lower dispersive surface energy than cellulose[74, 80]. It has also been shown that generally the surface of lignocellulosic materials is more basic than acidic[81-83] and lignin, extractives and hemicellulose have shown more Lewis basicity characteristic than cellulose [84-92].

IGC has been widely used for determining dispersive and acid-base surface energies of lignocellulosic materials [79, 87, 90, 93-100]. In this study IGC was used for measuring the surface energy.

Inverse gas chromatography (IGC)

IGC has been used for studying physicochemical properties such as surface area, work of cohesion, glass transition temperature, surface energy heterogeneity, acid-based properties, and polar functionality on the surface of materials in particle, fibrous, or powder form. In this study IGC was used to determine dispersive (nonpolar) and acid-based (polar) surface energies as well as surface acidity and basicity parameters of the wood/fiber. In the early days of IGC, surface energy was measured using probes at very low concentrations (infinite solution) which only resulted in one value for surface energy which was related to surface energy at high energy sites of the surface[69]. However in new IGC methods[101], surface energy distribution is obtained which is very useful and practical for wood and lignocellulosic materials since they are

very heterogeneous. In these new methods gas probes at different concentrations (finite dilution) are used and interact with the sample's surface[69].

In IGC, the sample is packed in a glass column and one gas probe is injected at a time and passes the sample column using an inert carrying gas which is typically helium, argon or nitrogen. The elution time of the gas, which is related to the interaction of the probe with the sample surface, is then detected by a flame ionization detector which results in a peak in a chromatogram. This peak can then be used to calculate surface energies and acid-base properties of the sample surface. It should be noted that in order to correct for the dead volume of the sample column, methane gas is injected and it is assumed that there is no interaction between methane gas and the sample. The surface property calculations in IGC are as follows:

Before starting the surface energy or surface acidity-basicity analysis the monolayer capacity for each gas probe should be calculated. This is necessary since the IGC is conducted in a range of surface coverage and in order to calculate the surface coverage, monolayer capacity for each probe should be known. For each gas probe, monolayer capacity is calculated based on the cross-sectional area of the probe molecule and the measured surface area using the BET gas adsorption method (IGC is capable of measuring surface area but in this study surface area was measured by Autosorb-1 instrument). From the monolayer capacity, surface coverage can be determined; which is the amount of probe moles divided by the monolayer capacity. In this study surface coverage of 0.01-0.15 was set for each gas probe. All the calculations including surface energies and surface acid-base properties are based on the net retention volume (V_N) which depends on the time of interaction between the injected gas probe and the solid surface (equation 7) [102].

7) $$V_N = \frac{j}{m} F (t_r - t_0) \frac{T}{273.15}$$

8) $$j = \frac{3}{2} \left[\frac{(\frac{P_{in}}{P_{out}})^2 - 1}{(\frac{P_{in}}{P_{out}})^3 - 1} \right]$$

where j is the James-Martin correction factor attributable to pressure drop (P_{in} and P_{out} are the column inlet and outlet pressures), m is the mass of the sample, F is the flow rate of the carrier

gas, t_r is the retention time of the probe, t_0 is the retention time of methane (for measuring the dead volume) and T is the temperature [102-103]. For determining the dispersive surface energy two methods can be used including the Dorris-Gray [98] or Schultz [104-105]. It has been stated that Dorris-Gray method gives more accurate and reproducible results [101, 106-107]. However some of the reported dispersive surface energies for hybrid materials did not show difference between Dorris-Gray and Schultz methods[108]. It has been reported that little difference was observed between Dorris-Gray and Schultz results when the analysis temperature was at 30°C[103]. The Dorri-Gray method was used in this project to calculate the dispersive surface energy.

The Dorris-Gray method is based on the free energy of adsorption of one methylene group (CH_2) from the gas probe molecule. The dispersive surface energy can be calculated from the correlation and slope of the free energy of adsorption of at least three alkanes (gas probes) plotted versus their carbon number. The free energy of adsorption of one CH_2 group is calculated as shown below (equation 9):

9) $$\Delta G^{CH_2} = -RTln(\frac{V_{N,n+1}}{V_{N,n}})$$

Where R is the universal gas constant, T is the temperature, V_N is the retention volume, and n is the carbon alkane number. The work of adhesion between the solid sample and the CH_2 group is described according to Fowke's theory [109] for van der Waals interactions (equation 10):

10) $$W_a^{CH_2} = 2\sqrt{\gamma_s^d \gamma CH_2}$$

where γ_s^d is the dispersive surface energy of the solid and γCH_2 is the free energy of the CH_2 group. The change in free energy of adsorption of one CH_2 group can be calculated as below (equation 11):

11) $$-\Delta G^{CH_2} = N a_{CH_2} W_a^{CH_2}$$

where N is Avogadro's number and a_{CH_2} is the cross-sectional area of the CH_2 group. Combining equations (10) and (11) gives the following equation (12):

12) $$\gamma_s^d = \frac{Slope^2}{4 \times N^2 (a_{CH_2})^2 \times \gamma CH_2}$$

The dispersive energy can be calculated from the slope of the free energy of adsorption versus the carbon number plot (Figure 1-4) by using equation (12) [69, 103].

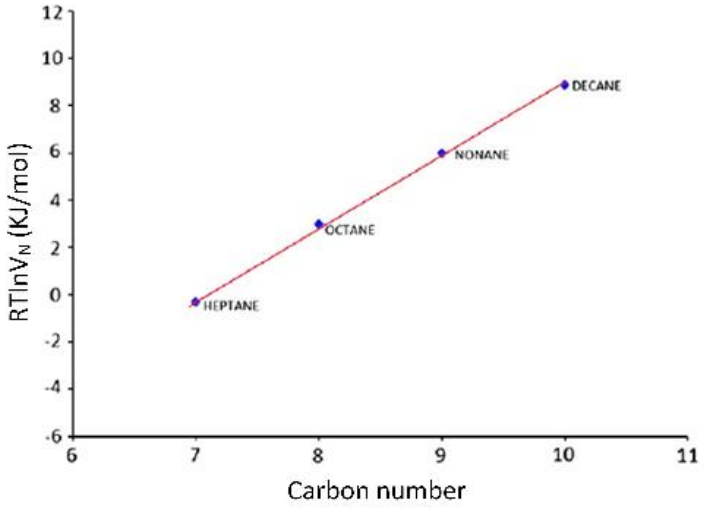

Figure 1-4. Dorris-Gray plot for determining the dispersive surface energy

For determining acid-base surface energy the Polarization method was used[110]. In this method deformation polarization (P_D) which is an intrinsic characteristic and is independent of the nature of the probe is calculated as below (equation 13):

13) $$P_D = \frac{n^2-1}{n^2+2} \times \frac{M}{\rho}$$

where n,M, and ρ are the refractive index, molar mass, and density. In the plot of RTlnV$_N$ versus the molar deformation polarization of n-alkane probes, the vertical distance between polar probe point and the alkane line gives the acid-base free energy ($\Delta G_{acid\text{-}base}$) [111] (Figure 1-5).

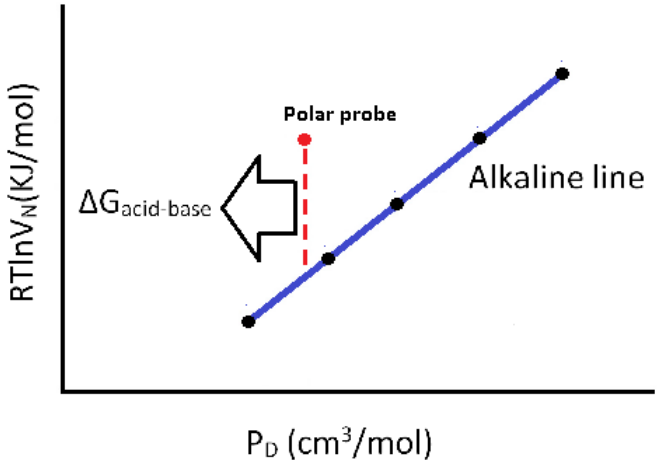

Figure 1-5. Polarization method plot for determining the acid-base free energy (ΔGacid-base)

The relationship between acid-base free energy and acid-base surface energy is as follows (equation 14)[107]:

14) $-\Delta G_{acid-base} = 2.N.a.(\sqrt{\gamma_S^+.\gamma_L^-} + \sqrt{\gamma_S^-.\gamma_L^+}$

where N is Avogadro's number, a is the molecular cross-sectional area of the adsorbed probe molecule, and γ_S^+ and γ_S^- are Lewis acid (electron acceptor) and Lewis base (electron donor) of the sample acid-base surface energy. $\gamma_L^+$and γ_L^- are Lewis acidity and Lewis basicity of the probes used: dichloromethane is used normally for Lewis acid ($\gamma_L^+ = 124.58$ KJ/mol,) and ethyl acetate for Lewis base ($\gamma_L^- = 475.67$ KJ/mol). Therefore in the case of having dichloromethane and ethyl acetate as acidic and basic probes respectively, equation (14) can be summarized as follows:

15) $\gamma_S^{acid-base} = 2.(\sqrt{\gamma_S^+.\gamma_S^-}$

where $\gamma_S^{acid-base}$ is the acid-base surface energy.

IGC is also capable of determining acid-base properties of the solid surface. The most common theory for that is the Gutmann concept[112-113]. The equation used in the Gutmann concept is shown below (equation 16). Different polar probes can be used in Gutmann concept and probes can be amphoteric such as acetone. Acetone can act as an electron acceptor because of the electron deficient carbon of the carbonyl group and at the same time can show basicity behavior through sharing the electrons on the oxygen atom.

16) $-\Delta G_{acid-base} = K_A.DN + K_B.AN$

where $\Delta G_{acid-base}$ is the acid-base free energy, AN and DN are acceptor number and donor number respectively and K_A and K_B are Lewis acid and base numbers of the solid reflecting its surface electron accepting and donating characteristics[102]. K_A and K_B can be calculated by plotting –ΔG/AN versus DN/AN as shown in Figure 1-6.In Figure 1-6, K_A and K_B are the slope and the intercept respectively.

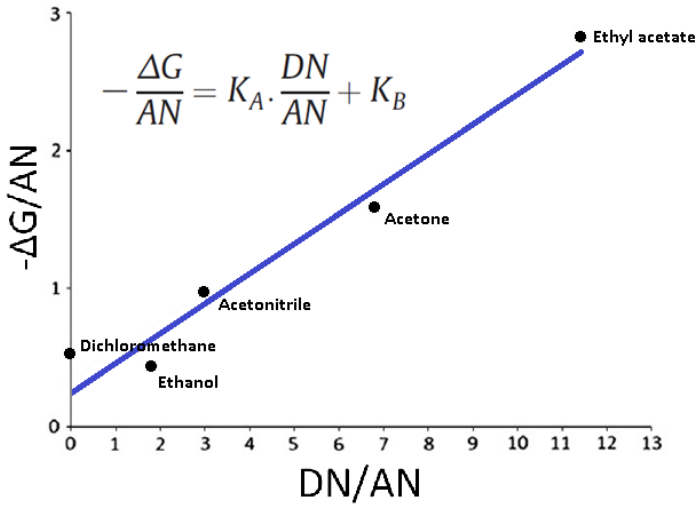

Figure 1-6. The Gutmann concept plot for determining KA and KB

AN and DN of some of the probes are shown in Table 1-2.

Table 1-2. AN and DN of some probes used for determining KA and KB using Gutmann concept

Probe	AN(Kcal/mol)	DN (Kcal/mol)
Dichloromethane	3.9	0
Acetonitrile	4.7	14.1
Acetone	2.5	17
Ethyl acetate	1.5	17.1

In new IGC instruments, controlling the relative humidity is also possible, which can be a very interesting option for studying lignocellulosic materials.

1.2.3.5. Compositional analysis

Polysaccharides

The only work that focused on the effect of refining energy (gap between the refiner plates) on Loblolly pine fiber dimensions, acidity and buffer capacity was done by Short and Lyon (2007)[20]. They did not see any effect of refining energy on fiber acidity and buffer capacity[20]. Most of the other research projects studied the effect of refining pressure and

steaming on fiber chemistry. Kelley et al. (2007) looked at the effect of refining pressure (0.2 – 1.8 MPa) on fiber chemistry. They reported that in general glucose increased while xylose and galactose decreased by increasing the refining pressure[8]. It was stated that higher refining pressures depress the glass transition temperature of lignin which can initiate the hydrolysis of carbohydrate bonds[8]. They also found that fiber crystallinity increased by increasing refining pressure; increasing refining pressure can result in decrease in the concentration of the amorphous cellulose and hemicellulose components which can increase the crystallinity[8]. Roffael et al. (2001) reported decrease in pentosan content by increasing the refining temperature from 140 to 180°C for thermomechanical spruce fibers [114]. Josefsson et al. (2001 and 2002) found degradation and dissolution of cellulose and hemicellulose due to steam explosion treatment; they also observed increase in glucose content[115-116]. Li et al. (2005) also found degradation of polysaccharides during high temperature steam treatment which resulted in formation of furfural and hydroxymethyl furfural [117]. It has been stated that both homolytic cleavage and acid hydrolysis of glucosidic linkages might take place during the steaming[118] and also linkages between lignin and polysaccharides can be cleaved[119] which all can lead to polysaccharide degradation. Wang et al. (2016) also reported degradation of both cellulose and hemicellulose by increasing steam treatment temperature[120]. Martin-Sampedro et al. (2011) showed that upon increasing the severity of steam treatment, no change was observed in glucan content, but the amounts of xylan and arabinan decreased [121]. Chung and Wang (2017) studied the effect of steaming on bamboo and found that holocellulose and alpha cellulose were decreased due to steam treatment [122]. Zhao et al. (2010) studied the effect of steam treatment temperature and time on bamboo and found that alpha-cellulose was very stable to temperature and time, however the hemicellulose content decreased substantially by increasing temperature [123]. Shao et al. also reported decrease of xylose content after steam explosion treatment of bamboo [124].

Fiber acidity

Many authors reported increases in wood acidity due to the effect of refining[38, 114]and steaming temperature[117, 125]. Zhao et al. (2010) found the same effect of steam temperature on bamboo[123].

Lignin

Wang et al. (2016) found that for steam treated samples the amount of soluble lignin was higher than untreated sample. They also reported that by increasing steam temperature the amount of acid soluble lignin decreased and that Klason lignin (acid insoluble lignin) decreased by increasing the steam temperature[120]. Martin-Sampedro et al. (2011) showed that by increasing the severity of steam treatment Klason lignin increased while acid soluble lignin decreased [121]. Others reported that refining pressure[8] and steam treatment[117, 122] had no significant effect on Klason lignin. Zhao et al. (2010) found that the amount of bamboo lignin slightly increased by increasing the steam temperature [123].

Extractives

Regarding the effect of refining and steam treatment on wood extractives, many authors reported that refining pressure and steam treatment resulted in increase in the amount of extractives. Roffael et al. (2001) showed that increasing the refining temperature caused increase in the ethanol and hot-water extracts wood extractives [114]. Increasing steam temperature also caused increase in the amount of extractives in Aspen[120], Eucalyptus[121], and Black walnut[126]. Chung and Wang (2017) and Zhao et al. (2010) found the same effect of steam temperature on bamboo extractives [122-123]. The reason for increasing the amount of extractives due to refining pressure or steam treatment was stated to be due to perhaps some delignification during ethanol extraction[116, 121, 127-128].

The method used in this research for studying the compositional analysis was the NREL procedure: determination of structural carbohydrates and lignin in biomass (NREL/TP-510-42618). We also studied the effect of refining energy on wood/fiber crystallinity using X-ray diffraction. Titration was also used for determining wood/fiber pH and the amount of weak acids (Appendix C)

NREL procedure (for studying compositional analysis)

NREL procedure: determination of structural carbohydrates and lignin in biomass (NREL/TP-510-42618) [129] was used for wood/fiber compositional analysis. First, Soxhlet extraction was performed on wood/fiber (mesh size 18-80) to remove the extractives using 95%

ethanol for 24 hours. Afterwards the extracted samples were dried and hydrolyzed in two consecutive steps 1: 72% sulfuric acid, 30°C, 1 hr and 2: 4% sulfuric acid, 120°C, 1 hr (in autoclave). Acid insoluble lignin was filtered and measured gravimetrically after being oven dried (105°C, overnight), while the acid soluble lignin content was measured using UV-Vis spectroscopy. After the two step acid hydrolysis which resulted in polysaccharide hydrolysis into sugar monomers, Ion chromatography was used for quantifying the sugars.

1.2.3.6. Lignin chemistry

Lignin is a phenylpropanoid macromolecule having both aliphatic and aromatic moieties [121]; it consists of three major monomers coniferyl, sinapyl and p-coumaryl alcohols (Figure 1-7). Softwoods contain guaiacyl lignins and these are derived mostly from coniferyl alcohol. Hardwoods contain syringyl/guaiacyl lignins and are derived mostly from sinapyl and coniferyl alcohols[130]. Grasses contain syringyl/guaiacyl/p-hydroxyphenyl propane lignins and are derived from sinapyl, coniferyl, and p-coumaryl alcohols.

There are different types of linkages in the lignin structure at different positions of the phenylpropane unit labeled in Figure 1-7.

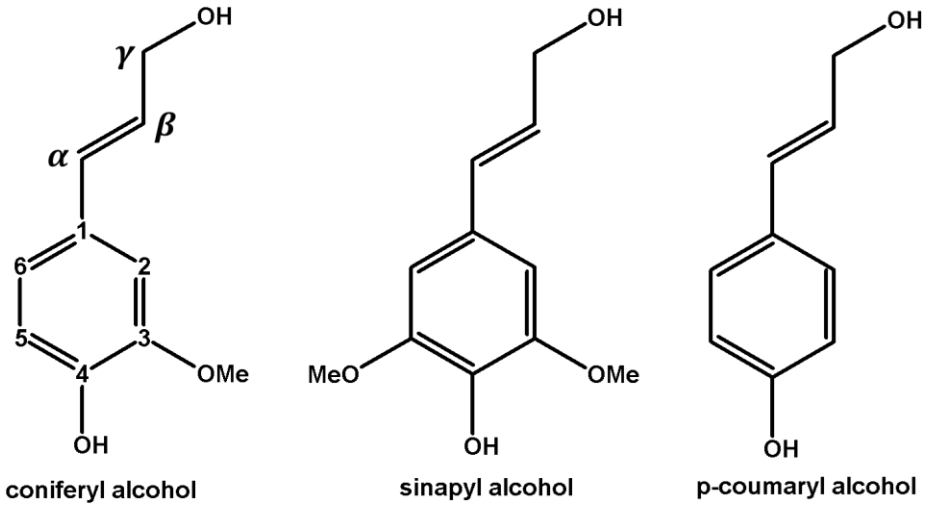

Figure 1-7. Lignin major monomers

The dominant linkages between phenylpropane units in softwood lignin are shown in Table 1-3.

Table 1-3. Dominant linkages in softwood lignin[131]

Linkage type	% Linkages
β-O-4	45-50
5-5	18-25
β-5	9-12
β-1	7-10
α-O-4	6-8
4-O-5	4-8
β-β	3

Among all the linkages shown in Table 2, β-O-4 is the most dominant one (Figure 1-8).

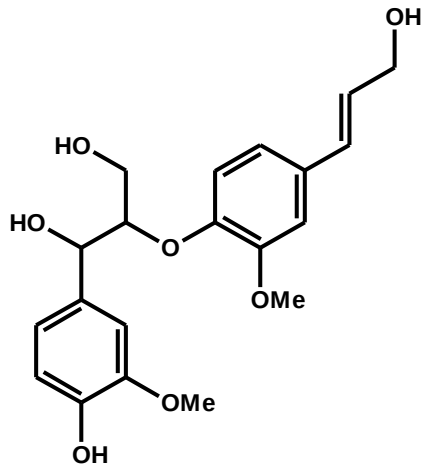

Figure 1-8. β-O-4 linkage in guaiacyl lignin

As mentioned before during refining, the temperature is high (about 170°C) and wood is slightly acidic (Douglas fir pH: 6.01). Under these conditions lignin acidolysis can take place[130]. The most important reaction during lignin acidolysis is the cleavage of β-O-4 linkages[130]. β-O-4 cleavage has been described[132-140] and the mechanism is known[133]. In lignin acidolysis, there are two routes for β-O-4 cleavage[130]. Both routes result in formation of phenols[130], but only one route releases formaldehyde[141-142] (Figure 8). However it has been observed that during lignin acidolysis, depolymerization (β-O-4 cleavage) and repolymerization (condensation) reactions

can occur[127, 143-147] (Figure 1-9) and these reactions can be more or less simultaneous[125, 127, 145, 148]. This is due to the fact that both of these reactions have a common intermediate, the carbonium ion at C_α of the side chain (Figure 1-9)[125].

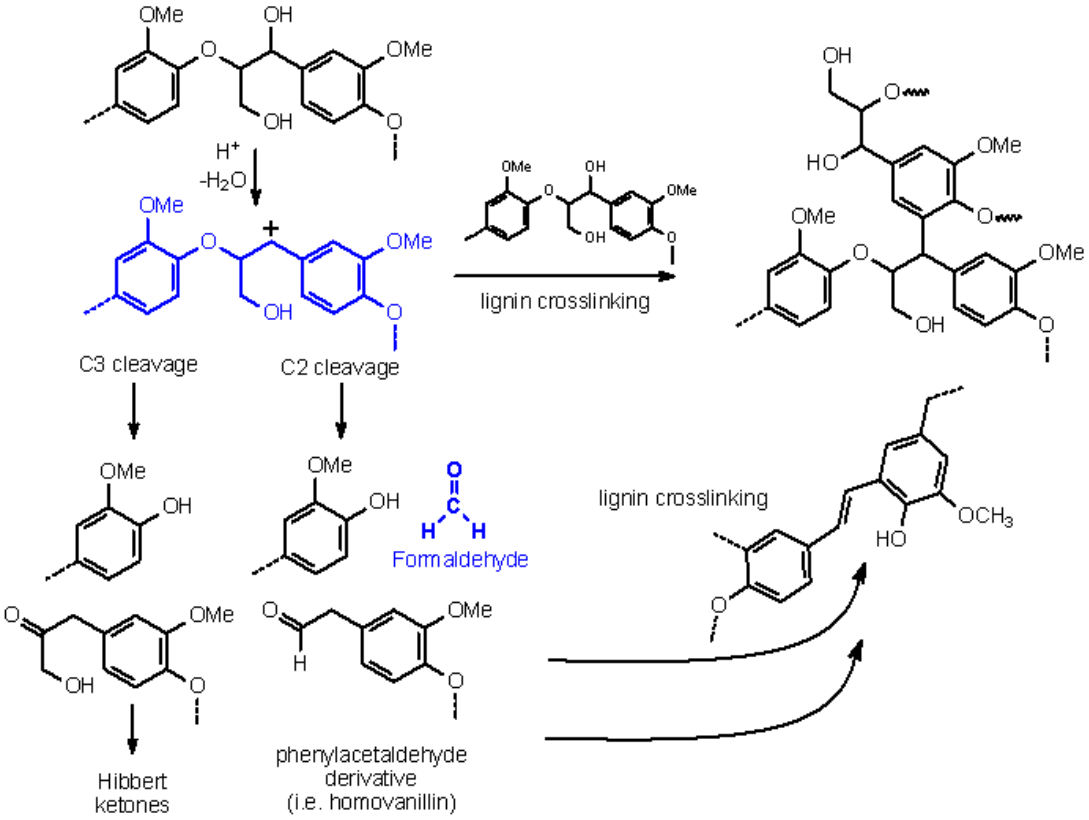

Figure 1-9. Different pathways in lignin acidolysis

The occurrence of lignin acidolysis due to wood steam treatment has been shown. Several studies focused on the effect of steam explosion or autohydrolysis treatments of aspen wood and reported cleavage of β-O-4 linkages and formation of phenols [120, 125, 145, 148-149]. Sudo et al. (1985) did steam treatment (183-230°C) on beech wood and they found extensive cleavage of β-O-4 linkages which resulted in high phenolic hydroxyl content [150].Shimizu et al. (1998) studied the steam explosion treatment on various wood species (hardwoods) at 180-230°C for 1-20 min. They found that α- and β-aryl ether (β-O-4) linkages were extensively cleaved due to steaming [151]. Jakobsons et al. (1995) focused on the steam explosion treatment of birch wood and observed that phenol concentration increased after steam explosion and lignin side chains were subjected to oxidation and partial destruction. They also reported that

pseudo-lignin (products of reactions between polysaccharide degradation products and lignin, and/or repolymerization of polysaccharide degradation products [152]) was incorporated into steam treated lignin structure[153]. Shao et al. (2008) studied the steam explosion of bamboo and found that the phenol content of steam-exploded fiber was 2.3 times higher than the control sample and they stated that the reason is due to β-O-4 cleavage [124]. Martin-Sampedro et al. (2011) studied lignin changes due to steam explosion of Eucalyptus wood chips and found significant decrease in β-O-4 and more phenol formation after steam treatment [121].

As previously mentioned besides phenols, formaldehyde formation also occurs in the C2 pathway of β-O-4 cleavage during lignin acidolysis (Figure 8). Roffael et al. (2001) measured the amount of formaldehyde released from thermomechanical spruce fibers produced at refining temperature from 140 to 160°C. They found that upon increasing the refining temperature formaldehyde release of spruce fibers increased[114], which is consistent with lignin acidolysis.

As discussed before during lignin acidolysis, lignin depolymerization (β-O-4 cleavage) and repolymerization (C-C condensation) occur more or less simultaneously. Several studies observed that in steam treatments, lignin repolymerization takes place [125, 127, 143-148] and some reported that lignin condensation reactions occurred when wood was steam treated at high severity [120-121]. They proved the occurrence of lignin condensation reactions by observing increase in the number of carbon-carbon linkages[120, 150, 154], lignin molecular weight[120-121, 125, 150], and degradation temperature[121].

In this research, for studying wood/fiber lignin chemistry, conductometric titration[155] (Appendix C) was used for measuring the phenols, serum bottle method [156] was used for formaldehyde determination and nitrobenzene oxidation reaction (Chapter 3, Appendix D) for studying lignin structure. 2D NMR heteronuclear single quantum correlation (HSQC) (Appendix E) analysis was also conducted, but it was not a sufficiently sensitive method for this study. Low sensitivity of HSQC has been observed before.

Nitrobenzene oxidation (NBO) reaction is an old method that was introduced by Freudenberg to confirm the aromatic nature of lignin[157]. In this method lignin is oxidized by nitrobenzene in alkaline condition (2M NaOH, 170°C, for 2-3 hrs), lignin linkages such as β-O-4, β-1, β-β and β-5 are cleaved[158-160], and benzaldehydes are recovered as the main products

together with small amounts of corresponding benzoic acids[161]. Therefore in softwoods the two main products of NBO are vanillin and vanillic acid[161]. The mechanism of NBO reaction was first proposed to be in such that nitrobenzene acts as a two-electron-transfer oxidant to produce quinone methide intermediates from free phenolic units[160]; however later studies showed that oxidation is a free radical procedure involving a one-electron transfer at the level of the benzylic alcohol group[162]. It is highly possible that both mechanisms coexist (Figure 1-10). Benzoic acid is formed in small amounts from benzaldehyde (3-10% based on the benzaldehyde yield[160, 163]) during NBO through Cannizzaro reaction which occurs under alkaline condition (Figure 1-11). The reason for having small amounts of corresponding benzoic acid is that aldehydes containing phenolic hydroxyls are stable under basic conditions. This is due to resonance stabilization on the carbonyl group by the phenolate anion which tends to protect it from the nucleophilic attack of hydroxide anion which is the initial step in the base-catalyzed Cannizzaro reaction (Figure 1-11).

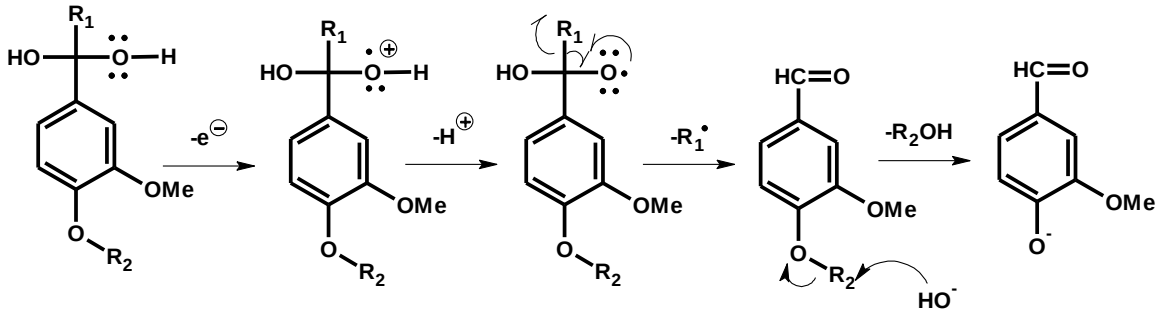

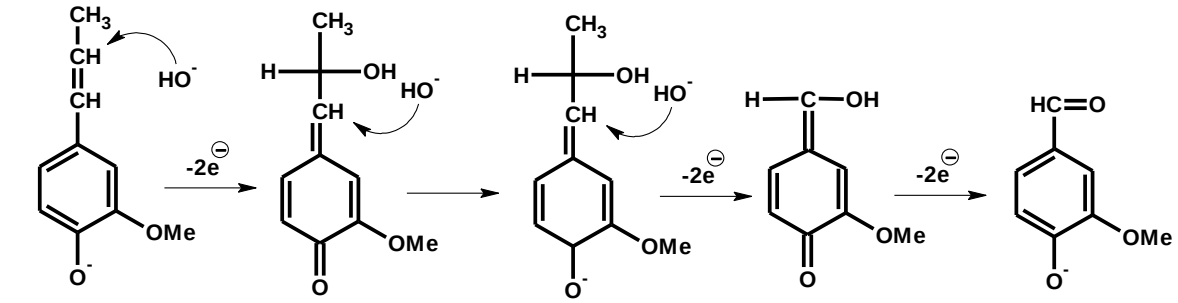

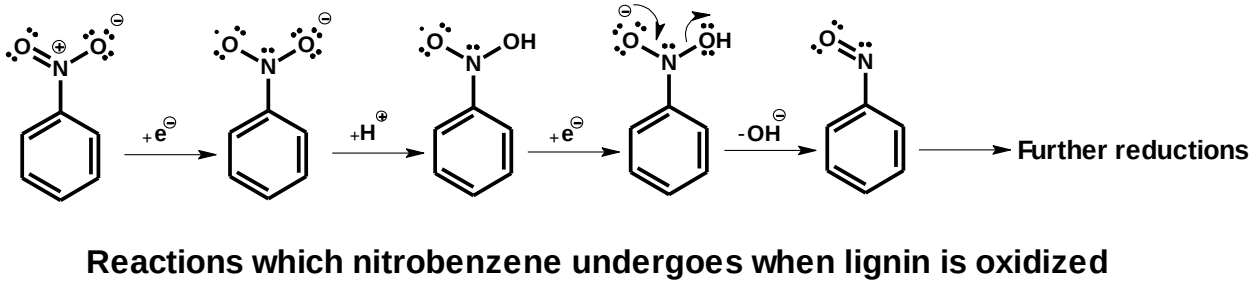

Figure 1-10. Proposed nitrobenzene oxidation mechanisms (Two-electron-transfer mechanism is shown for isoeugenol)

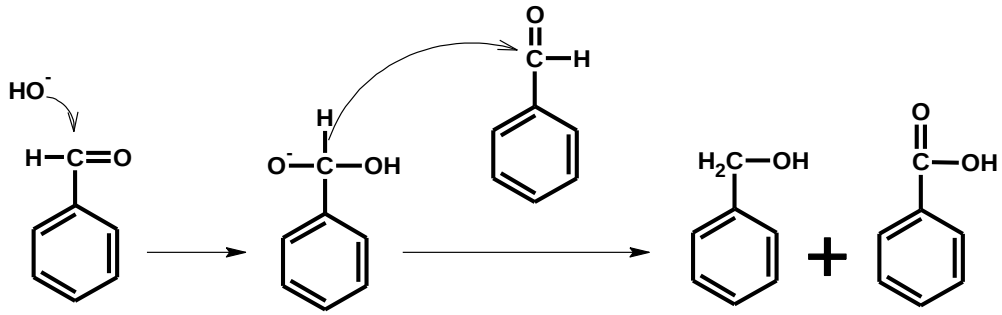

Figure 1-11. Cannizzaro reaction

It should be noted that in softwoods the yield of NBO reaction (vanillin formation) is about 17-20% (by weight) based on Klason (acid insoluble) lignin. The NBO reaction has been conducted in slightly different ways in the literature and in this study the method was adapted from Ohra et al. (2013) [164], Liyama (1990) [163], and Latahira and Nakatsubo (2001) [165]. However modified version of NBO has been developed which reduced the amount of sample and the reaction time[166]. In this study NBO was used in order to confirm the occurrence of lignin acidolysis reaction during the refining.

1.2.3.7. Rheology

The effect of refining on compaction and densification of wood fiber mat and also on lignin glass transition temperature was studied using rheometer.

Compaction and densification

In MDF production wood fibers blended with adhesive and other additives undergo cold press and then are subjected to heat and pressure in the process of forming the final board. The application of heat and pressure to moisture-containing wood fibers results in compaction and densification. Compaction and densification have significant effects on the final board properties. When MDF is hot pressed there will be a gradation in final board density throughout the thickness of the board which is called vertical density profile (VDP) [167]. In hot pressing, thermal and moisture-induced softening decrease the compression strength of the wood fibers and the modulus perpendicular to the grain as well as the bending modulus. Therefore when the press starts to close, the layers of the mat which are directly in contact with the platens get weakend and readily densified. However it should be mentioned that the extreme outer surfaces of the face layers have the lowest density which is mainly due to the adhesive overcure with the immediate contact of the extreme outer surfaces with the heated press platens. Steam generated from heating the surface layer is transferred to the core of the mat; this increases the core temperature and moisture content. The intermediate and core regions of the mat densify at a different rate and degree than the surface layers [167]. The result of this dynamic process develops the VDP throughout the board thickness (Figure 1-12). Vertical density profile formation is dependent upon some factors as stated by Wang and Winistorfer (2000) [168]: 1) the

moisture content of the mat, 2) mat structure which depends on the fiber geometry, dimensions and inherent density of the wood used for producing the fibers, and 3) pressing conditions including temperature, pressure and pressure cycle, and pressing time (total and press closing time). VDP has significant effects on physical properties of the final MDF. For example boards with considerably higher face density are better for laminating, gluing, and finishing. When the core density is homogenous the board is very suitable for embossing, molding, and general machining [169].

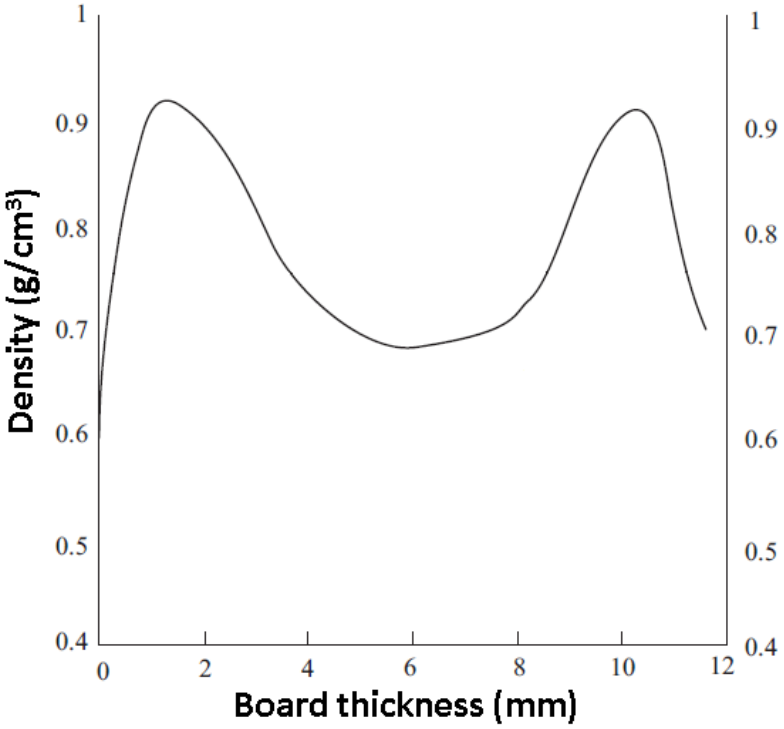

Figure 1-12. Example of vertical density profile (VDP)

During hot pressing since the moisture content of the mat changes, this will have effect on the viscoelastic behavior of the mat. When wood is under load and subjected to moisture content changes, it shows much greater deformation than under constant moisture content. This phenomenon is known as mechano-sorptive (mechano-sorption) effect and it seems that it can happen during the MDF hot pressing. The mechano-sorptive effect has been observed in wood and paper using dynamic mechanical analysis [170-172]. In this study the compaction and

densification of the fiber mat during cold and hot pressings were studied using a newly developed method which is described in Chapter 2.

Lignin glass transition

The effect of steam treatment on lignin structure has been discussed before in the lignin chemistry section and it was mentioned that during lignin acidolysis, lignin depolymerization (β-O-4 cleavage) and repolymerization (C-C condensation) occur more or less simultaneously. Several studies showed that in steam treatments, lignin repolymerization takes place [125, 127, 143-148] and this was found based on increase in number of carbon-carbon linkages[120, 150, 154], lignin molecular weight[120-121, 125, 150] and degradation temperature[121]. Dynamic mechanical analysis (DMA) can also be used for studying lignin repolymerization by measuring lignin glass transition temperature (T_g). If repolymerization/crosslinking reactions are more dominant than cleavage reactions, lignin polymeric flexibility is expected to decrease which results in lignin T_g increase. Thermal softening of lignin and its impact on energy consumption of pulping processes was first studied by Hoglund et al. (1976) [173]. DMA was first used to study the viscoelastic behavior of wood in 1960s, using a torsional pendulum mode on rectangular specimens [174-175]. After the 1960s torsion bending and tension modes were mostly used [176-182].The DMA analysis that was used in this study has been developed by Chowdhury et al. (2010) [183]. The method is solvent-submersion compressive torsion DMA where a fiber mat is compressed between parallel-plates while being immersed in a plasticizer. The reason for using plasticizer is that in dry conditions, the glass transition temperature of *in situ* lignin is about 205°C[184]; however by using plasticizing solvents, lignin T_g can effectively be reduced to lower temperatures. For example lignin T_g for water saturated wood has been reported to be between 60 and 95°C, while more stronger plasticizers such as formamide can reduce the lignin T_g to about 40°C[176]. In this study glycerol was used as plasticizer which is a less effective wood swelling agent compared to other plasticizers[185-186]. Glycerol was selected since it provides a crude approximation of moisture levels below wood fiber saturation point which is the condition used in MDF industry.

1.2.3.8. Resin cure

Resins that are normally used in MDF production are urea formaldehyde (UF) and melamine urea formaldehyde (MUF) resins (the amount of melamine is normally very small, 2% based on 100% liquid) [187]. Pizzi and Panamgama (1995) studied the curing of MUF resin in the presence of wood and cellulose. They reported that MUF in the presence of wood and cellulose had a lower activation energy compared to neat MUF [188]. Xing et al. (2004) reported that UF gelation time was directly correlated to wood pH. They also found that at low level of resin catalyst (NH_2Cl), UF gel time was inversely correlated with wood acid buffering capacity, however at higher catalyst levels wood acid buffering capacity did not have significant effect on UF gel time [189]. Johns and Niazi (2007) studied the effect of wood extract pH and buffering capacity on UF gelation time and reported that UF gelation time was directly correlated to the wood extract pH and inversely correlated with acid buffering capacity[190]. Xing et al. (2005) also studied the effect of wood on UF curing behavior. They found that the curing enthalpy of the UF resin decreased in the presence of wood; they stated that the reason is due to diffusion induced by wood since wood can absorb UF water and reduce the mobility of resin which can have effect on resin cure [191]. Gao et al. (2008) studied the curing characteristics of UF in the presence of various amounts of wood extracts. They found that the curing rates of UF increased in the presence of wood extracts when pH values decreased. They found that different wood species had mixed effect on UF activation energy. Based on that they suggested that activation energy does not reveal the whole picture of the resin cure, and other curing behaviors such as curing peak temperature must also be considered[192]. Lee et al. (2013) studied the effect of MDF flour, rice husk flour, silica powder, and tannin powder on the curing behavior of UF resin. They found that by adding MDF flour the thermal stability of UF increased but the curing activation energy decreased[193].

The curing behavior of phenol formaldehyde (PF) resins has also been affected by the wood substrates in the PF/wood mixtures[194-199]. Mixed findings were reported on the effect of wood on PF resin activation energy. Some authors reported that wood decreased the PF activation energy[194, 197] while others stated the opposite way[196, 199]. It has been also reported that in the presence of wood the reaction enthalpy of PF resin was reduced[199].

In this study, the effect of wood/fiber on the onset and enthalpy of cure as well as curing activation energy has been studied using differential scanning calorimetry as described in Chapter 4.

1.2.3.9. Resin crystallinity

The presence of crystallinity in UF resin has been reported by many authors [200-203]. It has been reported that UF crystallinity occured when F/U mole ratio was low (1.0) [201-204]. Dunker et al.(1986) related the semicrystalline nature of cured UF to hydrogen bonds between colloidal particles. They also stated that the UF crystalline regions could be formed from the crystallization of compounds containing ring structure[205]. Levendis et al. (1992) also stated that the crystallinity of the cured UF is dependent upon the F/U mole ratio and NH_4Cl hardener content [206]. The crystallinity of UF resin can be very important because it can affect the strength[200] of the resin and also its formaldehyde emission[201]. Ferg et al. (1993) reported that the cured UF crystallinity and strength appeared to be inversely related [207]. Park and Causin (2013) found that UF crystallinity was correlated to the improved hydrolytic stability of the resin which can reduce resin formaldehyde emissions [201-202].

Regarding the effect of wood on UF crystallinity Levendis et al. (1992) found that the cured UF can only be amorphous when it is cured in the presence of wood even at low F/U mole ratios [206]. Lee et al. reported the same for UF cured in the presence of MDF flour[193]. In contrast, Singh et al. (2014) showed that UF with low F/U mole ratio does crystallize when cured in the presence of wood[200].

In this research, the effect of wood/fiber on UF and MUF crystallinity was studied using X-ray diffraction as described in Chapter 4.

1.3. References

1. Suchsland, O.; Woodson, G. E., Fiberboard manufacturing practices in the United States. *Agriculture handbook/United States. Dept. of Agriculture (USA)* **1987**.
2. Panshin, A. J.; Zeeuw, C. d., *Textbook of wood technology, 3d ed*. McGraw-Hill Book Co.: **1970**; Vol. 1.
3. Park, B.-D.; Kim, Y.-S.; Riedl, B., Effect of wood-fiber characteristics on medium density fiberboard (MDF) performance. *Journal of the Korean Wood Science and Technology* **2001,** *29* (3), 27-35.
4. Hua, J.; Chen, G.; Xu, D.; Shi, S. Q., Impact of thermomechanical refining conditions on fiber quality and energy consumption by mill trial. *BioResources* **2012,** *7* (2), 1919-1930.
5. Benthien, J. T.; Hasener, J.; Pieper, O.; Tackmann, O.; Bähnisch, C.; Heldner, S.; Ohlmeyer, M. In *Determination of MDF fiber size distribution: Requirements and innovative solution*, Proc of the International Wood Composites Symposium, **2013**.
6. Ohlmeyer, M.; Helder, S.; Benthien, J. T.; Seppke, B. In *Effects of refining parameters on fibre quality measured by fibre cube*, Proceedings of the International Panel Products Symposium, **2015**; pp 17-25.
7. McMillin, C. W., Fiberboards from loblolly pine refiner groundwood: effects of gross wood characteristics and board density. **1968**.
8. Kelley, S. S.; Elder, T.; Groom, L. H., Changes in the chemical composition and spectroscopy of loblolly pine medium density fiberboard furnish as a function of age and refining pressure. *Wood and Fiber Science* **2007,** *37* (1), 14-22.
9. Groom, L. H.; Mott, L.; Shaler, S., Relationship between Fiber Furnish and the Structural Performance of MDF. **1999**.
10. Rials, T.; Groom, L.; Tze, W.; Gardner, D.; Snell, R. In *Effect of refining on the surface characteristics of loblolly pine fibers*, Abstracts of papers of the american chemical society Amer Chemical Soc 1155 16th ST, NW, Washington, DC 20036 USA **2001**; pp U182-U182.
11. Krug, D.; Kehr, E., Influence of high pulping pressures on permanent swelling-tempered medium density fiberboard. *Holz Roh-Werkst* **2001,** *59* (5), 342-343.
12. Groom, L. H.; So, C.-L.; Elder, T.; Pesacreta, T.; Rials, T. G., Effects of Refiner Pressure on the Properties of Individual Wood Fibers. *Characterization of the cellulosic cell wall* **2008**, 227.
13. Snell, R.; Groom, L. H.; Rials, T. G., Characterizing the surface roughness of thermomechanical pulp fibers with atomic force microscopy. *Holzforschung* **2001,** *55* (5), 511-520.
14. Yobp, R. D.; Janowiak, J. J.; Blankenhorn, P. R., Effect of steam pressure refining and resin levels on the properties of UF-bonded red maple MDF. *Forest Products Journal* **1993,** *43* (11, 12), 82.
15. Xing, C.; Deng, J.; Zhang, S., Effect of thermo-mechanical refining on properties of MDF made from black spruce bark. *Wood Science and Technology* **2007,** *41* (4), 329-338.
16. Xing, C.; Wang, S.; Pharr, G. M.; Groom, L. H., Effect of thermo-mechanical refining pressure on the properties of wood fibers as measured by nanoindentation and atomic force microscopy. *Holzforschung* **2008,** *62* (2), 230-236.
17. Groom, L.; Rials, T.; Snell, R., Effects of varying refiner pressure on the machanical properties of loblolly pine fibres. **2000**.

18. Xing, C.; Deng, J.; Zhang, S.; Riedl, B.; Cloutier, A., Properties of MDF from black spruce tops as affected by thermomechanical refining conditions. *European Journal of Wood and Wood Products* **2006,** *64* (6), 507-512.
19. Schäfer, M.; Roffael, E., On the formaldehyde release of wood. *European Journal of Wood and Wood Products* **2000,** *58* (4), 259-264.
20. Short, P. H.; Lyon, D. E., Pressure-refined fiber from low-grade southern hardwoods. *Wood and Fiber Science* **2007,** *10* (2), 82-94.
21. Lumiainen, J., Refining of chemical pulp. *Papermaking part* **2000,** *1*, 86-122.
22. Nugroho, D. D. P., Low consistency refining of mixtures of softwood & hardwood bleached kraft pulp: effects of refining power. *Asian Institute of Technology* **2012**.
23. Gharehkhani, S.; Sadeghinezhad, E.; Kazi, S. N.; Yarmand, H.; Badarudin, A.; Safaei, M. R.; Zubir, M. N. M., Basic effects of pulp refining on fiber properties—A review. *Carbohydrate polymers* **2015,** *115*, 785-803.
24. Genco, J. In *Fundamental processes in stock preparation and refining*, Tappi Pulping Conference, **1999**; pp 57-95.
25. Karlström, A.; Eriksson, K.; Sikter, D.; Gustavsson, M., Refining models for control purposes. *Nordic Pulp and Paper Research Journal* **2008,** *23* (1), 129-138.
26. Kerekes, R. J., Force-based characterization of refining intensity. *Nordic Pulp and Paper Research Journal* **2011,** *26* (1), 14.
27. Mohlin, U., Industrial refining of unbleached kraft pulps—The effect of pH and refining intensity. *Sweden: STFI AB, Swedish Pulp and Paper Research Institute* **2002**.
28. Olejnik, K., Impact of pulp consistency on refining process conducted under constant intensity determined by SEL and SEC factors. *BioResources* **2013,** *8* (3), 3212-3230.
29. Lumiainen, J., New theory can improve practice. *Pulp and Paper International* **1990,** *32* (7), 46-54.
30. Loijas, M., Factors affecting the axial force in low-consistency refining. Tampere, Finland: Tampere University of Applied Science. *Paper Technology, Valkeakoski Service Center* **2010**.
31. Kerekes, R., Energy and forces in refining. *Journal of Pulp and Paper* **2010,** *36* (1-2), 10-15.
32. Kerekes, R. J.; SENGER, J., Characterizing Refining Action in Low-Consistency Refiners by Forces on Fibres. *JOURNAL OF PULP AND PAPER SCIENCE* **2006,** *32* (1), 1-8.
33. Smook, G., *Third edition Handbook for Pulp & Paper Technologists (The Smook Book)*. Angus Wilde Publiationd Inc.: **2002**.
34. Franzén, R., General and selective upgrading of mechanical pulps [raw materials]. *Nordic Pulp and Paper Research Journal* **1986**.
35. Benthien, J. T.; Hasener, J.; Pieper, O.; Tackmann, O.; Bähnisch, C.; Heldner, S.; Ohlmeyer, M. In *Determination of MDF fiber size distribution: Requirements and innovative solution*, International Wood Composites Symposium, **2013**.
36. Groom, L.; Mott, L.; Shaler, S. In *Relationship between fiber furnish properties and the structural performance of MDF*, 33rd International Particleboard/Composite Materials Symposium Proceedings, April, **1999**; pp 13-15.
37. Myers, G. C., Relationship of fiber preparation and characteristics to performance of medium-density hardboards. *Forest products journal* **1983,** *33* (10), 43-51.

38. Xing, C.; Zhang, S.; Deng, J.; Riedl, B.; Cloutier, A., Medium-density fiberboard performance as affected by wood fiber acidity, bulk density, and size distribution. *Wood science and technology* **2006,** *40* (8), 637-646.
39. Moura, M.; Ferreira, P.; Figueiredo, M., Mercury intrusion porosimetry in pulp and paper technology. *Powder Technology* **2005,** *160* (2), 61-66.
40. Truong, M.; Zhong, W.; Boyko, S.; Alcock, M., A comparative study on natural fibre density measurement. *The Journal of The Textile Institute* **2009,** *100* (6), 525-529.
41. Maloney, T.; Paulapuro, H., The formation of pores in the cell wall. *Journal of pulp and paper science* **1999,** *25* (12), 430-436.
42. Stone, J.; Scallan, A.; Abrahamson, B., Influence of beating on cell wall swelling and internal fibrillation. *Svensk Papperstidning* **1971,** *71* (19), 687-694.
43. Stone, J.; Scallan, A., A structural model for the cell wall of water-swollen wood pulp fibres based on their accessibility to macromolecules. *Cellulose Chemistry and Technology* **1968,** *2*, 343-358.
44. Topgaard, D.; Söderman, O., Diffusion of water absorbed in cellulose fibers studied with 1H-NMR. *Langmuir* **2001,** *17* (9), 2694-2702.
45. Meng, X.; Foston, M.; Leisen, J.; DeMartini, J.; Wyman, C. E.; Ragauskas, A. J., Determination of porosity of lignocellulosic biomass before and after pretreatment by using Simons' stain and NMR techniques. *Bioresource technology* **2013,** *144*, 467-476.
46. Alince, B.; Van de Ven, T., Porosity of swollen pulp fibers evaluated by polymer adsorption. *The Fundamentals of Papermaking Materials* **1997,** *2*, 771-788.
47. Maloney, T. C., Thermoporosimetry of hard (silica) and soft (cellulosic) materials by isothermal step melting. *Journal of Thermal Analysis and Calorimetry* **2015,** *121* (1), 7-17.
48. Beaumont, M.; Kondor, A.; Plappert, S.; Mitterer, C.; Opietnik, M.; Potthast, A.; Rosenau, T., Surface properties and porosity of highly porous, nanostructured cellulose II particles. *Cellulose* **2017,** *24* (1), 435-440.
49. Yin, J.; Song, K.; Lu, Y.; Zhao, G.; Yin, Y., Comparison of changes in micropores and mesopores in the wood cell walls of sapwood and heartwood. *Wood science and technology* **2015,** *49* (5), 987-1001.
50. Liu, W. G.; De Yao, K., What causes the unfrozen water in polymers: hydrogen bonds between water and polymer chains? *Polymer* **2001,** *42* (8), 3943-3947.
51. Nakamura, K.; Hatakeyama, T.; Hatakeyama, H., Studies on bound water of cellulose by differential scanning calorimetry. *Textile research journal* **1981,** *51* (9), 607-613.
52. Ping, Z.; Nguyen, Q.; Chen, S.; Zhou, J.; Ding, Y., States of water in different hydrophilic polymers—DSC and FTIR studies. *Polymer* **2001,** *42* (20), 8461-8467.
53. Berlin, E.; Kliman, P.; Pallansch, M., Changes in state of water in proteinaceous systems. *Journal of Colloid and Interface science* **1970,** *34* (4), 488-494.
54. Park, S.; Venditti, R. A.; Jameel, H.; Pawlak, J. J., Changes in pore size distribution during the drying of cellulose fibers as measured by differential scanning calorimetry. *Carbohydrate polymers* **2006,** *66* (1), 97-103.
55. Fahlén, J.; Salmén, L., Ultrastructural changes in a holocellulose pulp revealed by enzymes, thermoporosimetry and atomic force microscopy. *Holzforschung* **2005,** *59* (6), 589-597.

56. Moro, F.; Böhni, H., Ink-bottle effect in mercury intrusion porosimetry of cement-based materials. *Journal of Colloid and Interface Science* **2002,** *246* (1), 135-149.
57. Stayton, C.; Hart, C., Determining pore-size distribution in softwoods with a mercury porosimeter. *Forest Products Journal* **1965,** *15* (10), 435-440.
58. Plötze, M.; Niemz, P., Porosity and pore size distribution of different wood types as determined by mercury intrusion porosimetry. *European Journal of Wood and Wood Products* **2011,** *69* (4), 649-657.
59. Pfriem, A.; Zauer, M.; Wagenführ, A., Alteration of the pore structure of spruce (Picea abies (L.) Karst.) and maple (Acer pseudoplatanus L.) due to thermal treatment as determined by helium pycnometry and mercury intrusion porosimetry. *Holzforschung* **2009,** *63* (1), 94-98.
60. Johnson, R. W.; Abrams, L.; Maynard, R. B.; Amick, T. J., Use of mercury porosimetry to characterize pore structure and model end-use properties of coated papers. I. Optical and strength properties. *Tappi journal.*-- **1999**.
61. Alince, B.; Porubska, J.; Van de Ven, T., Light scattering and microporosity in paper. *Journal of pulp and paper science* **2002,** *28* (3), 93-98.
62. Bhardwaj, N. K.; Hoang, V.; Nguyen, K. L., A comparative study of the effect of refining on physical and electrokinetic properties of various cellulosic fibres. *Bioresource technology* **2007,** *98* (8), 1647-1654.
63. Nikitin, Y. I.; Petasyuk, G., Specific surface area determination methods, devices, and results for diamond powders. *Journal of Superhard Materials* **2008,** *30* (1), 58-70.
64. Brunauer, S.; Emmett, P. H.; Teller, E., Adsorption of gases in multimolecular layers. *Journal of the American chemical society* **1938,** *60* (2), 309-319.
65. Romagnoli, M.; Gualtieri, M. L.; Hanuskova, M.; Rattazzi, A.; Polidoro, C., Effect of drying method on the specific surface area of hydrated lime: A statistical approach. *Powder technology* **2013,** *246*, 504-510.
66. Yang, X.; Frazier, C. E., Organic filler surface analysis by column wicking. *Journal of adhesion science and Technology* **2016,** *30* (6), 607-620.
67. Ormondroyd, G. A.; Källbom, S.; Curling, S.; Stefanowski, B.; Segerholm, B.; Wålinder, M.; Jones, D., Water sorption, surface structure and surface energy characteristics of wood composite fibres refined at different pressures. *Wood Material Science & Engineering* **2017,** *12* (4), 203-210.
68. Källbom, S.; Wålinder, M.; Segerholm, K.; Jones, D., Surface energy characterization of thermally modified spruce using inverse gas chromatography under cyclic humidity conditions. *Wood and Fiber Science* **2015,** *47* (4), 410-420.
69. Carvalho, M.; Santos, J.; Martins, A.; Figueiredo, M., The effects of beating, web forming and sizing on the surface energy of Eucalyptus globulus kraft fibres evaluated by inverse gas chromatography. *Cellulose* **2005,** *12* (4), 371-383.
70. Gamelas, J.; JMRCA, S.; Ferreira, P., Surface energetics of softwood kraft pulps by inverse gas chromatography. *Fine structure of papermaking fibres. COST Office, Brussels* **2011**, 39-49.
71. Aquino, A.; Ferreira, P.; Carvalho, M.; Amaral, J.; Figueiredo, M. In *Influence of cooking and bleaching conditions on the surface and paper properties of Eucalyptus globulus kraft pulps*, Proceedings of the 2nd Iberoamerican Congress on Pulp and Paper Research, CD-ROM, CIADICYP, Sa o Paulo, Brasil, **2002**.

72. Carvalho, M.; Ferreira, P.; Santos, J.; Amaral, J.; Figueiredo, M. In *Effect of extended cooking and oxigen prebleaching on the surface energy of Eucalyptus globulus Kraft pulp*, Journal of pulp and paper science, Pulp and Paper Technical Association of Canada: **2005**; pp 90-94.
73. Peterlin, S.; Planinšek, O.; Moutinho, I.; Ferreira, P.; Dolenc, D., Inverse gas chromatography analysis of spruce fibers with different lignin content. *Cellulose* **2010,** *17* (6), 1095-1102.
74. Gamelas, J. A., The surface properties of cellulose and lignocellulosic materials assessed by inverse gas chromatography: a review. *Cellulose* **2013,** *20* (6), 2675-2693.
75. Nussbaum, R., The critical time limit to avoid natural inactivation of spruce surfaces (Picea übles) intended for painting or gluing. *European Journal of Wood and Wood Products* **1996,** *54* (1), 26-26.
76. Gunnells, D. W.; Gardner, D. J.; Wolcott, M. P., Temperature dependence of wood surface energy. *Wood and Fiber Science* **2007,** *26* (4), 447-455.
77. Gulati, D.; Sain, M., Surface characteristics of untreated and modified hemp fibers. *Polymer Engineering & Science* **2006,** *46* (3), 269-273.
78. NACEUR BELGACEM, M., Characterisation of polysaccharides, lignin and other woody components by inverse gas chromatography: A review. *Cellulose chemistry and technology* **2000,** *34* (3-4), 357-383.
79. Lundqvist, A.; Odberg, L.; Berg, J. C., Surface characterization of non-chlorine-bleached pulp fibers and calcium carbonate coatings using inverse gas chromatography. *Tappi journal (USA)* **1995**.
80. Cordeiro, N.; Gouveia, C.; Moraes, A.; Amico, S., Natural fibers characterization by inverse gas chromatography. *Carbohydrate Polymers* **2011,** *84* (1), 110-117.
81. Cordeiro, N.; Ornelas, M.; Ashori, A.; Sheshmani, S.; Norouzi, H., Investigation on the surface properties of chemically modified natural fibers using inverse gas chromatography. *Carbohydrate Polymers* **2012,** *87* (4), 2367-2375.
82. Cordeiro, N.; Gouveia, C.; John, M. J., Investigation of surface properties of physico-chemically modified natural fibres using inverse gas chromatography. *Industrial Crops and Products* **2011,** *33* (1), 108-115.
83. Kamdem, D. P.; Bose, S. K.; Luner, P., Inverse gas chromatography characterization of birch wood meal. *Langmuir* **1993,** *9* (11), 3039-3044.
84. Shen, W.; Parker, I. H.; Sheng, Y. J., The effects of surface extractives and lignin on the surface energy of eucalypt kraft pulp fibres. *Journal of adhesion science and technology* **1998,** *12* (2), 161-174.
85. Wålinder, M. E.; Gardner, D. J., Surface energy of extracted and non-extracted Norway spruce wood particles studied by inverse gas chromatography (IGC). *Wood and fiber science* **2007,** *32* (4), 478-488.
86. Felix, J.; Gatenholm, P., Characterization of cellulose fibers using inverse gas chromatography. *Nordic Pulp and Paper Research Journal (Sweden)* **1993**.
87. Stenius, P.; Laine, J., Studies of cellulose surfaces by titration and ESCA. *Applied surface science* **1994,** *75* (1-4), 213-219.

88. Dorris, G. M.; Gray, D. G., The surface analysis of paper and wood fibers by Esca-electron spectroscopy for chemical analysis-I. Applications to cellulose and lignin. *Cellulose chemistry and technology* **1978,** *12*, 9-23.
89. Jacob, P. N.; Berg, J. C., Acid-base surface energy characterization of microcrystalline cellulose and two wood pulp fiber types using inverse gas chromatography. *Langmuir* **1994,** *10* (9), 3086-3093.
90. Lee, H.; Luner, P., Characterisation of AKD sized papers by inverse gas chromatography. *Nordic Pulp Paper Res J* **1989,** *4*, 164-172.
91. Gérardin, P.; Petrič, M.; Petrissans, M.; Lambert, J.; Ehrhrardt, J. J., Evolution of wood surface free energy after heat treatment. *Polymer degradation and stability* **2007,** *92* (4), 653-657.
92. Abdmeziem, K.; Passas, R.; Belgacem, M. N., Inverse gas chromatography as a tool to characterize the specific surface area of cellulose fibres. *Cellulose chemistry and technology* **2006,** *40* (3-4), 199-204.
93. Shen, W.; Parker, I. H., Surface composition and surface energetics of various eucalypt pulps. *Cellulose* **1999,** *6* (1), 41-55.
94. SHEN, W.; LI, M.; PARKER, I., Characterization of eucalypt fibre surface using inverse gas chromatography and X-ray photoelectron spectroscopy. *Appita journal* **1998,** *51* (2), 147-151.
95. Börås, L.; Sjöström, J.; Gatenholm, P., Characterization of surfaces of CTMP fibers using inverse gas chromatography combined with multivariate data analysis. *Nordic Pulp and Paper Research Journal (Sweden)* **1997**.
96. Kamdem, D.; Riedl, B., Characterization of wood fibers modified by phenol-formaldehyde. *Colloid and polymer science* **1991,** *269* (6), 595-603.
97. Dorris, G. M.; Gray, D. G., Adsorption of n-alkanes at zero surface coverage on cellulose paper and wood fibers. *Journal of Colloid and Interface Science* **1980,** *77* (2), 353-362.
98. Matuana, L. M.; Balatinecz, J. J.; Park, C. B.; Woodhams, R. T., Surface characteristics of chemically modified newsprint fibers determined by inverse gas chromatography. *Wood and fiber science* **2007,** *31* (2), 116-127.
99. Tze, W. T.; Wålinder, M. E.; Gardner, D. J., Inverse gas chromatography for studying interaction of materials used for cellulose fiber/polymer composites. *Journal of adhesion science and technology* **2006,** *20* (8), 743-759.
100. Ylä-Mäihäniemi, P. P.; Heng, J. Y.; Thielmann, F.; Williams, D. R., Inverse gas chromatographic method for measuring the dispersive surface energy distribution for particulates. *Langmuir* **2008,** *24* (17), 9551-9557.
101. Ho, R.; Heng, J. Y., A review of inverse gas chromatography and its development as a tool to characterize anisotropic surface properties of pharmaceutical solids. *KONA Powder and Particle Journal* **2013,** *30*, 164-180.
102. Mohammadi-Jam, S.; Waters, K., Inverse gas chromatography applications: A review. *Advances in colloid and interface science* **2014,** *212*, 21-44.
103. Schultz, J. a.; Lavielle, L.; Martin, C., The role of the interface in carbon fibre-epoxy composites. *The Journal of Adhesion* **1987,** *23* (1), 45-60.
104. Schultz, J.; Lavielle, L., Interfacial properties of carbon fiber—epoxy matrix composites. ACS Publications: **1989**.

105. Shi, B.; Wang, Y.; Jia, L., Comparison of Dorris–Gray and Schultz methods for the calculation of surface dispersive free energy by inverse gas chromatography. *Journal of Chromatography A* **2011,** *1218* (6), 860-862.
106. Gamble, J. F.; Leane, M.; Olusanmi, D.; Tobyn, M.; Šupuk, E.; Khoo, J.; Naderi, M., Surface energy analysis as a tool to probe the surface energy characteristics of micronized materials—A comparison with inverse gas chromatography. *International journal of pharmaceutics* **2012,** *422* (1-2), 238-244.
107. Kołodziejek, J.; Voelkel, A.; Heberger, K., Characterization of hybrid materials by means of inverse gas chromatography and chemometrics. *Journal of pharmaceutical sciences* **2013,** *102* (5), 1524-1531.
108. Fowkes, F. M., Attractive forces at interfaces. *Industrial & Engineering Chemistry* **1964,** *56* (12), 40-52.
109. Gamble, J. F.; Davé, R. N.; Kiang, S.; Leane, M. M.; Tobyn, M.; Wang, S. S., Investigating the applicability of inverse gas chromatography to binary powdered systems: An application of surface heterogeneity profiles to understanding preferential probe-surface interactions. *International journal of pharmaceutics* **2013,** *445* (1-2), 39-46.
110. Bandosz, T. J.; Jagiello, J.; Andersen, B.; Schwarz, J. A., Inverse gas chromatography study of modified smectite surfaces. *Clays and Clay Minerals* **1992,** *40* (3), 306-310.
111. Voelkel, A., Physicochemical measurements (inverse gas chromatography). *Gas chromatography. Elsevier, Amsterdam* **2012**, 477-494.
112. Thielmann, F., Introduction into the characterisation of porous materials by inverse gas chromatography. *Journal of chromatography A* **2004,** *1037* (1-2), 115-123.
113. Roffael, E.; Dix, B.; Schneider, T., Thermomechanical (TMP) and chemo-thermomechanical pulps (CTMP) for medium density fibreboards (MDF). *Holzforschung* **2001,** *55* (2), 214-218.
114. Josefsson, T.; Lennholm, H.; Gellerstedt, G., Changes in cellulose supramolecular structure and molecular weight distribution during steam explosion of aspen wood. *Cellulose* **2001,** *8* (4), 289-296.
115. Josefsson, T.; Lennholm, H.; Gellerstedt, G., Steam explosion of aspen wood. Characterisation of reaction products. *Holzforschung* **2002,** *56* (3), 289-297.
116. Li, J.; Henriksson, G.; Gellerstedt, G., Carbohydrate reactions during high-temperature steam treatment of aspen wood. *Applied biochemistry and biotechnology* **2005,** *125* (3), 175.
117. Iwanade, A.; Ohi, H.; Yamaguchi, A., Steam treatment of guiacyglycerol-β-guaiacyl ether on a holocellulose support. *Mokuzai Gakkaishi* **1995,** *41* (7), 683-688.
118. Avellar, B. K.; Glasser, W. G., Steam-assisted biomass fractionation. I. Process considerations and economic evaluation. *Biomass and Bioenergy* **1998,** *14* (3), 205-218.
119. Wang, P.; Fu, Y.; Shao, Z.; Zhang, F.; Qin, M., Structural changes to aspen wood lignin during autohydrolysis pretreatment. *BioResources* **2016,** *11* (2), 4086-4103.
120. Martin-Sampedro, R.; Capanema, E. A.; Hoeger, I.; Villar, J. C.; Rojas, O. J., Lignin changes after steam explosion and laccase-mediator treatment of eucalyptus wood chips. *Journal of agricultural and food chemistry* **2011,** *59* (16), 8761-8769.
121. jay Chung, M.; Wang, S. Y., Effects of peeling and steam-heating treatment on basic properties of two types of bamboo culms (Phyllostachys makinoi and Phyllostachys pubescens). *Journal of Wood Science* **2017,** *63* (5), 473-482.

122. Zhao, R.; Jiang, Z.; Hse, C.; Shupe, T., Effects of steam treatment on bending properties and chemical composition of moso bamboo (Phyllostachys pubescens). *Journal of Tropical Forest Science* **2010**, 197-201.
123. Shao, S.; Wen, G.; Jin, Z., Changes in chemical characteristics of bamboo (Phyllostachys pubescens) components during steam explosion. *Wood science and technology* **2008,** *42* (6), 439.
124. Li, J.; Henriksson, G.; Gellerstedt, G., Lignin depolymerization/repolymerization and its critical role for delignification of aspen wood by steam explosion. *Bioresource technology* **2007,** *98* (16), 3061-3068.
125. Chen, P. Y.; Workman, E. C., Effect of steaming on some physical and chemical properties of black walnut heartwood. *Wood and Fiber Science* **2007,** *11* (4), 218-227.
126. Lora, J.; Wayman, M., Delignification of hardwoods by autohydrolysis and extraction. *Tappi [Technical Association of the Pulp and Paper Industry]* **1978**.
127. Robert, D.; Gellerstedt, G.; Bardet, M., Carbon-13 NMR analysis of lignins obtained after sulfonation of steam exploded aspen wood [prehydrolysis, structural analysis]. *Nordic Pulp and Paper Research Journal (Sweden)* **1986**.
128. Sluiter, A.; Ruiz, R.; Scarlata, C.; Sluiter, J.; Templeton, D., Determination of extractives in biomass. *National Renewable Energy Laboratory, Laboratory Analytical Procedure (LAP), NREL/TP-510-42619* **2008**.
129. Santos, R. B.; Hart, P.; Jameel, H.; Chang, H.-m., Wood based lignin reactions important to the biorefinery and pulp and paper industries. *BioResources* **2013,** *8* (1), 1456-1477.
130. Patil, R. A., Cleavage of acetyl groups for acetic acid production in Kraft pulp mills. **2012**.
131. Adler, E.; Pepper, J.; Eriksoo, E., Action of mineral acid on lignin and model substances of guaiacylglycerol-β-aryl ether type. *Industrial & Engineering Chemistry* **1957,** *49* (9), 1391-1392.
132. Lundquist, K.; Lundgren, R., Acid Degradation of Lignin. Part VII. The cleavage of ether bonds. *Acta Chemica Scandinavica* **1972,** *26* (5), 2005-2023.
133. Lundquist, K., Acid degradation of lignin. Part VIII. Low molecular weight phenols from acidolysis of birch lignin. *Acta Chemica Scandinavica* **1973,** *27* (7), 2597-2606.
134. Ito, T.; Terashima, N.; Yasuda, S., Chemical structures of sulfuric acid lignin. III. Reaction of arylglycerol beta-aryl ether with five percent sulfuric acid. *Mokuzai Gakkai.= Journal of the Japan Wood Research Society* **1981**.
135. Yasuda, S.; Terashima, N., Chemical structures of sulfuric acid lignin. II. Chemical structures of condensation products from arylglycerol-bela-aryl ether type structures. *Mokuzai Gakkai.= Journal of the Japan Wood Research Society* **1981**.
136. Yasuda, S., Chemical structure of sulfuric acid lignin IV. Reaction of arylglycerol-β-aryl ether with seventy-two percent sulfuric acid. *Mokuzai Gakkaishi* **1981,** *27*, 879-884.
137. Yasuda, S.; Terashima, N., Chemical structures of sulfuric acid lignin. V. Reaction of three arylglycerol-beta-aryl ethers with seventy-two percent sulfuric acid. *Mokuzai Gakkai shi.= Journal of the Japan Wood Research Society* **1982**.
138. Hoo, L. H.; Sarkanen, K. V.; Anderson, C. D., Formation of C6 C2-Enol Ethers in the Acid-Catalyzed Hydrolysis of Erythro-Veratrylglycerol-β-(2-Methoxyphenyl) Ether. *Journal of Wood Chemistry and Technology* **1983,** *3* (2), 223-243.
139. Karlsson, O.; Lundquist, K.; Meuller, S.; Westlid, K., On the Acidolytic Cleavage of Arylglycerol β-Aryl Ethers. *ChemInform* **1988,** *19* (23).

140. Lundquist, K.; Ericsson, L., Acid degradation of lignin. III. Formation of formaldehyde. *Acta chemica scandinavica* **1970**.
141. Wan, G.; Frazier, C. E., Lignin acidolysis predicts formaldehyde generation in pine wood. *ACS Sustainable Chemistry & Engineering* **2017,** *5* (6), 4830-4836.
142. Wayman, M.; Lora, J., Aspen autohydrolysis: the effects of 2-naphthol and othe aromatic compounds. *Tappi Tech Assoc Pulp Paper Ind* **1978,** *61* (6), 55-57.
143. Chua, M. G.; Wayman, M., Characterization of autohydrolysis aspen (P. tremuloides) lignins. Part 1. Composition and molecular weight distribution of extracted autohydrolysis lignin. *Canadian Journal of Chemistry* **1979,** *57* (10), 1141-1149.
144. Robert, D.; Bardet, M.; Lapierre, C.; Gellerstedt, G., Structural changes in aspen lignin during steam explosion treatment. *Cellulose chemistry and technology* **1988**.
145. Robert, D.; Gellerstedt, G.; Bardet, M., Carbon-13 NMR analysis of lignins obtained after sulfonation of steam exploded aspen wood. *Nordic Pulp Pap. Res. J* **1986,** *1* (3), 18-25.
146. Li, S.; Lundquist, K.; Westermark, U., Cleavage of arylglycerol β-aryl ethers under neutral and acid conditions. *Nordic Pulp & Paper Research Journal* **2000,** *15* (4), 292-299.
147. Li, J.; Gellerstedt, G., Improved lignin properties and reactivity by modifications in the autohydrolysis process of aspen wood. *Industrial Crops and Products* **2008,** *27* (2), 175-181.
148. Marchessault, R.; Coulombe, S.; Morikawa, H.; Robert, D., Characterization of aspen exploded wood lignin. *Canadian Journal of Chemistry* **1982,** *60* (18), 2372-2382.
149. Sudo, K.; Shimizu, K.; Sakurai, K., Characterization of steamed wood lignin from beech wood. *Holzforschung-International Journal of the Biology, Chemistry, Physics and Technology of Wood* **1985,** *39* (5), 281-288.
150. Shimizu, K.; Sudo, K.; Ono, H.; Ishihara, M.; Fujii, T.; Hishiyama, S., Integrated process for total utilization of wood components by steam-explosion pretreatment. *Biomass and Bioenergy* **1998,** *14* (3), 195-203.
151. Hu, F.; Jung, S.; Ragauskas, A., Pseudo-lignin formation and its impact on enzymatic hydrolysis. *Bioresource technology* **2012,** *117*, 7-12.
152. Jakobsons, J.; Hortling, B.; Erins, P.; Sundquist, J., Characterization of alkali soluble fraction of steam exploded birch wood. *Holzforschung-International Journal of the Biology, Chemistry, Physics and Technology of Wood* **1995,** *49* (1), 51-59.
153. Robert, D.; Bardet, M.; Lapierre, C.; Gellerstedt, G., Structural changes in aspen lignin during steam explosion treatment. *Cellulose chemistry and technology* **1988,** *22* (2), 221-230.
154. Fras, L.; Laine, J.; Stenius, P.; Stana-Kleinschek, K.; Ribitsch, V.; Doleček, V., Determination of dissociable groups in natural and regenerated cellulose fibers by different titration methods. *Journal of Applied Polymer Science* **2004,** *92* (5), 3186-3195.
155. Tasooji, M.; Frazier, C. E., Simple milligram-scale extraction of formaldehyde from wood. *ACS Sustainable Chemistry & Engineering* **2016,** *4* (9), 5041-5045.
156. Chen, C.-L., Nitrobenzene and cupric oxide oxidations. In *Methods in lignin chemistry*, Springer: **1992**, pp 301-321.
157. Chan, F. D.; Nguyen, K. L.; Wallis, A. F., Contribution of lignin sub-structures to nitrobenzene oxidation products. *Journal of wood chemistry and technology* **1995,** *15* (3), 329-347.
158. Leopold, B., Aromatic keto-and hydroxy-polyethers as lignin models. III. *Acta Chem. Scand* **1950,** *4*, 1523-1537.

159. Sarkanen, K. V.; Ludwig, C. H., *Liguins. Occurrence, formation, structure, and reactions*. New York.; Wiley-Interscience: **1971**.
160. Heitner, C.; Dimmel, D.; Schmidt, J., *Lignin and lignans: advances in chemistry*. CRC press: **2016**.
161. Schultz, T. P.; Templeton, M. C., Proposed mechanism for the nitrobenzene oxidation of lignin. *Holzforschung-International Journal of the Biology, Chemistry, Physics and Technology of Wood* **1986,** *40* (2), 93-97.
162. Iiyama, K.; Lam, T. B. T., Lignin in wheat internodes. Part 1: The reactivities of lignin units during alkaline nitrobenzene oxidation. *Journal of the Science of Food and Agriculture* **1990,** *51* (4), 481-491.
163. Ohra-Aho, T.; Gomes, F.; Colodette, J.; Tamminen, T., S/G ratio and lignin structure among Eucalyptus hybrids determined by Py-GC/MS and nitrobenzene oxidation. *Journal of analytical and applied pyrolysis* **2013,** *101*, 166-171.
164. Katahira, R.; Nakatsubo, F., Determination of nitrobenzene oxidation products by GC and 1 H-NMR spectroscopy using 5-iodovanillin as a new internal standard. *Journal of wood science* **2001,** *47* (5), 378-382.
165. Zheng, M.; Gu, S.; Chen, J.; Luo, Y.; Li, W.; Ni, J.; Li, Y.; Wang, Z., Development and validation of a sensitive UPLC–MS/MS instrumentation and alkaline nitrobenzene oxidation method for the determination of lignin monomers in wheat straw. *Journal of Chromatography B* **2017,** *1055*, 178-184.
166. Stokke, D. D.; Wu, Q.; Han, G., Consolidation Behavior of Lignocellulosic Materials. *Introduction to Wood and Natural Fiber Composites* **2013**, 85-127.
167. Wang, S.; Winistorfer, P. M., Consolidation of flakeboard mats under theoretical laboratory pressing and simulated industrial pressing. *Wood and Fiber Science* **2000,** *32* (4), 527-538.
168. Wang, S.; Winistorfer, P. M.; Young, T. M., Fundamentals of vertical density profile formation in wood composites. Part III. MDF density formation during hot-pressing. *Wood and fiber science* **2007,** *36* (1), 17-25.
169. Ebrahimzadeh, P.; Bertilsson, H., Effect of impregnation on mechanosorption in wood and paper studied by dynamic mechanical analysis. *Wood science and technology* **1998,** *32* (2), 101-118.
170. Ebrahimzadeh, P.; Kubát, J.; McQueen, D., Dynamic mechanical characterization of mechanosorptive effects in wood and paper. *European Journal of Wood and Wood Products* **1996,** *54* (4), 263-271.
171. Lindström, S. B.; Karabulut, E.; Kulachenko, A.; Sehaqui, H.; Wågberg, L., Mechanosorptive creep in nanocellulose materials. *Cellulose* **2012,** *19* (3), 809-819.
172. Hoglund, H.; Sohlin, U.; Tistad, G., Physical properties of wood in relation to chip refining. *Tappi* **1976**.
173. Norimoto, M.; Yamada, T., *Dynamic Torsional Visco-elasticity of Wood*. Canada, Department of Forestry and Rural Development: **1967**.
174. Becker, H.; Noack, D., Studies on dynamic torsional viscoelasticity of wood. *Wood Science and Technology* **1968,** *2* (3), 213-230.
175. Sadoh, T., Viscoelastic properties of wood in swelling systems. *Wood Science and Technology* **1981,** *15* (1), 57-66.

176. Salmen, L., Viscoelastic properties ofin situ lignin under water-saturated conditions. *Journal of Materials Science* **1984,** *19* (9), 3090-3096.
177. Kelley, S. S.; Rials, T. G.; Glasser, W. G., Relaxation behaviour of the amorphous components of wood. *Journal of materials science* **1987,** *22* (2), 617-624.
178. Olsson, A.; Salmén, L., Viscoelasticity of in situ lignin as affected by structure: softwood vs. hardwood. ACS Publications: **1992**.
179. Kojiro, K.; Furuta, Y.; Ishimaru, Y., Influence of histories on dynamic viscoelastic properties and dimensions of water-swollen wood. *Journal of wood science* **2008,** *54* (2), 95-99.
180. Das, S.; Frazier, C. In *Dynamic mechanical analysis of wood-polymeric isocyanate adhesive interactions*, ABSTRACTS OF PAPERS OF THE AMERICAN CHEMICAL SOCIETY, AMER CHEMICAL SOC 1155 16TH ST, NW, WASHINGTON, DC 20036 USA: **2004**; pp U243-U243.
181. Sun, N.; Das, S.; Frazier, C. E., Dynamic mechanical analysis of dry wood: linear viscoelastic response region and effects of minor moisture changes. *Holzforschung* **2007,** *61* (1), 28-33.
182. Chowdhury, S.; Fabiyi, J.; Frazier, C. E., Advancing the dynamic mechanical analysis of biomass: comparison of tensile-torsion and compressive-torsion wood DMA. *Holzforschung* **2010,** *64* (6), 747-756.
183. Back, E.; Salmen, N., Glass transitions of wood components hold implications for molding and pulping processes [Wood and paper materials]. *TAPPI; journal of the Technical Association of the Pulp and Paper Industry* **1982**.
184. Chowdhury, S.; Frazier, C. E., Thermorheological complexity and fragility in plasticized lignocellulose. *Biomacromolecules* **2013,** *14* (4), 1166-1173.
185. Chowdhury, S.; Frazier, C. E., Compressive-torsion DMA of yellow-poplar wood in organic media. *Holzforschung* **2013,** *67* (2), 161-168.
186. Pizzi, A.; Mittal, K., Urea-formaldehyde adhesives. *Handbook of adhesive technology* **2003,** *2*.
187. Pizzi, A.; Panamgama, L., Diffusion hindrance vs. wood-induced catalytic activation of MUF adhesive polycondensation. *Journal of applied polymer science* **1995,** *58* (1), 109-115.
188. Xing, C.; Zhang, S.; Deng, J., Effect of wood acidity and catalyst on UF resin gel time. *Holzforschung* **2004,** *58* (4), 408-412.
189. Johns, W. E.; Niazi, K. A., Effect of pH and buffering capacity of wood on the gelation time of urea-formaldehyde resin. *Wood and fiber science* **2007,** *12* (4), 255-263.
190. Xing, C.; Deng, J.; Zhang, S.; Riedl, B.; Cloutier, A., Differential scanning calorimetry characterization of urea–formaldehyde resin curing behavior as affected by less desirable wood material and catalyst content. *Journal of Applied Polymer Science* **2005,** *98* (5), 2027-2032.
191. Gao, Z.; Wang, X. M.; Wan, H.; Liu, Y., Curing characteristics of urea–formaldehyde resin in the presence of various amounts of wood extracts and catalysts. *Journal of Applied Polymer Science* **2008,** *107* (3), 1555-1562.
192. Lee, Y.-K.; Kim, H.-J., Relationship between curing activation energy and free formaldehyde content in urea-formaldehyde resins. *Journal of Adhesion Science and Technology* **2013,** *27* (5-6), 598-609.
193. Chow, S., A kinetic study of the polymerization of phenol-formaldehyde resin in the presence of cellulosic materials. *Wood Sci* **1969,** *1* (4), 215-221.

194. Chow, S.; Mukai, H., Effect of thermal degradation of cellulose on wood-polymer bonding. *Wood Sci* **1972,** *4* (4), 202-208.
195. Mizumachi, H., Activation energy of the curing reaction of phenolic resin in the presence of woods. *Wood Sci* **1975,** *7*, 256-260.
196. Pizzi, A.; Mtsweni, B.; Parsons, W., Wood-induced catalytic activation of PF adhesives autopolymerization vs. PF/wood covalent bonding. *Journal of applied polymer science* **1994,** *52* (13), 1847-1856.
197. Lee, S.; Wu, Q.; Strickland, B., The influence of flake chemical properties and zinc borate on gel time of phenolic resin for oriented strandboard. *Wood and fiber science* **2007,** *33* (3), 425-436.
198. He, G.; Riedl, B., Curing kinetics of phenol formaldehyde resin and wood-resin interactions in the presence of wood substrates. *Wood Science and Technology* **2004,** *38* (1), 69-81.
199. Singh, A. P.; Causin, V.; Nuryawan, A.; Park, B.-D., Morphological, chemical and crystalline features of urea–formaldehyde resin cured in contact with wood. *European Polymer Journal* **2014,** *56*, 185-193.
200. Park, B.-D.; Jeong, H.-W., Hydrolytic stability and crystallinity of cured urea–formaldehyde resin adhesives with different formaldehyde/urea mole ratios. *International Journal of Adhesion and Adhesives* **2011,** *31* (6), 524-529.
201. Park, B.-D.; Causin, V., Crystallinity and domain size of cured urea–formaldehyde resin adhesives with different formaldehyde/urea mole ratios. *European Polymer Journal* **2013,** *49* (2), 532-537.
202. Stuligross, J.; Koutsky, J. A., A morphological study of urea-formaldehyde resins. *The Journal of Adhesion* **1985,** *18* (4), 281-299.
203. Park, B. D.; Jeong, H. W.; Lee, S. M., Morphology and chemical elements detection of cured urea–formaldehyde resins. *Journal of applied polymer science* **2011,** *120* (3), 1475-1482.
204. Dunker, A. K.; John, W. E.; Rammon, R.; Farmer, B.; Johns, S. J., Slightly bizarre protein chemistry: urea-formaldehyde resin from a biochemical perspective. *The Journal of Adhesion* **1986,** *19* (2), 153-176.
205. Levendis, D.; Pizzi, A.; Ferg, E., The correlation of strength and formaldehyde emission with the crystalline/amorphous structure of UF resins. *Holzforschung-International Journal of the Biology, Chemistry, Physics and Technology of Wood* **1992,** *46* (3), 263-269.
206. Ferg, E.; Pizzi, A.; Levendis, D., 13C NMR analysis method for urea–formaldehyde resin strength and formaldehyde emission. *Journal of Applied Polymer Science* **1993,** *50* (5), 907-915.

Chapter 2 Physical, surface, and rheological characterization of thermomechanical wood fiber

Mohammad Tasooji and Charles E. Frazier *

Sustainable Biomaterials, Virginia Tech, Cheatham Hall, RM 230 West Campus Drive, Blacksburg, Virginia 24061, United States

Macromolecules Innovation Institute, Virginia Tech, ICTAS II, 240 West Campus Drive, Blacksburg, Virginia 24061, United States

2.1. Abstract

Resin and additive-free Douglas fir thermomechanical fiber was refined at two energies (188 and 349 kW•h/ton) by a North American fiberboard mill; specimens were studied for aspects of fiber quality. The highest refining energy produced relative reductions in fiber width and length, and an increase in bulk density. Thermoporosimetry revealed increases in sub-micron scale porosity, greatest at the highest refining energy. Mercury intrusion porosimetry (MIP) revealed porosity changes on a higher dimensional scale, associated with fiber lumens, inter-fiber voids, and fiber damage. Brunauer-Emmett-Teller gas adsorption and MIP demonstrated that refining increased the specific surface area, the greatest effect occurring at the highest refining energy. Inverse gas chromatography showed that the lowest refining energy produced surfaces dominated by lignin and/or extractives. The highest refining energy produced more fiber damage and this seemed to uncover higher energy active sites. A novel rheological analysis (nonlinear compression simultaneous with linear torsional oscillation) was devised to study fiber compaction and densification. The method did not clearly distinguish the fiber types studied, but aspects of mechano-sorption and fiber densification were observed, and it is suggested that this method merits further development for new insights into wood fiber rheology. These observations were generally consistent with the industry standard of visual and tactile evaluation of fiber quality. The effects observed are expected to cause bulk chemical changes, and changes in fiber/resin interaction that are described elsewhere.

KEYWORDS: Thermomechanical wood fiber, Medium density fiberboard, Refining energy, Fiber quality, Wood fiber characterization,

2.2. Introduction

Among the variety of wood-based composites, medium density fiberboard (MDF) is special because it is made from wood that is processed into individual cells (fibers). At roughly 3000 x 30 microns, length-to-diameter, these fibers are reconsolidated with thermosetting adhesives such that inter and intra-fiber compaction produces very smooth, machine-moldable surfaces that make MDF ideal for furniture production and interior decoration[1-2]. MDF is typically manufactured with wood residues such as chips, shavings, and sawdust. While processes vary, a common MDF production sequence involves: 1) steam treatment (digestion) and wood softening above the glass transition, 2) refining, or rotary shearing between circular plates under steam pressure, 3) blending with resin, wax, and other additives, 4) drying, and 5) mat formation and hot-pressing. Since the objective is to process wood into isolated fibers, refining causes cleavage in and around the middle lamella[3]. However transverse fractures also occur thereby shortening the fibers, and producing sub-fiber fragments. Fiber separation is imperfect, and refining conditions will affect the occurrence of fiber bundles, which are collections of two or more wood cells that fail to separate. Normally, greater quantities of fiber bundles (shives) are associated with lower fiber quality[4].

MDF fiber quality is most commonly evaluated by visual and tactile inspection[4], suggesting that average fiber length, the occurrence of fiber bundles, fiber morphology, and bulk density are implicit indicators of fiber quality. Besides tree species[2, 5-7], several production variables will affect fiber quality; these include digester and refining pressure[6, 8-16], digester retention time[13, 16-17], refining temperature[17], rotational speed of the refiner plates, and the gap between refiner plates[18], which changes as the plates wear. The most important production variable is perhaps the refining energy (kW•h/ton of fiber)[19], which is controlled by the refiner-plate gap while other variables remain fixed.

Considering the complex structure and chemical reactivity of wood, it seems unlikely that all aspects of fiber quality could be reflected in visual and tactile inspections. Consequently, this effort is an industry/university cooperation intended to seek other aspects of fiber quality that might affect product performance or process efficiency. The context for this study was an industrial MDF production facility processing Douglas fir (*Pseudotsuga*

menziesii); and the principal experimental variable was refining energy via changes in gap settings. Using a variety of species not including Douglas fir, Short and Lyon found that refiner-plate gap settings had no impact on fiber pH, alkaline buffering capacity, and ash content; only the fiber size and bulk fiber density were affected[18]. This is in contrast to our observations, presented here and elsewhere, and the discrepancy speaks to a practical challenge in MDF research: it is very difficult to relate pilot-scale refining (as for Short and Lyon[18]) to industrial practice, and critical aspects of processing vary substantially among industrial producers. In other words, wood fiber-based composites like MDF are the most technologically and scientifically complex wood-based composites. Our expectation is that refining energy will affect multiple aspects of fiber chemistry and other fiber properties, and that these effects could be expected to alter the fiber/resin interaction. Specifically however, this publication focuses on how fiber dimensions, porosity, surface area, surface energy, and aspects of fiber rheology are affected by changes in refining energy.

2.3. Experimental

Materials

Douglas fir (*Pseudotsuga menziesii)* refined and unrefined samples were collected at Arauco's MDF production facility in Eugene, Oregon, U.S.A. Normal production at this facility uses Douglas fir particles (30% shavings, 70% sawdust) softened in a steam digester (0.77 MPa, 174°C, 3.5 min retention time). Steam digested material is sprayed with additives (urea and wax), then fed into a Sprout-Bauer SB150 thermomechanical refiner (0.77 MPa, 174°C, 1800 revolutions per min; disk configuration: spiral, 152 cm diameter). After passing through the plant drying system, the fibers are resinated, formed and hot-pressed. For this research, additive inlet valves were closed and fiber was processed so as to clear additives from the system. Once clear of additives, and after the drying stage, fiber sampling occurred in an emergency fiber-dump section (a fire safety feature of the plant). Collected specimens had a moisture content of 5-6% (wet basis), and were identified as DF188 and DF349 corresponding to the refining energies used: 188 and 349 kW•h/ton. These refining energies (adjusted by changing the refiner-plate gap) are the practical range for production at this facility; the low

and high refining energies produce “low” and “high” quality fiber as needed for commercial production. Unrefined control specimens (identified as DF; moisture content ~25%) were sampled from the production feedstock. All samples were collected in one day and sample preparation (below) started on the following day. Besides two different refining energies, all other production parameters were fixed. Fiber specimens were free of adhesive and additives.

Sample preparation

The unrefined sample (DF) was vacuum dried (0.10 mmHg, 25°C, overnight), ground by a Wiley mill, screened (18-80 mesh) and vacuum dried (0.10 mmHg, 25°C, overnight). Refined samples (DF188, DF349) were not milled, but similarly screened and dried as described. All samples were then sealed/stored at room temperature.

Solvent-exchange drying: previously screened and vacuum dried samples (~3 g) were sequentially stirred (25°C, 1h) in the following solvents (300 mL): distilled water, acetone:water (25:75, 50:50, 75:25, 100:0 vol:vol), and hexane. Solvents were exchanged by filtration, and washing occurred using 100 mL of the next solvent (disposed) before immersion in the next solvent, then the sample was vacuum dried (0.10 mmHg, 25°C, overnight).

Fiber size distribution

An IMAL FiberCam 100 was used to measure fiber width/length distributions. Fibers were separated manually and dropped inside the vibrating FiberCam conveyance system, where after the system high-speed camera then collected images that were processed into fiber length and width measurements using image analysis software. Tangled or overlapping fibers were excluded by the software and a minimum of 250,000 fibers were analyzed for each sample repetition. Note that the fiber width results were downwardly and uniformly adjusted by a factor of 10; this made the results consistent with microscope images (not shown here) that demonstrated that most fibers had been reduced to individual tracheid cells.

Brunauer-Emmett-Teller (BET) gas adsorption

A Quantachrome Autosorb-1 was used to measure specimen specific surface area. Sample (0.2-0.5 g) was loaded into a 9 mm large bulb cell. The loaded cell was degassed (25^{o}C, 24h) until the vacuum was less than 50 µmHg. Eleven point BET analysis was conducted at 77 K. Freeze dried specimens were analyzed with Kr gas (equilibration time: 4 min; tolerance: 0).

Solvent-exchange dried specimens were analyzed with N_2 gas (equilibration time: 3 min; tolerance: 0). Measurement were conducted at 0.05-0.3 relative pressure (P/P_0). Specific surface area values were calculated from gas adsorption isotherms using the BET model[20-23].

Mercury intrusion porosimetry

Mercury intrusion porosimetry (MIP) analysis was conducted by Quantachrome using a Quantachrome Poremaster-60. Solvent-exchanged dried sample (0.05-0.1 g) was placed in a suitable penetrometer and degassed (25°C, 16h) until the pressure was less than 20 µmHg and then filled with mercury to completely surround the sample. Pressure (0.001-400 MPa) was incrementally applied and the volume of mercury intruded to the sample pores was measured. The Washburn equation was used for calculating pore size distribution[24]. Surface area was calculated from the area above the cumulative intrusion volume vs pressure graph[25]. Bulk density was measured from the difference in mercury volume of empty and sample-containing penetrometers. For all samples, the maximum mercury pressure was 0.7 MPa, since the cumulative intrusion volume vs pressure graph reached a plateau after 0.7 MPa.

Inverse gas chromatography

Inverse gas chromatography (IGC) analysis was conducted by Surface Measurements Systems. IGC measurements were carried out on a Surface Measurements Systems IGC-SEA equipped with a flame ionization detector. Freeze dried sample (350-400 mg) was packed into a silanized glass column (3 mm ID, 300 mm long, silanized glass wool packed into each end) using the Surface Measurements Systems sample-packing device. The packed column was conditioned (30°C, 2 h, 0% RH) and analysis conducted at 30°C with He carrier gas (10 ml/min) and methane used for column dead volume correction. For measuring dispersive surface energy, non-polar probes (decane, nonane, octane, heptane) were used and polar probes (dichloromethane, ethyl acetate) were used to measure acid-base surface energy. Surface acidity and basicity parameters (Ka and Kb) were calculated using polar probes (dichloromethane, acetone, acetonitrile, ethyl acetate). All probes were HPLC grade (99% purity, Sigma-Aldrich). Surface coverage range for all probes was set at 1-15% (0.01-0.15 n/nm). BET specific surface area (above) was used for the surface coverage calculation. The Dorris-

Gray[26-27] and polarization[27-28] methods were used for calculating dispersive and acid-base surface energies respectively. The Gutmann[27, 29-30] concept was used for Ka and Kb calculations.

Thermoporosimetry

A TA Instruments Discovery differential scanning calorimeter (DSC) was used for thermoporosimetry; temperature and enthalpy measurements were calibrated with high purity water and mercury. Vacuum dried sample (0.3 g) was saturated in distilled water using a vacuum/pressure treatment (mix water and fiber; apply 70mBar vacuum for 45 min; open to atmospheric pressure) then sealed/stored (25°C, 24 h). Sample was centrifuged (10min, 5000 RPM) and decanted. Fully saturated sample (0.07 g) was placed in an aluminum thermogravimetric analysis pan, loaded into the TGA (Q500 TGA, TA instruments) and dried (20°C/min to 90°C, then hold at 90°C). Drying was interrupted to produce samples with moisture content ratio of 2.47±0.64 g H_2O/g dry sample. Then the sample (~2.5 mg) was sealed into a DSC aluminum hermetic pan and analyzed. An isothermal step scan program was applied and the data developed as described by others[31]. After analysis was complete, the specimen holder was punctured, and heated (20°C/min to 110°C, then hold) on the TGA to obtain the dry sample mass.

Fiber mat rheology: compaction and densification

TA Instruments AR2000 was used for rheological analysis. Vacuum dried sample (0.05 g) was dispersed in distilled water (15 mL), then formed into a fiber mat (~5 mm thickness, 8 mm dia.) by filtration into a mold. The fiber mat was placed in an aluminum thermogravimetric analysis pan, loaded into the TGA (Q500 TGA, TA instruments) and dried (20°C/min to 90°C, then hold at 90°C); drying was interrupted to produce mats with different wet basis moisture contents (10%, and 75%). The fiber mat was placed between 8 mm diameter parallel-plates and subjected to 1) a compaction analysis at room temperature, where the specimen was simply compacted without application of oscillation stress, and then 2) a densification analysis while heating, where an oscillation stress was applied. Compaction analysis: gap set (5000 μm); equilibrate (25°C, 1min); gap closed to 1500 μm (58.3 μm/s); monitor normal force during gap closing. Densification analysis: equilibrate (40N normal force, 25°C, 2 min), temperature ramp

(40N normal force, 25-200°C, 3°C/min, 30000 Pa, 1 Hz). The oscillation stress applied during the densification study was conducted within the linear viscoelastic response, as determined using stress sweep experiments at 25°C and 200°C. Compaction and densification analyses were always conducted sequentially on the same specimen.

2.4. Results and discussion

As expected, increasing refining energy shifted fiber size distributions to lower average dimensions, and with greater effect on width than length, Figure 2-1. The reduced fiber dimensions were consistent with similar measurements described in the literature[4, 18], and with the increased bulk density measured here (Table 2-1). While not directly comparable to this work, others have reported mixed findings regarding the impact of refining pressure on fiber dimensions[8-9, 14].

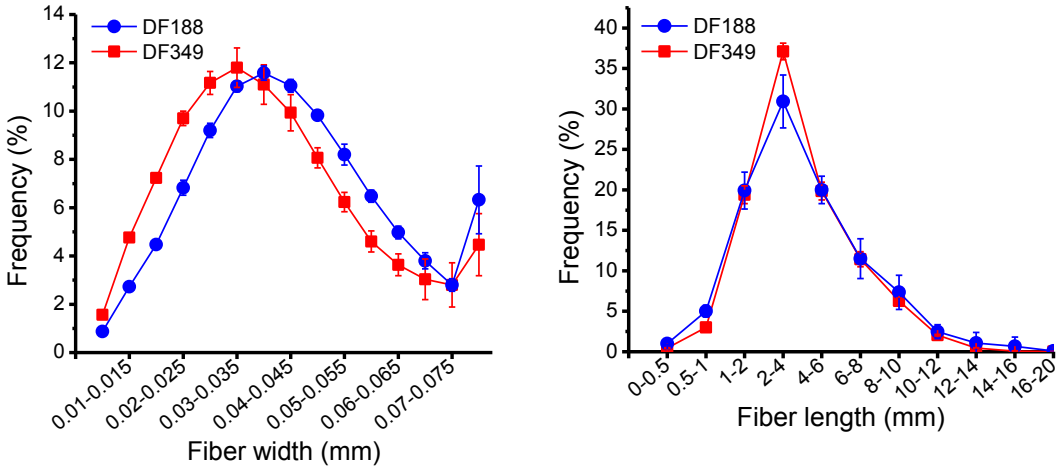

Figure 2-1. Fiber size distributions of refined fibers (DF188 and DF349) Left: fiber width distribution; right: fiber length distribution. Error bars represent ± 1 standard deviation, n=5.

Since increased refining energy reduced average fiber dimensions, it is reasonable to expect a corresponding effect on fiber porosity. Figure 2-2 confirms this where it is seen that the cumulative freezing bound water was increased by refining, and more so at the highest refining energy. Thermoporosimetry detects freezing bound water on the sub-micron scale within the fiber cell wall and within other features such as the fiber pits and the tips of fiber lumens (Appendix A) [32-33]. Consequently, an increase in the freezing bound water correlates

with increased porosity on the sub-micron scale. A similar conclusion was found using mercury intrusion porosimetry (MIP), Figure 2-3. MIP detects a broader pore size range, which includes intra-fiber and inter-fiber voids, respectively below and above about 30 µm. For instance, the unrefined specimens exhibited a roughly bimodal pore size distribution, with major pore sizes centered near about 25 and 250 µm. Respectively, these two ranges are believed to correlate to fiber lumens, and inter-fiber voids. After refining, the pore size distributions were more unimodal in nature, but with shoulders that revealed more cumulative pore volume below 20 µm. For the refined specimens, we interpret pore sizes at about 20 µm and lower to indicate fiber lumens, and smaller openings into the lumens as from fractures near the fiber tips and pit apertures via the ink-bottle effect [34-36]. Furthermore, refining appeared to have reduced the inter-fiber pore sizes to about 100 and 40 µm for DF188 and DF349 respectively. This is consistent with the reduced average fiber sizes, and increased bulk density mentioned above; and it suggests that fiber compaction would be greater in MDF panels prepared at the higher refining energy (contradictory to results described below). Finally, the change from a roughly bimodal to mostly unimodal pore size distribution probably reflects the nature of fracture during refining (at or near the middle lamella) whereas the unrefined specimens were reduced solely through milling where fractures parallel and perpendicular to the fiber axis are expected to occur with similar frequency [3].

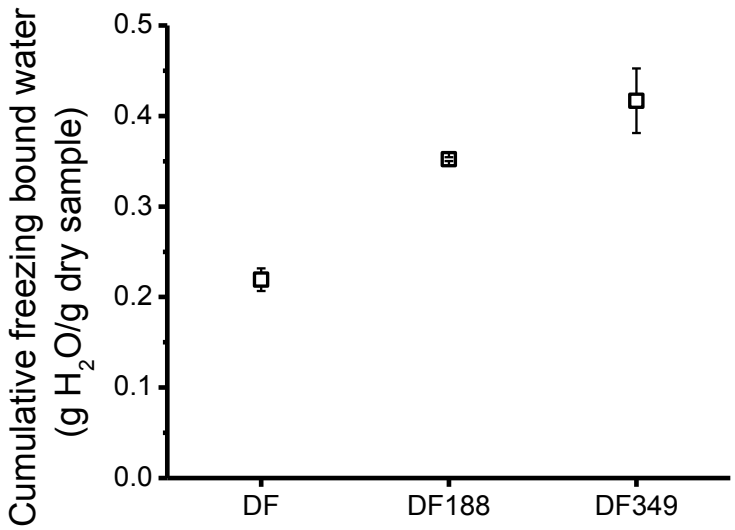

Figure 2-2. Cumulative freezing bound water by thermoporosimetry for refined (DF188 and DF349) and unrefined (DF) samples. Error bars represent ± 1 standard deviation, n=3.

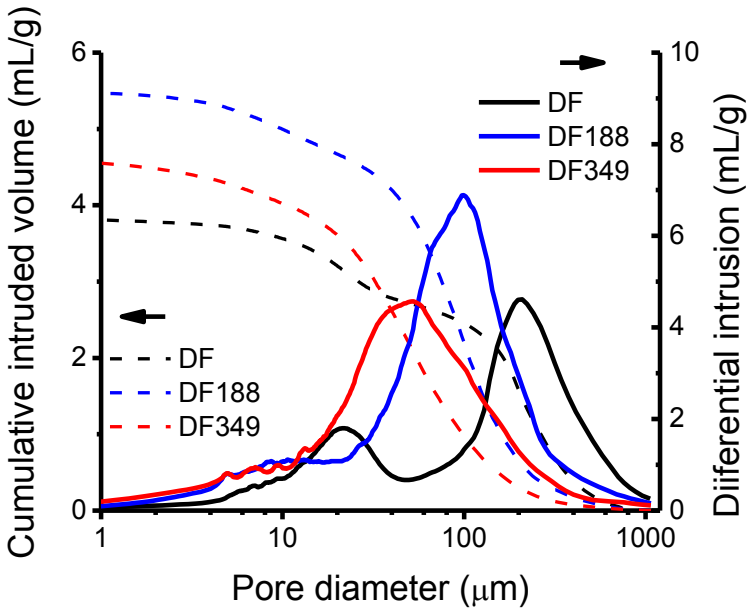

Figure 2-3. Example cumulative intruded volume and pore size distribution for refined (DF188 and DF349) and unrefined (DF) samples obtained with MIP; one measurement of two is shown.

Consistent with reductions in average fiber size, and with increases in fiber porosity discussed above, refining also increased the specific surface area, and again more so at the highest refining energy, Table 2-1. The fibrillation and fines production (fiber damage) resulting

from refining are known to increase specific surface area, and the effect is known to increase with increasing refining energy and time [37-40]. Table 2-1 indicates that gas adsorption detected more surface area than mercury intrusion, and that gas adsorption was also much more sensitive to increasing refining energy. The effects of fiber drying method are also seen in Table 2-1, where surface tension effects in solvent-exchange drying prevented void collapse, as others have shown [41-43].

Table 2-1. Specific surface area values of freeze dried and solvent exchange dried samples measured using BET gas adsorption and MIP; bulk density values measured using MIP. Standard deviation in parentheses; n=3 for BET, and 2 for MIP.

	BET gas adsorption		**MIP**	
Specimen	Specific surface area (m^2/g)		Specific surface area (m^2/g)	Bulk density (g/cm^3)
	Freeze dried	Solvent exchange	Solvent exchange	
DF	0.48 (0.02)	3.90 (0.48)	0.39 (0.00)	0.21 (0.00)
DF188	0.81 (0.04)	34.62 (2.19)	0.65 (0.03)	0.14 (0.02)
DF349	1.02 (0.09)	69.82 (5.55)	0.75 (0.03)	0.19 (0.00)

The changes in fiber dimension, porosity, and specific surface area so far mentioned suggest that refining should also impact fiber chemistry. While bulk chemical effects are reported elsewhere, Figure 2-4 demonstrates that refining caused surface chemical changes, as measured using inverse gas chromatography (IGC). Because IGC involves the introduction of different volumes of probe, the resulting sorption/desorption data provides surface energies as a function of surface coverage. Data in the low surface coverage range preferentially reflects the highest surface activity[27] and this is why the energies are generally higher in this range. Relative to the unrefined sample, Figure 2-4 shows that the lowest refining energy caused a significant reduction in dispersive energy across the entire range of surface coverage. This might be due to the effect of extractives[44-47], which are expected to undergo broad dispersal

during the steam pressure refining. For instance it was reported that extractives removal from wood/pulp resulted in a higher dispersive surface energy[48-53]. In this study recall that the unrefined sample was processed by milling and this is expected to cause more fractures perpendicular to the fiber axis. In contrast the refined samples are believed to experience preferential cleavage at the middle lamella (parallel to the fiber axis). Cleavage perpendicular to the fiber axis might expose more lignin-free surfaces, perhaps suggesting that the unrefined sample will exhibit an artificially high surface energy. However there are mixed findings on the relative dispersive surface energies of lignin and cellulose [54]. Some have shown that *in-situ* lignin has a lower dispersive surface energy than cellulose [55-56], which could be consistent with the reduction in surface energy found here. If that is true, then there is perhaps a limit to this effect because the highest refining energy caused an apparent reversal; the highest refining energy resulted in a dispersive surface energy that was more similar to the unrefined sample. However the IGC measurement of DF349 was highly variable and all of the IGC data is only based upon two measurements per sample type. Nevertheless, if it is assumed that *in situ* lignin has a lower surface energy than cellulose, it is reasonable to expect that higher refining energies will cause more fibrillation and damage, thereby increasing the number of active sites and increasing dispersive surface energy [57] because of greater cellulose exposure [44, 48, 58]. In fact others have shown that energy inputs such as fiber beating and refining. increase dispersive surface energy [59-62]. Regarding the acid-base surface energy and besides the lowest surface coverage, no difference was observed between the two refined samples; and generally they were lower than for the unrefined sample, Figure 2-4.

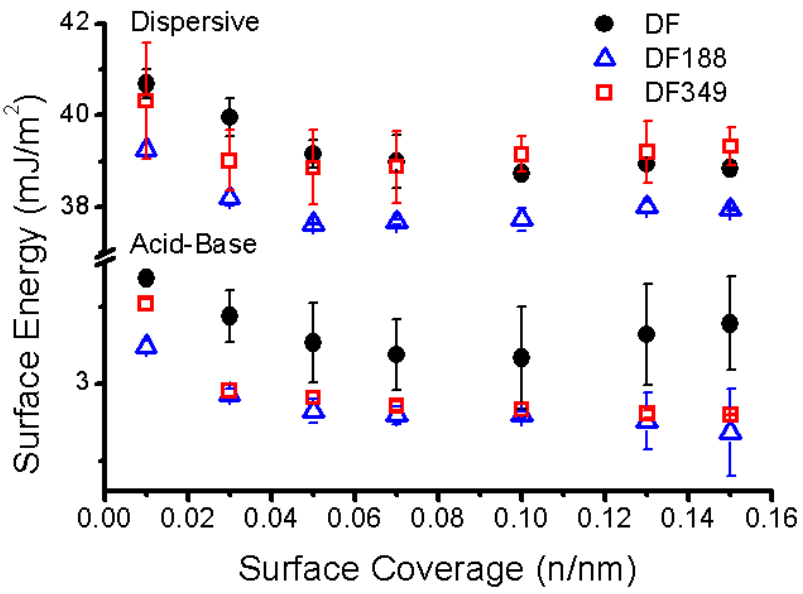

Figure 2-4 .Dispersive and acid-base surface energies for refined (DF188 and DF349) and unrefined (DF) samples as a function of surface coverage. Error bars represent ± 1 standard deviation, n=2.

The relative acidity and basicity are reflected in the acid/base ratio (K_a/K_b), and as typical for lignocellulose [63-65] all specimens exhibited a principally basic nature, Figure 2-5. At low surface coverage, refining reduced this ratio (the surface became more basic), but the effects of refining energy levels were not clearly distinguishable. At higher surface coverage the data variation prevented any reliable interpretation. As mentioned, refining can promote the effects of extractives and lignin, while the unrefined but milled samples might present more cellulose. It has been reported that lignin and extractives exhibit more Lewis basicity than cellulose[48, 52, 66-71]. Furthermore, hemicellulose might also decrease surface acidity[72]. Summarizing the surface analysis, interpretations were limited since only duplicate (n=2) analysis was obtained, but it seems that the lowest refining energy produced surfaces dominated by the effects of lignin and extractives. The highest refining energy produced substantially more fiber damage and this perhaps resulted in more cellulose exposure. This interpretation is perhaps consistent with our bulk chemical analysis that will be reported elsewhere; relative to the unrefined samples, those analyses showed that DF188 and DF349 respectively showed 20% and 43% reduction

(degradation) in neutral sugars, and substantial β-aryl ether cleavage in lignin (according to nitrobenzene oxidation).

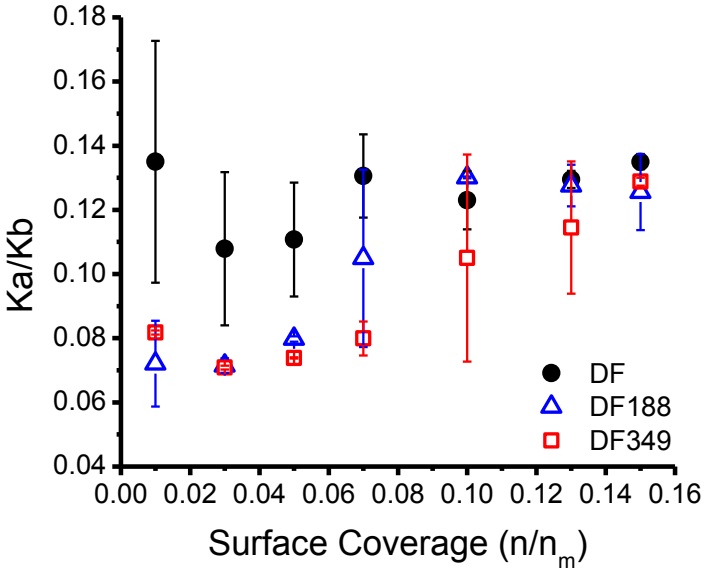

Figure 2-5. Surface acidity (Ka) and basicity (Kb) components of Gutmann concept for refined (DF188 and DF349) and unrefined (DF) samples as a function of surface coverage. Error bars represent ± 1 standard deviation, n=2.

In conventional production, MDF panels develop a characteristic density profile through the thickness (vertical density profile); high density regions are produced near the panel surfaces with a lower density material forming at the core[73-76]. Strongly coupled to panel performance and created during hot-pressing, this vertical density profile arises from viscoelastic phenomena[73-74] and probably also mechano-sorption effects (strains amplified by stresses acting during a change in moisture content)[77-79]. It was of interest to determine whether aspects of fiber compaction and densification (related to the vertical density profile) could be detected using a simple rotational rheometer. Consequently we applied a two-stage sequential analysis: Stage-1, compaction, at room temperature where parallel-plates compress specimens under a linear displacement to a maximum stress of ~ 1 MPa and; Stage-2, densification, where the compressive normal force was reduced to 40 N (0.8 MPa) and a 1 Hz torsional oscillation was applied while heating to 200°C. At high moisture levels (far exceeding typical production conditions) all three sample types exhibited a similar degree of compaction

over the 60 second acquisition period, Figure 2-6. Whereas at 10% moisture (industrially relevant) the unrefined sample compacted substantially more than the refined samples. Furthermore DF188 perhaps compacted slightly more than DF349, noting that the error bars are smaller than the symbols in this figure. If DF188 did compact more than DF349, this would seem contradictory to the measured bulk densities where the latter was about 36% more dense than the former, Table 2-1. Perhaps fiber curling and kinking (caused by refining) affects compaction without detectable effects in mercury intrusion measurements. This suggests that that the bulk density results are a function of the measurement technique because it seems that the compaction and bulk density results are in contradiction.

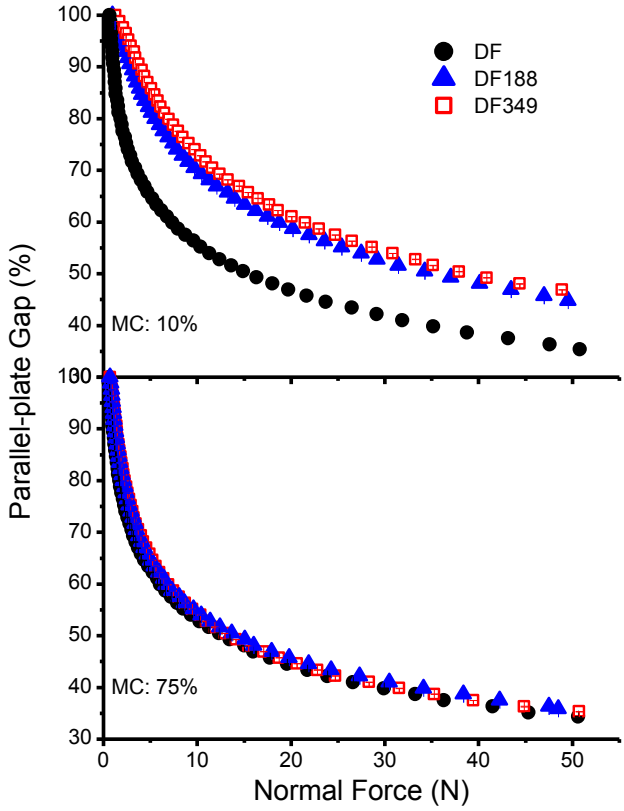

Figure 2-6. Compaction analysis: percent parallel-plate gap as a function of applied normal force for 10% and 75% moisture content (MC) refined (DF188 and DF349) and unrefined (DF) samples over a 60 second period at room temperature. Maximum stress ~ 1 MPa. Average curves presented; error bars represent ± 1 standard deviation, n=3; nonvisible error bars are smaller than symbols

Such morphological details were not measured. But even if differences in fiber morphology did affect the compaction depicted in Figure 2-6, apparently subsequent stress relaxation resulted in no difference between the refined specimens. That conclusion is reached because the refined samples exhibited the same storage moduli and (parallel-plate) gap changes during the temperature ramp, Figure 2-7. Likewise the relative storage moduli and gap changes indicated that the refined specimens densified more than the unrefined sample, regardless of moisture content. For all sample types, densification was greatest at the highest moisture level, as seen in the substantially higher storage moduli and the greater gap changes. At the respective moisture contents mechano-sorption effects were revealed by the increase in loss moduli corresponding to the increasing storage moduli caused by drying[78], Figure 2-7. Note that the normal stress applied in this sequential analysis (1-0.8 MPa) was approximately 40-30% of the stress actually applied during MDF production[40], easily exceeding the linear compressive response as seen in Figure 2-6.

The oscillation stress (Figure 2-7) was within the linear torsional response and so the viscous loss accompanied by stiffening/drying was attributed to mechano-sorptive dissipation. However at best this data must be qualified as not simply linear viscoelastic; specimen drying occurred and the compressive normal force could feasibly couple with the torsional oscillation in complex fashion. For instance, during heating the compressive normal force caused an additional 20-30% gap reduction. Stress ramps conducted before and after the Figure 2-7 temperature ramps demonstrated that torsional oscillation was within the linear response; but we cannot know if that was true during the densifying temperature ramp. Furthermore we are suggesting that the gap changes themselves indicate mechano-sorptive effects that suggest possible coupling of torsion and compression stresses. For example at 10% moisture, the initial stiffening attributed to drying occurred near 40°C, and the corresponding gap change exhibited a slope increase near this temperature. In other words the compressive strain rate increased during the moisture loss corresponding to torsional stiffening, consistent with the definition of mechano-sorption. At the higher moisture level two such events were observed: near 35°C the storage moduli leveled-off and at 70°C a sharp stiffness increase occurred. Both stiffness changes corresponded to increases in compressive strain rate (increasing slope in the parallel-

plate gap change). Considering all aspects of Figure 2-7 it is clear that specimen moisture loss may cause complex interactions of the two stress states, and so cautious interpretation must be emphasized. Given that caution, Figure 2-7 does indicate mechano-sorption in both stress modes. Furthermore the torsional storage moduli and compressive gap changes clearly demonstrate specimen densification. Because mechano-sorption and fiber mat densification are critical aspects of MDF manufacture, we are suggesting that this unusual rheological approach may yet provide novel insight. Unfortunately, the conditions employed here only distinguished refined and unrefined specimens. Perhaps the effects of refining energy could be discerned with careful modifications of this method; modifications might include higher temperature ramp rates and perhaps also compaction (Figure 2-6) conducted during heating (Figure 2-7).

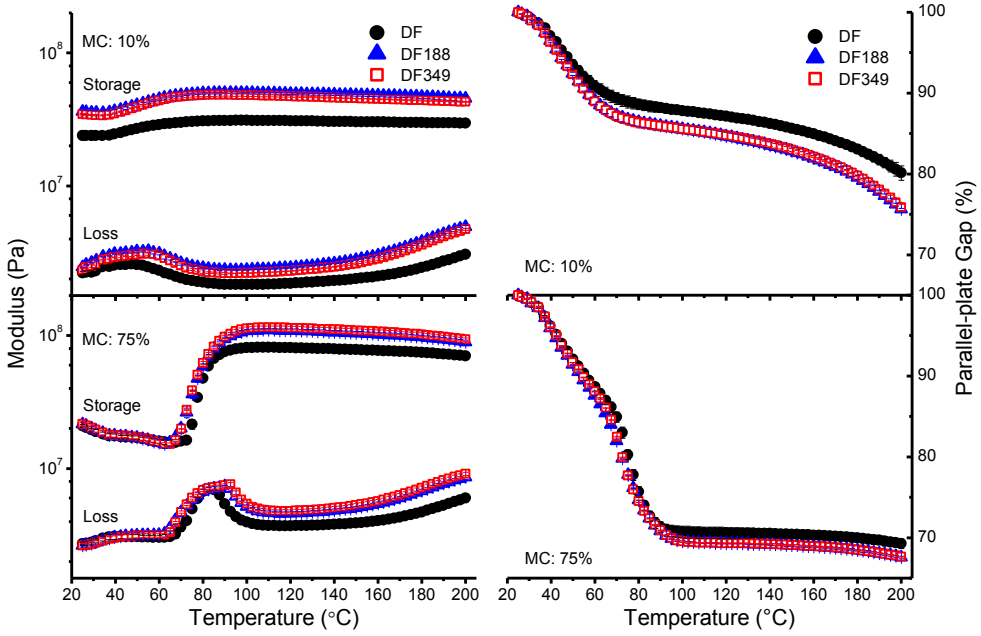

Figure 2-7. Densification analysis during temperature ramp: comparison of moisture content effects (10% and 75%) for refined (DF188, DF349) and unrefined (DF) samples. Left: Dynamic moduli under linear torsional oscillation. Right: Parallel-plate gap change due to the nonlinear compressive normal force. Average curves are presented; error bars represent ± 1 standard deviation, n=3; nonvisible error bars are smaller than symbols.

2.5. Summary and conclusions

In cooperation with a North American MDF mill using Douglas fir feedstock, two different refining energies (188 and 349 kW•h/ton) were used to produce resin and additive-free specimens studied for novel aspects of fiber quality. These refining energies represent the practical range commonly employed for production at this facility. The highest refining energy produced relative reductions in fiber width and length, and an increase in bulk density, all consistent with industry standard visual and tactile evaluations of fiber quality. Thermoporosimetry revealed increases in sub-micron scale porosity, and this was greatest at the higher refining energy. Mercury intrusion porosimetry (MIP) revealed porosity changes on a higher dimensional scale, interpreted to reflect fiber lumens, inter-fiber voids, and the effects of fiber damage. BET gas adsorption and MIP both demonstrated that refining increased the fiber specific surface area, where the greatest effect was at the highest refining energy. Consistent with these observations was that inverse gas chromatography revealed changes in fiber surface chemistry. The lowest refining energy produced surfaces dominated by the effects of lignin and extractives. In contrast, the highest refining energy produced substantially more fiber damage and this perhaps resulted in more cellulose exposure, uncovering higher energy active sites. These findings were generally consistent with the results of others, but the only directly comparable effort utilized a pilot-scale refiner. Our results suggest that the bulk fiber chemistry and also the fiber/resin interactions could be expected to vary between the low and high refining energy fibers. These topics will be addressed in subsequent publications. Finally, a novel rheological analysis was devised to probe aspects of fiber compaction and densification as related to the development of the panel vertical density profile. The method appeared to reveal mechano-sorptive dissipation and related aspects of fiber densification. The method failed to distinguish densification characteristics of the respective fiber types studied, but we suggest that the method merits further study for potentially novel insights.

Acknowledgments:

This project was supported by the Wood-Based Composites center, a National Science Foundation Industry/University Cooperative Research Center (Awards IIP-1035009 and IIP 1624536). Funding for this work was provided in part by the Virginia Agricultural Experiment

Station and the McIntire Stennis Program of the National Institute of Food and Agriculture, U.S. Department of Agriculture. The authors would like to thank Daniel Burnett from Surface Measurements Systems and Riaz Ahmad from Quantachrome respectively for providing inverse gas chromatography and mercury intrusion analyses. Special thanks are extended to the many collaborators at Arauco for providing samples and insight.

2.6. References

1. Hua, J.; Chen, G.; Xu, D.; Shi, S. Q., Impact of thermomechanical refining conditions on fiber quality and energy consumption by mill trial. *BioResources* **2012,** *7* (2), 1919-1930.
2. Park, B.-D.; Kim, Y.-S.; Riedl, B., Effect of wood-fiber characteristics on medium density fiberboard (MDF) performance. *Journal of the Korean Wood Science and Technology* **2001,** *29* (3), 27-35.
3. Franzén, R., General and selective upgrading of mechanical pulps [raw materials]. *Nordic Pulp and Paper Research Journal* **1986**.
4. Ohlmeyer, M.; Helder, S.; Benthien, J. T.; Seppke, B. In *Effects of refining parameters on fibre quality measured by fibre cube*, Proceedings of the International Panel Products Symposium, **2015**; pp 17-25.
5. McMillin, C. W., Fiberboards from loblolly pine refiner groundwood: effects of gross wood characteristics and board density. **1968**.
6. Kelley, S. S.; Elder, T.; Groom, L. H., Changes in the chemical composition and spectroscopy of loblolly pine medium density fiberboard furnish as a function of age and refining pressure. *Wood and Fiber Science* **2007,** *37* (1), 14-22.
7. Groom, L. H.; Mott, L.; Shaler, S., Relationship between Fiber Furnish and the Structural Performance of MDF. **1999**.
8. Rials, T.; Groom, L.; Tze, W.; Gardner, D.; Snell, R. In *Effect of refining on the surface characteristics of loblolly pine fibers*, Abstracts of papers of the american chemical society Amer Chemical Soc 1155 16th ST, NW, Washington, DC 20036 USA **2001**; pp U182-U182.
9. Krug, D.; Kehr, E., Influence of high pulping pressures on permanent swelling-tempered medium density fiberboard. *Holz Roh-Werkst* **2001,** *59* (5), 342-343.
10. Groom, L. H.; So, C.-L.; Elder, T.; Pesacreta, T.; Rials, T. G., Effects of Refiner Pressure on the Properties of Individual Wood Fibers. *Characterization of the cellulosic cell wall* **2008**, 227.
11. Snell, R.; Groom, L. H.; Rials, T. G., Characterizing the surface roughness of thermomechanical pulp fibers with atomic force microscopy. *Holzforschung* **2001,** *55* (5), 511-520.
12. Yobp, R. D.; Janowiak, J. J.; Blankenhorn, P. R., Effect of steam pressure refining and resin levels on the properties of UF-bonded red maple MDF. *Forest Products Journal* **1993,** *43* (11, 12), 82.
13. Xing, C.; Deng, J.; Zhang, S., Effect of thermo-mechanical refining on properties of MDF made from black spruce bark. *Wood Science and Technology* **2007,** *41* (4), 329-338.
14. Xing, C.; Wang, S.; Pharr, G. M.; Groom, L. H., Effect of thermo-mechanical refining pressure on the properties of wood fibers as measured by nanoindentation and atomic force microscopy. *Holzforschung* **2008,** *62* (2), 230-236.
15. Groom, L.; Rials, T.; Snell, R., Effects of varying refiner pressure on the machanical properties of loblolly pine fibres. **2000**.

16. Xing, C.; Deng, J.; Zhang, S.; Riedl, B.; Cloutier, A., Properties of MDF from black spruce tops as affected by thermomechanical refining conditions. *European Journal of Wood and Wood Products* **2006,** *64* (6), 507-512.
17. Schäfer, M.; Roffael, E., On the formaldehyde release of wood. *European Journal of Wood and Wood Products* **2000,** *58* (4), 259-264.
18. Short, P. H.; Lyon, D. E., Pressure-refined fiber from low-grade southern hardwoods. *Wood and Fiber Science* **2007,** *10* (2), 82-94.
19. Benthien, J. T.; Hasener, J.; Pieper, O.; Tackmann, O.; Bähnisch, C.; Heldner, S.; Ohlmeyer, M. In *Determination of MDF fiber size distribution: Requirements and innovative solution*, Proc of the International Wood Composites Symposium, **2013**.
20. Brunauer, S.; Emmett, P. H.; Teller, E., Adsorption of gases in multimolecular layers. *Journal of the American chemical society* **1938,** *60* (2), 309-319.
21. Fagerlund, G., Determination of specific surface by the BET method. *Materials and structures* **1973,** *6* (3), 239-245.
22. Graf, K.; Kappl, M., *Physics and chemistry of interfaces*. John Wiley & Sons: **2006**.
23. Lowell, S.; Shields, J. E., Langmuir and BET theories (kinetic isotherms). In *Powder Surface Area and Porosity*, Springer: **1991**, pp 14-29.
24. Washburn, E. W., Note on a method of determining the distribution of pore sizes in a porous material. *Proceedings of the National Academy of Sciences* **1921,** *7* (4), 115-116.
25. Lowell, S.; Shields, J. E., Interpretation of mercury porosimetry data. In *Powder Surface Area and Porosity*, Springer: **1984**, pp 97-120.
26. Dorris, G. M.; Gray, D. G., Adsorption of n-alkanes at zero surface coverage on cellulose paper and wood fibers. *Journal of Colloid and Interface Science* **1980,** *77* (2), 353-362.
27. Mohammadi-Jam, S.; Waters, K., Inverse gas chromatography applications: A review. *Advances in colloid and interface science* **2014,** *212*, 21-44.
28. Dong, S.; Brendle, M.; Donnet, J., Study of solid surface polarity by inverse gas chromatography at infinite dilution. *Chromatographia* **1989,** *28* (9), 469-472.
29. Gutmann, V., *donor-acceptor approach to molecular interactions*. Plenum Press: **1978**.
30. Papirer, E.; Balard, H.; Vidal, A., Inverse gas chromatography: a valuable method for the surface characterization of fillers for polymers (glass fibres and silicas). *European polymer journal* **1988,** *24* (8), 783-790.
31. Park, S.; Venditti, R. A.; Jameel, H.; Pawlak, J. J., Changes in pore size distribution during the drying of cellulose fibers as measured by differential scanning calorimetry. *Carbohydrate polymers* **2006,** *66* (1), 97-103.
32. Książczak, A.; Radomski, A.; Zielenkiewicz, T., Nitrocellulose porosity-thermoporometry. *Journal of thermal analysis and calorimetry* **2003,** *74* (2), 559-568.
33. Yin, J.; Song, K.; Lu, Y.; Zhao, G.; Yin, Y., Comparison of changes in micropores and mesopores in the wood cell walls of sapwood and heartwood. *Wood science and technology* **2015,** *49* (5), 987-1001.
34. Plötze, M.; Niemz, P., Porosity and pore size distribution of different wood types as determined by mercury intrusion porosimetry. *European Journal of Wood and Wood Products* **2011,** *69* (4), 649-657.
35. Moro, F.; Böhni, H., Ink-bottle effect in mercury intrusion porosimetry of cement-based materials. *Journal of Colloid and Interface Science* **2002,** *246* (1), 135-149.
36. Moura, M.; Ferreira, P.; Figueiredo, M., Mercury intrusion porosimetry in pulp and paper technology. *Powder Technology* **2005,** *160* (2), 61-66.
37. Bhardwaj, N. K.; Hoang, V.; Nguyen, K. L., A comparative study of the effect of refining on physical and electrokinetic properties of various cellulosic fibres. *Bioresource technology* **2007,** *98* (8), 1647-1654.

38. Fardim, P.; Durán, N., Modification of fibre surfaces during pulping and refining as analysed by SEM, XPS and ToF-SIMS. *Colloids and Surfaces A: Physicochemical and Engineering Aspects* **2003,** *223* (1), 263-276.
39. Maloney, T.; Paulapuro, H., The formation of pores in the cell wall. *Journal of pulp and paper science* **1999,** *25* (12), 430-436.
40. Suchsland, O.; Woodson, G. E., Fiberboard manufacturing practices in the United States. *Agriculture handbook/United States. Dept. of Agriculture (USA)* **1987**.
41. Comstock, G., Longitudinal permeability of wood to gases and nonswelling liquids. *Forest products journal* **1967,** *17* (10), 41-46.
42. Hart, C.; Thomas, R., Mechanism of bordered pit aspiration as caused by capillarity. *Forest Products Journal* **1967,** *17* (11), 61-68.
43. Petty, J.; Puritch, G., The effects of drying on the structure and permeability of the wood of Abies grandis. *Wood Science and Technology* **1970,** *4* (2), 140-154.
44. Gamelas, J. A., The surface properties of cellulose and lignocellulosic materials assessed by inverse gas chromatography: a review. *Cellulose* **2013,** *20* (6), 2675-2693.
45. Nussbaum, R., The critical time limit to avoid natural inactivation of spruce surfaces (Picea übles) intended for painting or gluing. *European Journal of Wood and Wood Products* **1996,** *54* (1), 26-26.
46. Gunnells, D. W.; Gardner, D. J.; Wolcott, M. P., Temperature dependence of wood surface energy. *Wood and Fiber Science* **2007,** *26* (4), 447-455.
47. Gulati, D.; Sain, M., Surface characteristics of untreated and modified hemp fibers. *Polymer Engineering & Science* **2006,** *46* (3), 269-273.
48. Shen, W.; Parker, I. H.; Sheng, Y. J., The effects of surface extractives and lignin on the surface energy of eucalypt kraft pulp fibres. *Journal of adhesion science and technology* **1998,** *12* (2), 161-174.
49. Börås, L.; Sjöström, J.; Gatenholm, P., Characterization of surfaces of CTMP fibers using inverse gas chromatography combined with multivariate data analysis. *Nordic Pulp and Paper Research Journal (Sweden)* **1997**.
50. Belgacem, M.; Czeremuszkin, G.; Sapieha, S.; Gandini, A., Surface characterization of cellulose fibres by XPS and inverse gas chromatography. *Cellulose* **1995,** *2* (3), 145-157.
51. Belgacem, M. N.; Blayo, A.; Gandini, A., Surface characterization of polysaccharides, lignins, printing ink pigments, and ink fillers by inverse gas chromatography. *Journal of Colloid and Interface Science* **1996,** *182* (2), 431-436.
52. Wålinder, M. E.; Gardner, D. J., Surface energy of extracted and non-extracted Norway spruce wood particles studied by inverse gas chromatography (IGC). *Wood and fiber science* **2007,** *32* (4), 478-488.
53. Liu, F. P.; Rials, T. G.; Simonsen, J., Relationship of wood surface energy to surface composition. *Langmuir* **1998,** *14* (2), 536-541.
54. NACEUR BELGACEM, M., Characterisation of polysaccharides, lignin and other woody components by inverse gas chromatography: A review. *Cellulose chemistry and technology* **2000,** *34* (3-4), 357-383.
55. Peterlin, S.; Planinšek, O.; Moutinho, I.; Ferreira, P.; Dolenc, D., Inverse gas chromatography analysis of spruce fibers with different lignin content. *Cellulose* **2010,** *17* (6), 1095-1102.
56. Lundqvist, A.; Odberg, L.; Berg, J. C., Surface characterization of non-chlorine-bleached pulp fibers and calcium carbonate coatings using inverse gas chromatography. *Tappi journal (USA)* **1995**.
57. Reutenauer, S.; Thielmann, F., The characterisation of cotton fabrics and the interaction with perfume molecules by inverse gas chromatography (IGC). *Journal of materials science* **2003,** *38* (10), 2205-2208.
58. Mills, R. H.; Gardner, D. J.; Wimmer, R., Inverse gas chromatography for determining the dispersive surface free energy and acid–base interactions of sheet molding compound—Part II 14 Ligno-

cellulosic fiber types for possible composite reinforcement. *Journal of Applied Polymer Science* **2008,** *110* (6), 3880-3888.
59. Ormondroyd, G. A.; Källbom, S.; Curling, S.; Stefanowski, B.; Segerholm, B.; Wålinder, M.; Jones, D., Water sorption, surface structure and surface energy characteristics of wood composite fibres refined at different pressures. *Wood Material Science & Engineering* **2017,** *12* (4), 203-210.
60. Gamelas, J.; JMRCA, S.; Ferreira, P., Surface energetics of softwood kraft pulps by inverse gas chromatography. *Fine structure of papermaking fibres. COST Office, Brussels* **2011**, 39-49.
61. Carvalho, M.; Santos, J.; Martins, A.; Figueiredo, M., The effects of beating, web forming and sizing on the surface energy of Eucalyptus globulus kraft fibres evaluated by inverse gas chromatography. *Cellulose* **2005,** *12* (4), 371-383.
62. Källbom, S.; Wålinder, M.; Segerholm, K.; Jones, D., Surface energy characterization of thermally modified spruce using inverse gas chromatography under cyclic humidity conditions. *Wood and Fiber Science* **2015,** *47* (4), 410-420.
63. Cordeiro, N.; Gouveia, C.; Moraes, A.; Amico, S., Natural fibers characterization by inverse gas chromatography. *Carbohydrate Polymers* **2011,** *84* (1), 110-117.
64. Cordeiro, N.; Ornelas, M.; Ashori, A.; Sheshmani, S.; Norouzi, H., Investigation on the surface properties of chemically modified natural fibers using inverse gas chromatography. *Carbohydrate Polymers* **2012,** *87* (4), 2367-2375.
65. Cordeiro, N.; Gouveia, C.; John, M. J., Investigation of surface properties of physico-chemically modified natural fibres using inverse gas chromatography. *Industrial Crops and Products* **2011,** *33* (1), 108-115.
66. Kamdem, D. P.; Bose, S. K.; Luner, P., Inverse gas chromatography characterization of birch wood meal. *Langmuir* **1993,** *9* (11), 3039-3044.
67. Felix, J.; Gatenholm, P., Characterization of cellulose fibers using inverse gas chromatography. *Nordic Pulp and Paper Research Journal (Sweden)* **1993**.
68. Stenius, P.; Laine, J., Studies of cellulose surfaces by titration and ESCA. *Applied surface science* **1994,** *75* (1-4), 213-219.
69. Dorris, G. M.; Gray, D. G., The surface analysis of paper and wood fibers by Esca-electron spectroscopy for chemical analysis-I. Applications to cellulose and lignin. *Cellulose chemistry and technology* **1978,** *12*, 9-23.
70. Jacob, P. N.; Berg, J. C., Acid-base surface energy characterization of microcrystalline cellulose and two wood pulp fiber types using inverse gas chromatography. *Langmuir* **1994,** *10* (9), 3086-3093.
71. Lee, H.; Luner, P., Characterisation of AKD sized papers by inverse gas chromatography. *Nordic Pulp Paper Res J* **1989,** *4*, 164-172.
72. Gérardin, P.; Petrič, M.; Petrissans, M.; Lambert, J.; Ehrhrardt, J. J., Evolution of wood surface free energy after heat treatment. *Polymer degradation and stability* **2007,** *92* (4), 653-657.
73. Winistorfer, P. M.; Moschler, W. W.; Wang, S.; DePaula, E.; Bledsoe, B. L., Fundamentals of vertical density profile formation in wood composites. Part I. In-situ density measurement of the consolidation process. *Wood and fiber science* **2007,** *32* (2), 209-219.
74. Stokke, D. D.; Wu, Q.; Han, G., Consolidation Behavior of Lignocellulosic Materials. *Introduction to Wood and Natural Fiber Composites* **2014**, 85-127.
75. Winistorfer, P. M.; Young, T. M.; Walker, E., Modeling and comparing vertical density profiles. *Wood and Fiber Science* **2007,** *28* (1), 133-141.
76. Wang, S.; Winistorfer, P. M.; Young, T. M., Fundamentals of vertical density profile formation in wood composites. Part III. MDF density formation during hot-pressing. *Wood and fiber science* **2007,** *36* (1), 17-25.
77. Ebrahimzadeh, P.; Bertilsson, H., Effect of impregnation on mechanosorption in wood and paper studied by dynamic mechanical analysis. *Wood science and technology* **1998,** *32* (2), 101-118.

78. Ebrahimzadeh, P.; Kubát, J.; McQueen, D., Dynamic mechanical characterization of mechanosorptive effects in wood and paper. *European Journal of Wood and Wood Products* **1996,** *54* (4), 263-271.
79. Lindström, S. B.; Karabulut, E.; Kulachenko, A.; Sehaqui, H.; Wågberg, L., Mechanosorptive creep in nanocellulose materials. *Cellulose* **2012,** *19* (3), 809-819.

Chapter 3 Lignin acidolysis without repolymerization during thermomechanical refining of Douglas fir wood

Mohammad Tasooji and Charles E. Frazier *

Sustainable Biomaterials, Virginia Tech, Cheatham Hall, RM 230 West Campus Drive, Blacksburg, Virginia 24061, United States

Macromolecules Innovation Institute, Virginia Tech, ICTAS II, 240 West Campus Drive, Blacksburg, Virginia 24061, United States

3.1. Abstract

Thermomechanical refining of Douglas fir wood caused substantial polysaccharide degradation, and other degradative effects that sometimes correlated with higher refining energy. Lignin acidolysis was detected using nitrobenzene oxidation, conductometric titration of free phenols, and determination of formaldehyde extracted from dried fiber. Formaldehyde was generated via the C2 lignin acidolysis pathway, but C3 cleavage was the dominant lignin reaction. Observations suggested that in-line formaldehyde monitoring might be useful for process control during biomass processing, perhaps indicating the C2/C3 pathway ratio with implications yet unknown. Lignin acidolysis was not accompanied by repolymerization and crosslinking: the lignin glass transition temperature (T_g) was reduced by refining, and thermogravimetric analysis confirmed that T_g reduction was due to lignin cleavage, and not damage to the fibril network. Lignin repolymerization must have been prevented by the reaction of benzyl cations with non-lignin nucleophiles, but identification of the corresponding sugar-benzyl ether was not clear. This nevertheless raises consideration of additives that compete for lignin benzyl cations, perhaps to promote lignin crosslinking and/or augment the lignin network with structures that impart useful properties. The variety of chemical effects detected here suggest that fiber/resin interactions might be affected by refining energy, possibly impacting fiber composite properties.

KEYWORDS: Thermomechanical refining, Medium density fiberboard, Lignin acidolysis, Wood fiber rheology,

3.2. Introduction

Among the most common wood-based composites, medium density fiberboard (MDF) is special because it is made from wood that is processed into individual cells (fibers). At roughly 3000 x 30 microns, length-to-diameter, these fibers are reconsolidated with thermosetting adhesives such that inter and intra-fiber compaction produces very smooth, machine-moldable surfaces that make MDF ideal for applications like cabinetry and decorative moldings[1]. MDF is normally manufactured with wood residues like chips, shavings, and sawdust. While processes vary, a common MDF production sequence involves: 1) steam digestion and softening above the glass transition, 2) refining, or rotary shearing between circular plates under steam pressure, 3) blending with resin, wax, and other additives, 4) drying, and 5) mat formation and hot-pressing. The objective is to process wood into isolated fibers, and refining promotes cleavage in and around the middle lamella[2]. However transverse fractures also occur, shortening the fibers, and producing sub-fiber fragments. Fiber separation is imperfect, and refining conditions affect the occurrence of fiber bundles, which are collections of multiple wood cells that fail to separate. Normally, greater quantities of fiber bundles (shives) are associated with lower fiber quality[3].

MDF fiber quality is most commonly evaluated by visual and tactile inspection[3], suggesting that average fiber length, the occurrence of shives, fiber morphology, and bulk density are intrinsic indicators of fiber quality. Besides tree species[4-7] , several production variables affect fiber quality; these include digester and refining pressure[4, 8-14], digester retention time[11, 14-15], refining temperature[15], rotational speed of the refiner plates, and the gap between refiner plates (changing as plates wear)[16]. The most important production variable is perhaps the refining energy (kW•h/ton of fiber)[17], which is controlled by the gap, or distance, between refiner-plates. In a prior publication we described how refining energy affected Douglas fir (*Pseudotsuga menziesii*) fiber dimensions, porosity, specific surface area, surface chemistry, and rheological aspects of compaction and densification[18]. In a comparable effort not using Douglas fir, Short and Lyon found that refiner-plate gap settings had no impact on fiber pH, alkaline buffering capacity, and ash content; only the fiber size and bulk fiber density were affected[16]. This is in contrast to our observations here and elsewhere[18], and the

discrepancy speaks to a practical challenge in MDF research: it is very difficult to relate pilot-scale refining (as for Short and Lyon[16]) to industrial practice, and critical aspects of processing vary substantially among industrial producers. In other words, wood fiber-based composites like MDF are the most technologically and scientifically complex wood-based composites.

Considering the complex structure and chemical reactivity of wood, it is unlikely that all aspects of fiber quality are reflected in visual and tactile inspections. Consequently, this effort is an industry/university cooperation intended to seek other aspects of fiber quality that might affect product performance or process efficiency. The context for this study was an industrial MDF production facility processing Douglas fir; and the principal experimental variable was refining energy via changes in gap settings. Our expectation is that refining energy will affect multiple aspects of fiber chemistry and properties, and that these effects could be expected to alter the fiber/resin interaction. Specifically however, this publication addresses how refining energy affects fiber acidity, cellulose crystallinity, chemical composition (with emphasis on lignin), and thermomechanical softening.

3.3. Experimental

Materials

Douglas fir (*Pseudotsuga menziesii)* refined and unrefined samples were collected at Arauco's MDF production facility in Eugene, Oregon, U.S.A. Normal production at this facility uses Douglas fir particles (30% shavings, 70% sawdust) softened in a steam digester (0.77 MPa, 174°C, 3.5 min retention time). Steam digested material is sprayed with additives (urea and wax), fed into a Sprout-Bauer SB150 thermomechanical refiner (0.77 MPa, 174°C, 1800 revolutions per min; disk configuration: spiral, 152 cm diameter). After passing through the plant drying system, the fibers are resinated, formed and hot-pressed. For this research, additive inlet valves were closed and fiber was processed so as to clear additives from the system. Once clear of additives, and after the drying stage, fiber sampling occurred in an emergency fiber-dump section (a fire safety feature of the plant). Collected specimens had a moisture content of 5-6% (wet basis), and were identified as DF188 and DF349 corresponding to the refining energies used: 188 and 349 kW•h/ton. These refining energies (adjusted by

changing the refiner-plate gap) are the practical range for production at this facility; the low and high refining energies produce “low” and “high” quality fiber as needed for commercial production. Unrefined control specimens (identified as DF; moisture content ~25%) were sampled from the production feedstock. All samples were collected in one day and sample preparation (below) started on the following day. Besides two different refining energies, all other production parameters were fixed. Fiber specimens were free of resin and additives.

Sample preparation

The unrefined sample (DF) was vacuum dried (0.10 mmHg, 25°C, overnight), ground by a Wiley mill, screened (18-80 mesh) and vacuum dried (0.10 mmHg, 25°C, overnight). Refined samples (DF188, DF349) were not milled, but similarly screened and dried as described. All samples were then sealed/stored at room temperature.

Compositional analysis

Samples were soxhlet extracted (95% ethanol, 24 hours) and vacuum dried (0.10 mmHg, 25°C, overnight). Ethanol soluble extractives were quantified as described [19]. Extractive-free vacuum dried sample was subjected to compositional analysis for determination of structural carbohydrates, soluble and insoluble lignin[20]. A Metrohm Ion chromatograph was used for sugar analysis (Hamilton RCX-30, 250-4.6 mm, column, DI water eluent: 1 ml/min, column temperature: 32°C, pulsed amperometric detector) was used.

Water chemistry

A Metrohm 905 titrando autotitrator equipped with 856 conductivity module was used. pH (Syntrode with Pt 1000) and conductivity (5-ring conductivity measuring cell with Pt 1000, C=0.7 cm^{-1}) probes were calibrated using Fisher Scientific buffer solutions (pH of 2, 4, 7 and 10) and Metrohm conductivity standard solution (100 µS/cm at 25°C) respectively. Vacuum dried and un-extracted sample (0.5 g) was placed in saline water (1mM NaCl, 300 mL) and stirred under N_2. Initial pH was measured after the suspension was equilibrated (10 min). The suspension was acidified with hydrochloric acid (0.1M, 2.6 mL) and equilibrated (15 min) prior to conductometric titration. Weak acids were titrated with sodium bicarbonate (0.1 M) and phenols were determined by difference after titrating separate specimens with sodium hydroxide (0.1 M)[21].

Thermogravimetric analysis

TA Instruments Q-100 was used for thermal analysis. Thermogravimetric analysis (from ambient to 600°C, 10°C/min) was conducted on vacuum dried and un-extracted samples (45-50 mg) in air (60 mL/min).

Nitrobenzene oxidation

The methods of Ohra et al.[22], Iiyama[23], and Katahira and Nakatsubo[24] were adopted. Extractive-free vacuum dried sample (200 mg, 18-80 mesh) was placed in a stainless steel reactor (10 x 2 cm, length × I.D.) followed by sodium hydroxide (2M, 7 mL) and nitrobenzene (0.5 mL). The reactor was tightly sealed (Teflon™ tape), placed in an oil bath (170°C, 160 min) and shaken occasionally. The reactor was cooled to room temperature; the contents were transferred and acidified to pH 2 (4 M HCl, 3mL). The organic phase was collected after liquid/liquid extraction (chloroform, 6 × 30 mL). After drying (sodium sulfate), the chloroform was removed by rotary evaporation and the residue was stored in a desiccator overnight. The residue was transferred to a volumetric flask (50 mL) and filled to mark with internal standard (0.2M acetovanillone in dichloromethane, 5 mL) and dichloromethane. From this an aliquot (2 mL) was derivatized using N,O-bis (trimethylsilyl)acetamide (10 µL), filtered (PTFE, 0.45 µm) and injected (1 µL) into an Agilent 7890 gas chromatograph (GC). The GC was equipped with a HP-5 5% phenyl methyl siloxane capillary column (30 m, 0.32 mm, length×I.D., 0.25 µm film thickness), a flame ionization detector with nitrogen (1 mL/min) carrier gas. GC conditions and temperature profile were as described by Chen[25]. Calibration curves using vanillin and vanillic acid standards were obtained in the concentrations of (0.04-2 mM for vanillin and 0.1-1 mM for vanillic acid (solvent: dichloromethane). Response factors (vanillin: 0.857, vanillic acid: 1.441) were calculated from the calibration curves and relative to the internal standard. Gas chromatography-mass spectrometry (Agilent 6890 GC, 5973 MSD) was used to verify chromatogram peaks.

Formaldehyde content

The formaldehyde content of vacuum dried and un-extracted samples (about 30 mg) was measured as described in the literature[26-27] . Besides the drying that occurred as part of sample collection, no heat treatment was applied to the samples prior to formaldehyde analysis.

Crystallinity

A D8 Bruker X-ray diffractometer with a Cu Kα radiation source (λ = 0.154 nm) generated at 40 kV and 40 mA was used. 2theta scan was performed from 10 to 50° at a scan speed of 2.4 °/min, using a 1 mm slit. Vacuum dried and un-extracted sample was flattened on a quartz slide (1-2 mm thickness) to collect the diffraction profile. Segal[28], deconvolution, and amorphous subtraction methods were used to calculate percent crystallinity[29]. For deconvolution, a Gaussian function was selected, five crystalline peaks (1-10, 110, 102, 200, 004[30]) and one amorphous peak were assumed and curve fitting was conducted using least squares fitting. For the amorphous subtraction method, the amorphous region was selected and subtracted using Bruker DIFRAC plus EVA software.

Rheology

TA Instruments AR2000 was used for rheological analysis. Vacuum dried and un-extracted sample (0.05 g) was dispersed in glycerol (15 mL), formed into a fiber mat (~5 mm thickness, 8 mm dia.) by filtration into a mold. Compressive torsion solvent-submersion dynamic mechanical analysis (DMA) was performed generally as described in previous studies[31-32]. The fiber mat was placed between 8 mm diameter parallel-plates and subsequently subjected to compressive-torsion DMA while immersed in glycerol as follows: Under a 10 N clamping normal force, impose sequential heating and cooling ramps: equilibrate (30°C, 2 min), temperature ramp (30-170 °C, 3°C/min, 15000 Pa,1Hz), equilibrate, (170°C, 2 min), temperature ramp (170-30°C, 3°C/min, 15000 Pa, 1 Hz). The oscillation stress was within the linear viscoelastic response, as determined using stress sweep experiments at 30°C and 170°C. DMA was conducted such that the specimen was surrounded by a stainless steel cup that maintained solvent immersion. An aluminum cover was used to reduce evaporative losses.

2D NMR (HSQC)

Extractive-free vacuum dried sample were ball milled[33] and screened (passed 325 mesh). Screened ball-milled powder (50 mg) was suspended into DMSO-d6/pyridine-d5 (4:1, v:v, 1 mL) and magnetically stirred (4 hrs) until reaching visual homogeneity, then transferred into NMR tube (5 mm, 600 MHz). NMR spectra were acquired on a Bruker Advance III A600 MHz equipped with triple resonance broad band (TBI) probe using Z gradient. An HSQC experiment (heteronuclear single quantum correlation, pulse program: hsqcedetgpsisp2.2) was performed with the following parameters: temperature: 24°C, number of scans: 96, relaxation delay: 1 sec, acquisition time: 0.125 sec, number of increments: 512, spectral width (1H): 13.66 ppm, centered at 5.75 ppm, spectral width (^{13}C): 240 ppm, centered at 100 ppm. The central solvent (DMSO) peak was used as an internal chemical shift reference point (δC: 39.52, δH: 2.50ppm). MNOVA was used for spectral processing and OriginPro was used for plotting. For qualitative comparison the signal intensities were normalized based on the pyridine peak (δC: 135.91, δH: 7.58ppm).

3.4. Results and discussion

Douglas fir samples are identified as DF188 and DF349 corresponding to the refining energies used: 188 and 349 kW•h/ton (unrefined control: DF). Previously, we showed that fiber damage and size reductions were associated with higher refining energy, as were increases in porosity, specific surface area, and changes in fiber surface chemistry[18]. As expected, compositional analysis of ethanol-extracted samples revealed that bulk chemical changes also resulted, Table 3-1. Among the neutral sugars analyzed, glucose and arabinose suffered the greatest losses; but all sugars were degraded and the effects were greatest at the highest refining energy. This degradation of cellulose and hemicellulose is consistent with other reports[34-39]. Relative to the control (DF), refining slightly increased insoluble lignin in DF188; but DF349 was no different from the control. In contrast, for soluble lignin, refining caused a slight reduction, and the highest refining energy caused a substantial reduction, Table 3-1. Similar effects have been reported for soluble[40] and insoluble lignin[4, 36, 41]. Finally, refining increased levels of ethanol extractives, but no difference was seen at the respective refining energies. The increase in ethanol soluble extractives found here is similar to that reported under steam

treatment and pressurized refining[40-45], and this is perhaps attributed to some delignification during ethanol extraction[34, 40, 46-47]. However, Table 3-1 does not clearly support this possibility, and the increase in ethanol extractives might also relate to the sugar degradation.

Conductometric titration was used to measure weak acids and phenols, but discussion of the latter appears below. Table 3-2 shows that refining increased fiber acidity, and more so at the highest energy; but the increase in weak acids was the same at the respective refining energies. These changes could be associated with the sugar degradation mentioned, and perhaps also with ester cleavage in both hemicellulose[48-50] and lignin carbohydrate complexes (LCC)[51-52]. Others have also reported acid formation due to steam treatments[36, 42, 53] and refining[44, 54], and this increased acidity will catalyze wood polymer hydrolysis[4, 36].

Table 3-1. Compositional analysis of refined (DF188 and DF349) and unrefined (DF) samples (% of dry extracted sample). Standard deviations in parentheses; n=3.

	Sugars						**Lignin**		**Extractives**
	Glu	Xyl	Gal	Arab	Man	Total	Sol.	Insol.	
DF	44.49	4.12	2.69	0.95	12.31	64.56	5.71	27.31	3.33
	(0.37)	(0.63)	(0.10)	(0.04)	(0.70)	(1.10)	(0.13)	(0.02)	(0.00)
DF188	35.62	3.16	2.16	0.41	10.28	51.63	5.27	27.76	5.73
	(2.24)	(0.22)	(0.19)	(0.03)	(0.61)	(3.30)	(0.09)	(0.10)	(0.34)
DF349	25.34	2.10	1.50	0.24	7.35	36.53	3.64	27.38	5.23
	(3.62)	(0.32)	(0.17)	(0.03)	(0.98)	(5.13)	(0.07)	(0.22)	(0.36)

Table 3-2. Fiber pH and weak acids of refined (DF188 and DF349) and unrefined (DF) samples. Standard deviations in parentheses; n=10 for pH and 2 for weak acids.

Specimen	pH	Weak acids (µmol / g dry sample)
DF	6.01 (0.01)	128.93 (0.02)
DF188	5.84 (0.01)	138.53 (0.45)
DF349	5.80 (0.01)	138.44 (0.10)

The sugar degradation due to refining could be expected to appear in cellulose crystallinity measurements. Figure 3-1 shows that the amorphous halo[55] decreased after refining, and Figure 3-2 gives the corresponding percent crystallinity according to three calculation methods, Segal, deconvolution, and amorphous subtraction. Among these calculation methods, the relative values found here were consistent with other reports[29]. Furthermore, all calculation methods exhibited similar trends regarding the effects of refining and refining energy, similar to related reports on the effects of refining pressure[4].

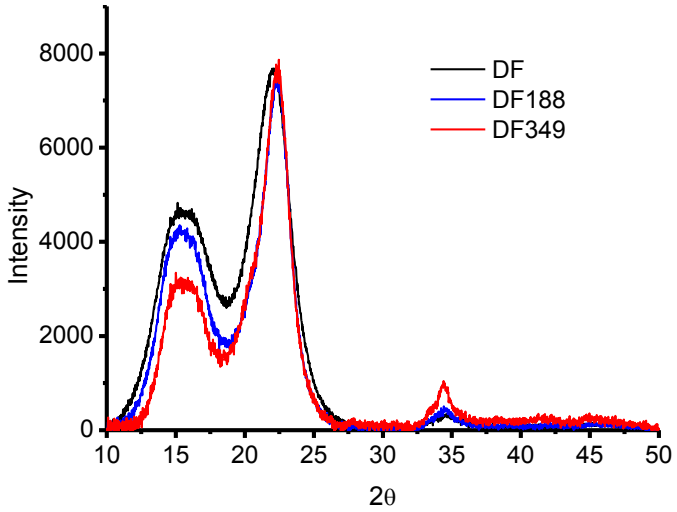

Figure 3-1. Example X-ray diffraction data for refined (DF188 and DF349) and unrefined (DF) samples; one measurement of three is shown.

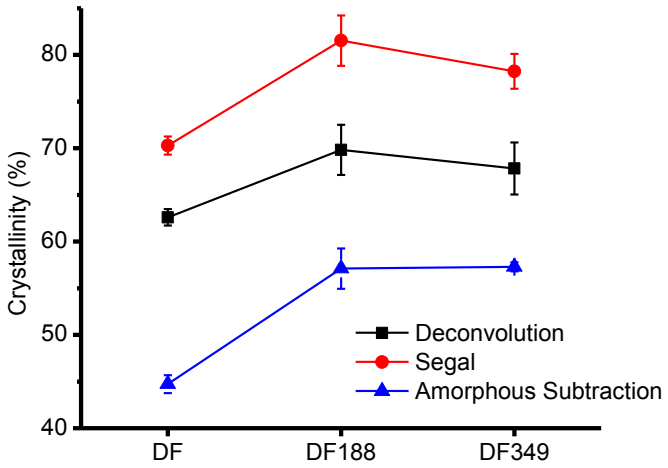

Figure 3-2. Percent crystallinity for refined (DF188 and DF349) and unrefined (DF) samples calculated using Segal, deconvolution and amorphous subtraction methods. Error bars represent ± 1 standard deviation, n=3.

Given the extensive fiber damage demonstrated so far, we could also expect lignin cleavage through acidolysis, and this was confirmed with nitrobenzene oxidation (NBO), by determination of free phenols (conductometric titration), and by formaldehyde determination through water extraction, Table 3-3 and Figure 3-3. This data is in units of µmol/gram of dry sample because NBO employed ethanol-extracted material, whereas un-extracted specimens were used for the other two analyses. NBO yields benzaldehydes for more than just β-aryl ethers[56-59], but these are by far the major reactants and for convenience the NBO discussion is simplified to consideration of only β-O-4 linkages (β-aryl ethers). Refining caused a statistically significant reduction in β-aryl ethers, but only about 6% for DF188 and 11% for DF349. The higher refining energy appeared to cause more lignin cleavage but the effect was not highly significant ($p=0.06$ between DF188 and DF349). Consistent with the lignin acidolysis mechanism[60-61], β-aryl ether cleavage generates free phenols and Table 3-3 indicates that refining increased phenol levels by about 42%, substantially greater than the corresponding decrease in NBO vanillin yields. However, free phenol levels and NBO yields were respectively obtained from un-extracted and extract-free samples; so a stoichiometric comparison is not feasible. Both data sets are consistent with lignin acidolysis, as are the formaldehyde levels measured in un-extracted samples. It seems as if all lignocellulosic organics can generate

formaldehyde[62], but lignin is most capable due to the structure of its benzyl cation, product of the first step in lignin acidolysis, Figure 3-4. After formation of the benzyl cation, either C2 cleavage or C3 cleavage (as in C6C2 vs C6C3 products) can occur; the former produces formaldehyde and both pathways generate a free phenol[61]. Model compound studies have demonstrated that different acid catalysts are highly selective for C2 or C3 cleavage[63-65]. These model studies were predictive of catalytic effects in whole wood, but pathway selectivity was much lower than observed in model compounds[62]. In the present case, unrefined samples contained formaldehyde that perhaps originated from the living tree[27], but it could have been absorbed from the environment as well. Upon refining, it appears that formaldehyde was generated via lignin acidolysis, and fiber drying captured that lignin-derived formaldehyde in the form of hemiformals, because dry lignocellulose retains formaldehyde[66-67]. Regarding the impact of refining energy, DF349 contained significantly more formaldehyde than DF188, but the formaldehyde generated in DF188 and DF349 accounted for only about 1% of the β-aryl ethers cleaved as measured using NBO. In other words, C3 cleavage appears to have been highly favored over C2 cleavage (this ignores any consumption of lignin benzyl cations due to aromatic substitution, as is believed to occur[68-69]). Although not proven, it is probable that most formaldehyde generated during refining originated from lignin acidolysis, and fiber drying preserves the evidence since the corresponding hemiformals are stable in dried fiber. Using simple water extraction, this biogenic formaldehyde is easily quantified[26]. Formaldehyde generation through lignin acidolysis raises the possibility of in-line formaldehyde measurements[70] for process control during biomass processing. Of course, C2 cleavage (formaldehyde generation) is but one acidolysis pathway, and we do not yet understand how the C2/C3 pathway ratio affects biomass properties. It is known that acid catalyst selection can promote C2 cleavage[62]. In any case, it is feasible to consider in-line formaldehyde measurement as potentially valuable for biomass processing. A possible complication (or perhaps opportunity) for in-line formaldehyde monitoring is that formaldehyde generation potential can be highly variable among different tree species, for reasons not yet understood[27]. Finally the observation of lignin acidolysis in this work is consistent with other reports involving steam processing [38, 40, 45-46, 71-72].

Table 3-3. Corrected vanillin yields from nitrobenzene oxidation using ethanol-extracted specimens, and free phenol and formaldehyde levels in un-extracted specimens for refined (DF188 and DF349) and unrefined (DF) samples. Standard deviations in parentheses; n=3 for formaldehyde and nitrobenzene oxidation; n=2 for phenols.

Specimen	Vanillin*	Phenols	Formaldehyde
	(µmol/ g dry sample)		
DF	394.2 (3.0)	167.5 (0.2)	0.67 (0.03)
DF188	369.4 (5.8)	238.2 (1.1)	0.83 (0.04)
DF349	350.0 (11.3)	237.0 (1.0)	0.95 (0.03)

* Corrected vanillin = vanillin + vanillic acid

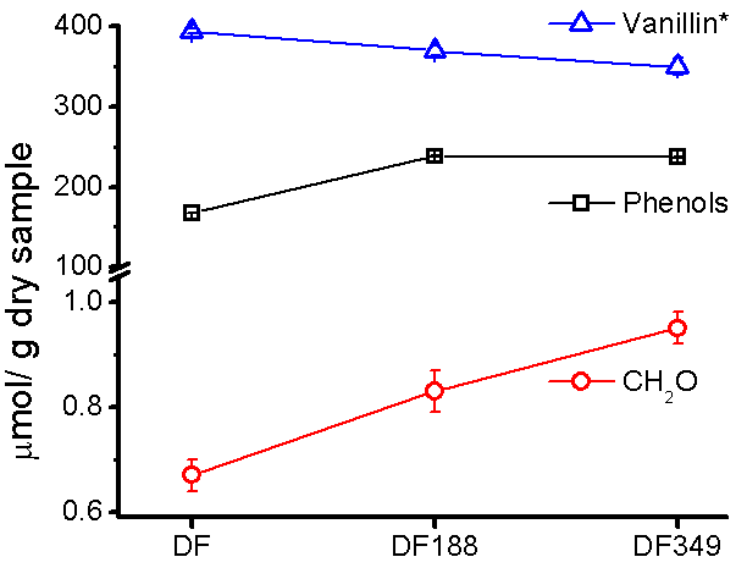

Figure 3-3. Corrected vanillin* (vanillin + vanillic acid) from nitrobenzene oxidation of ethanol-extracted specimens; free phenols and formaldehyde measured in un-extracted specimens, refined (DF188 and DF349) and unrefined (DF). Error bars represent ± 1 standard deviation; n=3 for formaldehyde and nitrobenzene oxidation; n=2 for phenols; note the broken y-axis.

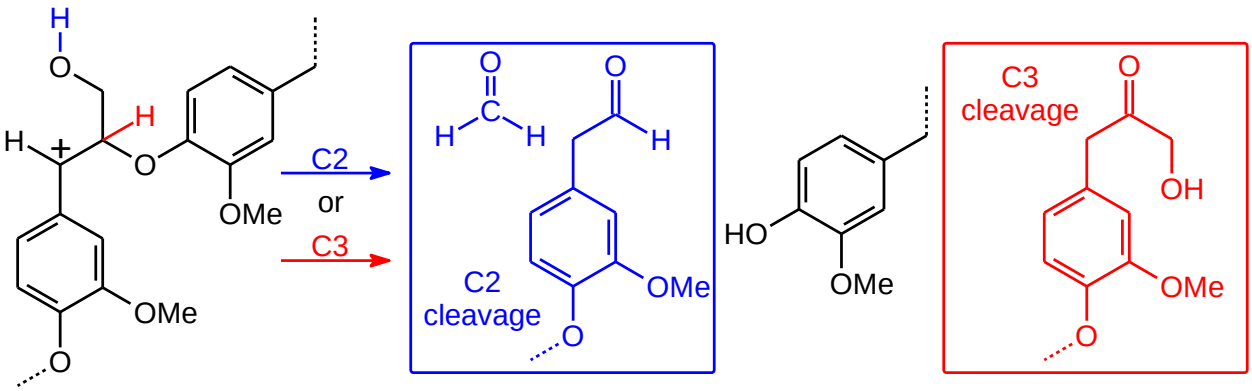

Figure 3-4. The first step in lignin acidolysis is formation of the benzyl cation, left; thereafter β-aryl ether cleavage can produce formaldehyde and a phenylacetaldehyde derivative (C2 Cleavage), or a phenylacetone derivative (C3 cleavage), both pathways generate a free phenol.

The properties of thermomechanical fibers are remarkably dependent upon wood softening in the refiner[2, 73-74], and chemical changes due to refining will likely affect fiber compaction and densification in the hot-press. Consequently, it was of interest to observe the lignin glass transition using solvent-submersion compressive-torsion rheology[31]. Specimen mats were saturated in glycerol, compressed between parallel-plates and subjected to torsional oscillation while immersed in glycerol, Figure 3-5. In contrast to water or ethylene glycol, glycerol is a less effective wood swelling agent[32, 75], and here its use as a plasticizer provides a crude approximation of moisture levels below fiber saturation. In the first heat, unrefined samples (DF) exhibited a lignin glass transition temperature (T_g: temperature of tan δ maximum) of about 120°C, with a shoulder near 90°C (origin unknown, but a similar shoulder is discussed[31]). Refined samples DF188 and DF349 exhibited lower T_g values, respectively 97°C and 92°C, and the tan δ signals were substantially narrowed and intensified. Upon cooling, the T_g values were higher than in the 1st heat (due to additional T_g related swelling[31]), but the T_g values exhibited the same trend; and while the difference among refined specimens seems negligible in Figure 3-5, the measured T_g values are statistically distinct (p-value of 1st cool T_g values for DF188 vs DF349 = 0.01). Since the fiber densification occurring during MDF hot-pressing is due to viscoelastic[76-77] and probably also mechano-sorptive effects[18], these rheological results indicate that refining energy will impact the evolution of density gradients in

panels made at the respective refining energies. However, the heat and mass transfer in the hot-press is so complex that it is very difficult, or not yet possible, to predict how these rheological differences would translate into distinguishable panel properties. In fact for refined and unrefined samples, the only readily apparent differences are the compaction and densification potentials[18]. For instance, in Figure 3-5 the low temperature storage moduli (heating and cooling) are greater for refined specimens, and this is due to densification (consistent with the correspondingly higher loss moduli in the same low temperature region). A final point about fiber rheology relates to the implications of lignin acidolysis discussed above. Lignin acidolysis is commonly associated with repolymerization (a.k.a "condensation"), the formation of carbon-carbon linkages and overall increasing crosslink density in lignin's well-known self-healing tendency[46-47, 53, 72, 78-80]. The reduced T_g values resulting from refining strongly suggest that acidolysis occurred without lignin repolymerization, and this is noteworthy considering that much of lignin's recalcitrance in biorefinery technologies is associated with repolymerization to create more carbon-carbon linkages[68]. However, some caution is required with this interpretation. The reduced lignin T_g was conceivably caused by the substantial polysaccharide degradation demonstrated above. It is known that *in situ* lignins can exhibit a great deal of orientation[81-82] imposed by the highly organized polysaccharide fibrillar network (however this is apparently most common in hardwoods[83]). In other words, the lignin glass transition is conceivably affected by restrictions imposed by the fibril network, and substantial fibril damage might in fact cause a reduction in the lignin T_g.

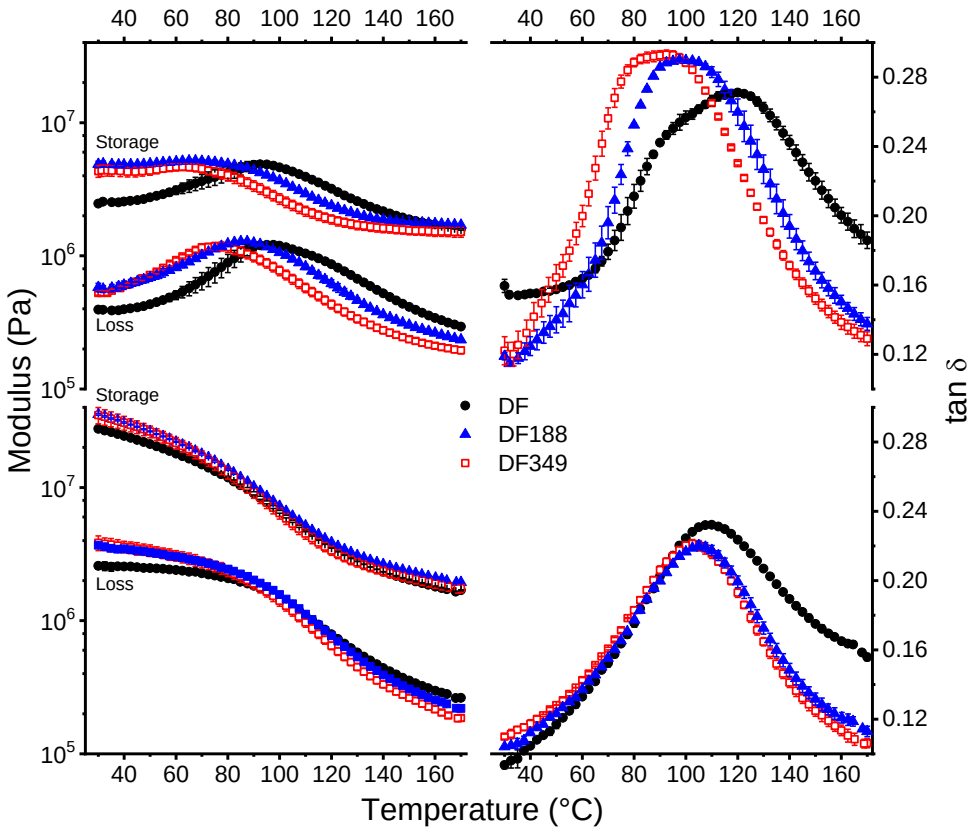

Figure 3-5. Dynamic mechanical analysis (torsional oscillation, 1 Hz, while under 10 N compressive force) for glycerol-plasticized samples; refined (DF188 and DF349) and unrefined (DF). Top: 1st heating ramp, bottom: 1st cooling ramp. Average curves are presented; error bars represent ± 1 standard deviation, n=3; nonvisible error bars are smaller than symbols

However, thermogravimetric analysis (TGA) suggested that lignin in refined samples did not undergo repolymerization, Figure 3-6. This interpretation extends from Martin-Sampedro et al. (2011) who showed compelling evidence for the use of TGA as an indicator of lignin repolymerization and crosslinking. They demonstrated that steam explosion of *Eucalyptus globulus* chips caused substantial reductions in β-aryl ether content, and that the corresponding increases in lignin degradation temperature (via the derivative weight, %/°C) were due to lignin repolymerization and crosslinking. Figure 3-6 shows that refined samples exhibited significant reductions in lignin degradation temperature, and besides the findings of Martin-Sampedro et al. (2011), the fundamental application of TGA[84] suggests that cleavage, not repolymerization,

was the ultimate fate of lignin acidolysis in this work. This conclusion is consistent with the rheology discussed above, and with HSQC NMR that showed no evidence for repolymerization in the aromatic region, Figure 3-7 (evidence would be broadening of existing signals and appearance of new signals, all in the 6.5 – 6.7 ppm range) [85]. Given the lignin acidolysis that was detected here, it is likely that lignin benzyl cations were consumed by non-lignin nucleophiles, perhaps sugars or sugar degradation products. This scenario is similar to naturally occurring lignin carbohydrate complexes (LCC) known to occur as benzyl ethers via sugar primary hydroxyls. Benzyl ether LCC chemical shifts have been established with model compounds [86], and applied in HSQC spectra [87]. A tentative identification of the benzyl ether LCC was made here, Figure 3-8, where in refined samples very weak signals were detected at or near the expected chemical shifts. Figure 8 displays the lowest contours, below which noise becomes problematic. Considering that LCC's are detected in isolated lignins, and not whole tissue preparations as used here, it is clear that the benzyl ether identification made here is highly tentative. If they did form, it is again noteworthy that the lignin T_g was reduced in refined samples, suggesting that the lignin softening relaxation is not affected by fibril network constraints. Regardless of the LCC detection, discussion of lignin benzyl cation reaction raises consideration of the addition of nucleophiles that might compete for benzyl cations (during refining or during subsequent hot-pressing) thereby resulting in useful functionalities that could improve panel properties. Similar strategies have been demonstrated in biofuels research where additives capture lignin benzyl cations, preventing repolymerization and improving delignification[61, 72]. However and precisely opposite the intention for biofuels production, various nucleophiles might be added to promote lignin crosslinking and/or augment the lignin network with structures that impart useful properties in fiber composites.

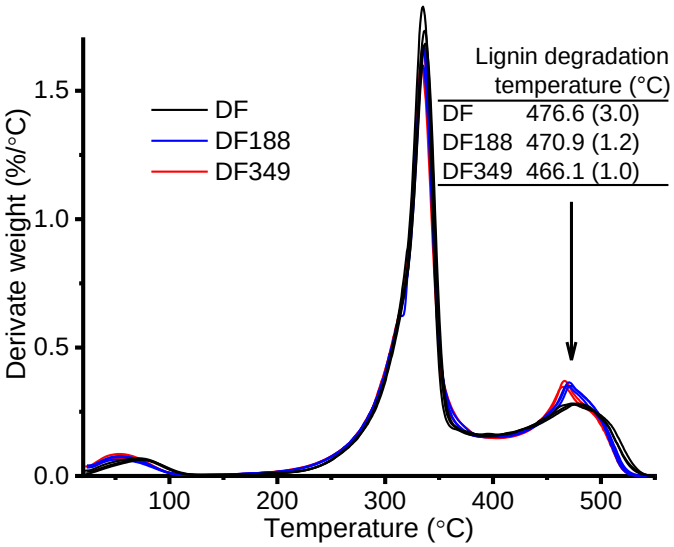

Figure 3-6. Thermogravimetric analysis (derivative weight) in air of refined (DF188 and DF349) and unrefined samples (DF). Standard deviation in parentheses; n=3.

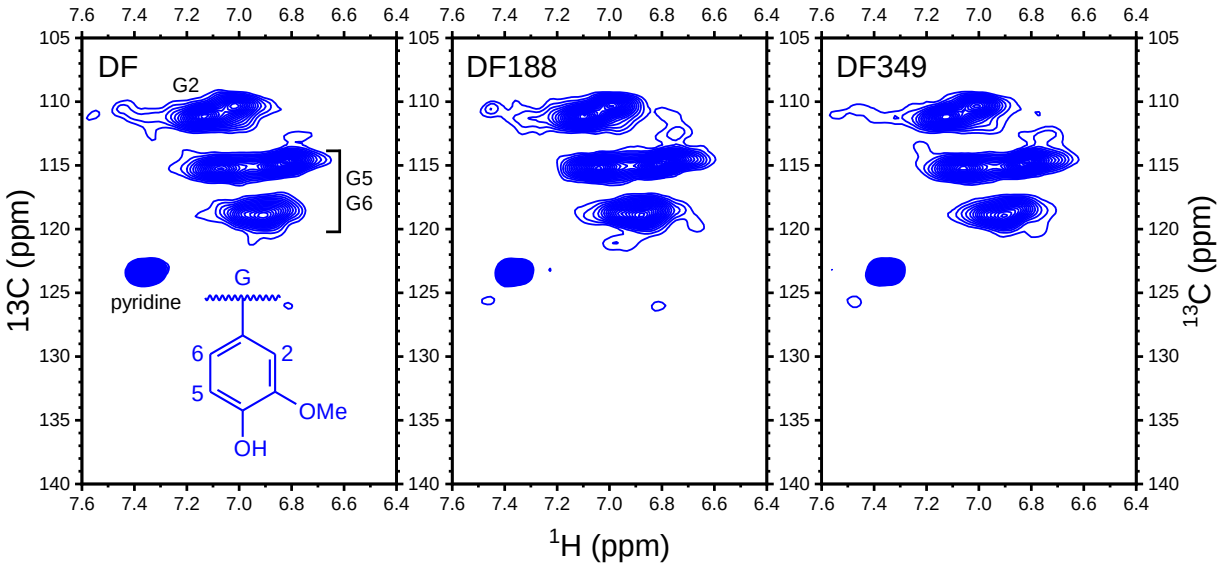

Figure 3-7. ^{13}C-^{1}H heteronuclear single quantum correlation (HSQC) spectra (aromatic region) of refined (DF188 and DF349) and unrefined (DF) samples.

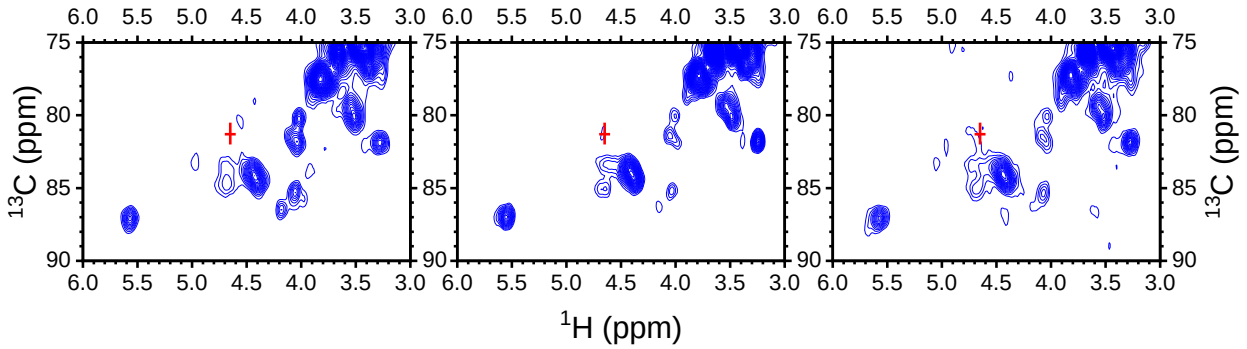

Figure 3-8. ^{13}C-^{1}H heteronuclear single quantum correlation (HSQC) spectra (LCC benzyl ether region) of refined (DF188 and DF349) and unrefined (DF) samples. Red cross indicates the expected chemical shifts for benzyl ether LCC.

3.5. Summary and conclusions

As part of an industry/university cooperation, a North American medium density fiberboard (MDF) plant was the setting to study refining energy effects on bulk chemical and rheological behavior of Douglas fir feedstock. Normal production at this facility involves only two energy levels controlled by refiner-plate gap settings. Refining caused substantial polysaccharide degradation and increased acidity, more so at the highest energy. A corresponding crystallinity increase was observed, but with no dependence on refining energy. Lignin acidolysis was detected using nitrobenzene oxidation, conductometric titration of free phenols, and determination of formaldehyde extracted from dried fiber. Formaldehyde was produced via the C2 lignin acidolysis pathway, but the low levels generated indicated that C3 cleavage was the dominant lignin reaction. These observations suggested that in-line formaldehyde monitoring might be useful for process control during biomass processing. Prior efforts demonstrated that the C2/C3 pathway ratio can be manipulated, but we do not yet understand the implications for biomass properties. Lignin acidolysis is commonly accompanied by repolymerization and crosslinking, but not in this study. The lignin glass transition temperature (T_g) was reduced by refining, and thermogravimetric analysis confirmed that the T_g reduction was due to lignin cleavage, and not damage to the surrounding fibril network. Lignin repolymerization must have been prevented by the reaction of benzyl cations with non-lignin nucleophiles, but in the case of sugar primary hydroxyls no clear evidence was found.

Nevertheless, this raises consideration of additives that compete for lignin benzyl cations, perhaps to promote lignin crosslinking and/or augment the lignin network with structures that impart useful properties. Finally, the variety of chemical effects detected here suggest that wood fiber/resin interactions might be affected by refining energy, possibly impacting MDF panel properties.

Acknowledgments

This project was supported by the Wood-Based Composites center, a National Science Foundation Industry/University Cooperative Research Center (Awards IIP-1035009 and IIP 1624536). Funding for this work was provided in part by the Virginia Agricultural Experiment Station and the McIntire Stennis Program of the National Institute of Food and Agriculture, U.S. Department of Agriculture. Special thanks are extended to the many collaborators at Arauco for providing samples and insight.

3.6. References

1. Stokke, D. D.; Wu, Q.; Han, G., *Introduction to wood and natural fiber composites*. John Wiley & Sons: **2013**.
2. Franzén, R., General and selective upgrading of mechanical pulps [raw materials]. *Nordic Pulp and Paper Research Journal* **1986**.
3. Ohlmeyer, M.; Helder, S.; Benthien, J. T.; Seppke, B. In *Effects of refining parameters on fibre quality measured by fibre cube*, Proceedings of the International Panel Products Symposium, **2015**; pp 17-25.
4. Kelley, S. S.; Elder, T.; Groom, L. H., Changes in the chemical composition and spectroscopy of loblolly pine medium density fiberboard furnish as a function of age and refining pressure. *Wood and Fiber Science* **2007,** *37* (1), 14-22.
5. McMillin, C. W., Fiberboards from loblolly pine refiner groundwood: Effects of gross wood characteristics and board densi ty. *Forest Prod. J* **1968,** *18* (8), 51-59.
6. Park, B.-D.; Kim, Y.-S.; Riedl, B., Effect of wood-fiber characteristics on medium density fiberboard (MDF) performance. *Journal of the Korean Wood Science and Technology* **2001,** *29* (3), 27-35.
7. Groom, L.; Mott, L.; Shaler, S. In *Relationship between fiber furnish properties and the structural performance of MDF*, Proceedings of the 33rd International Particleboard/Composite Materials, **1999**; pp 13-15.
8. Snell, R.; Groom, L. H.; Rials, T. G., Characterizing the surface roughness of thermomechanical pulp fibers with atomic force microscopy. *Holzforschung* **2001,** *55* (5), 511-520.
9. Groom, L. H.; So, C. L.; Elder, T.; Pesacreta, T.; Rials, T. G., Effects of refiner pressure on the properties of individual wood fibers. *Characterization of the cellulosic cell wall* **2006**, 227-240.
10. Yobp, R. D.; Janowiak, J. J.; Blankenhorn, P. R., Effect of steam pressure refining and resin levels on the properties of UF-bonded red maple MDF. *Forest Products Journal* **1993,** *43* (11, 12), 82.
11. Xing, C.; Deng, J.; Zhang, S., Effect of thermo-mechanical refining on properties of MDF made from black spruce bark. *Wood Science and Technology* **2007,** *41* (4), 329-338.
12. Xing, C.; Wang, S.; Pharr, G. M.; Groom, L. H., Effect of thermo-mechanical refining pressure on the properties of wood fibers as measured by nanoindentation and atomic force microscopy. *Holzforschung* **2008,** *62* (2), 230-236.
13. Groom, L.; Rials, T.; Snell, R. In *Effects of varying refiner pressure on the machanical properties of loblolly pine fibres*, Proceedings of the Fourth Panel Products Symposium, Llandudno, Wales UK, October 11-13, Hague; Griffiths; McLauchlin; Mayhead; Skinner; Tomkinson, eds., **2000**.
14. Xing, C.; Deng, J.; Zhang, S.; Riedl, B.; Cloutier, A., Properties of MDF from black spruce tops as affected by thermomechanical refining conditions. *Holz als Roh-und Werkstoff* **2006,** *64* (6), 507-512.
15. Schäfer, M.; Roffael, E., On the formaldehyde release of wood. *European Journal of Wood and Wood Products* **2000,** *58* (4), 259-264.
16. Short, P. H.; Lyon, D. E., Pressure-refined fiber from low-grade southern hardwoods. *Wood and Fiber Science* **2007,** *10* (2), 82-94.
17. Benthien, J. T.; Hasener, J.; Pieper, O.; Tackmann, O.; Bähnisch, C.; Heldner, S.; Ohlmeyer, M. In *Determination of MDF fiber size distribution: Requirements and innovative solution*, International Wood Composites Symposium, **2013**.
18. Tasooji, M.; Frazier, C. E., Physical, surface and rheological characterization of thermomechanical wood fiber. *Bioresource technology; submitted for publication* **2018**.
19. Sluiter, A.; Ruiz, R.; Scarlata, C.; Sluiter, J.; Templeton, D., Determination of extractives in biomass. *National Renewable Energy Laboratory, Laboratory Analytical Procedure (LAP), NREL/TP-510-42619* **2008**.

20. Sluiter, A.; Hames, B.; Ruiz, R.; Scarlata, C.; Sluiter, J.; Templeton, D.; Crocker, D., Determination of structural carbohydrates and lignin in biomass. *Laboratory analytical procedure NREL/TP-510-42618* **2011,** *1617*, 1-16.
21. Fras, L.; Laine, J.; Stenius, P.; Stana-Kleinschek, K.; Ribitsch, V.; Doleček, V., Determination of dissociable groups in natural and regenerated cellulose fibers by different titration methods. *Journal of Applied Polymer Science* **2004,** *92* (5), 3186-3195.
22. Ohra-Aho, T.; Gomes, F.; Colodette, J.; Tamminen, T., S/G ratio and lignin structure among Eucalyptus hybrids determined by Py-GC/MS and nitrobenzene oxidation. *Journal of analytical and applied pyrolysis* **2013,** *101*, 166-171.
23. Iiyama, K.; Lam, T. B. T., Lignin in wheat internodes. Part 1: The reactivities of lignin units during alkaline nitrobenzene oxidation. *Journal of the Science of Food and Agriculture* **1990,** *51* (4), 481-491.
24. Katahira, R.; Nakatsubo, F., Determination of nitrobenzene oxidation products by GC and 1 H-NMR spectroscopy using 5-iodovanillin as a new internal standard. *Journal of wood science* **2001,** *47* (5), 378-382.
25. Chen, C.-L., Characterization of lignin by oxidative degradation: use of gas chromatography-mass spectrometry technique. *Methods in Enzymology* **1988,** *161*, 110-136.
26. Tasooji, M.; Frazier, C. E., Simple milligram-scale extraction of formaldehyde from wood. *ACS Sustainable Chemistry & Engineering* **2016,** *4* (9), 5041-5045.
27. Tasooji, M.; Wan, G.; Lewis, G.; Wise, H.; Frazier, C. E., Biogenic formaldehyde: Content and heat generation in the wood of three tree species. *ACS Sustainable Chemistry & Engineering* **2017,** *5* (5), 4243-4248.
28. Segal, L.; Creely, J.; Martin Jr, A.; Conrad, C., An empirical method for estimating the degree of crystallinity of native cellulose using the X-ray diffractometer. *Textile Research Journal* **1959,** *29* (10), 786-794.
29. Park, S.; Baker, J. O.; Himmel, M. E.; Parilla, P. A.; Johnson, D. K., Cellulose crystallinity index: measurement techniques and their impact on interpreting cellulase performance. *Biotechnology for biofuels* **2010,** *3* (1), 10.
30. French, A. D., Idealized powder diffraction patterns for cellulose polymorphs. *Cellulose* **2014,** *21* (2), 885-896.
31. Chowdhury, S.; Fabiyi, J.; Frazier, C. E., Advancing the dynamic mechanical analysis of biomass: comparison of tensile-torsion and compressive-torsion wood DMA. *Holzforschung* **2010,** *64* (6), 747-756.
32. Chowdhury, S.; Frazier, C. E., Compressive-torsion DMA of yellow-poplar wood in organic media. *Holzforschung* **2013,** *67* (2), 161-168.
33. Mansfield, S. D.; Kim, H.; Lu, F.; Ralph, J., Whole plant cell wall characterization using solution-state 2D NMR. *Nature protocols* **2012,** *7* (9), 1579.
34. Josefsson, T.; Lennholm, H.; Gellerstedt, G., Steam explosion of aspen wood. Characterisation of reaction products. *Holzforschung* **2002,** *56* (3), 289-297.
35. Josefsson, T.; Lennholm, H.; Gellerstedt, G., Changes in cellulose supramolecular structure and molecular weight distribution during steam explosion of aspen wood. *Cellulose* **2001,** *8* (4), 289-296.
36. Li, J.; Henriksson, G.; Gellerstedt, G., Carbohydrate reactions during high-temperature steam treatment of aspen wood. *Applied biochemistry and biotechnology* **2005,** *125* (3), 175.
37. Avellar, B. K.; Glasser, W. G., Steam-assisted biomass fractionation. I. Process considerations and economic evaluation. *Biomass and Bioenergy* **1998,** *14* (3), 205-218.
38. Shao, S.; Wen, G.; Jin, Z., Changes in chemical characteristics of bamboo (Phyllostachys pubescens) components during steam explosion. *Wood science and technology* **2008,** *42* (6), 439.
39. Zhang, L.; Wang, T.; Jiao, S.; Hao, C.; Mao, Z., Effect of steam-explosion on biodegradation of lignin in wheat straw. *Bioresource technology* **2008,** *99* (17), 8512-8515.

40. Martin-Sampedro, R.; Capanema, E. A.; Hoeger, I.; Villar, J. C.; Rojas, O. J., Lignin changes after steam explosion and laccase-mediator treatment of eucalyptus wood chips. *Journal of agricultural and food chemistry* **2011,** *59* (16), 8761-8769.
41. M.J. Chung, M.; Wang, S. Y., Effects of peeling and steam-heating treatment on basic properties of two types of bamboo culms (Phyllostachys makinoi and Phyllostachys pubescens). *Journal of Wood Science* **2017,** *63* (5), 473-482.
42. Zhao, R.; Jiang, Z.; Hse, C.; Shupe, T., Effects of steam treatment on bending properties and chemical composition of moso bamboo (Phyllostachys pubescens). *Journal of Tropical Forest Science* **2010**, 197-201.
43. Chen, P. Y.; Workman, E. C., Effect of steaming on some physical and chemical properties of black walnut heartwood. *Wood and Fiber Science* **2007,** *11* (4), 218-227.
44. Roffael, E.; Dix, B.; Schneider, T., Thermomechanical (TMP) and chemo-thermomechanical pulps (CTMP) for medium density fibreboards (MDF). *Holzforschung* **2001,** *55* (2), 214-218.
45. Wang, P.; Fu, Y.; Shao, Z.; Zhang, F.; Qin, M., Structural changes to aspen wood lignin during autohydrolysis pretreatment. *BioResources* **2016,** *11* (2), 4086-4103.
46. Robert, D.; Gellerstedt, G.; Bardet, M., Carbon-13 NMR analysis of lignins obtained after sulfonation of steam exploded aspen wood. *Nordic Pulp Pap. Res. J* **1986,** *1* (3), 18-25.
47. Lora, J.; Wayman, M., Delignification of hardwoods by autohydrolysis and extraction. *Tappi [Technical Association of the Pulp and Paper Industry]* **1978,** *61* (6), 47-50.
48. Kisonen, V.; Xu, C.; Bollström, R.; Hartman, J.; Rautkoski, H.; Nurmi, M.; Hemming, J.; Eklund, P.; Willför, S., O-acetyl galactoglucomannan esters for barrier coatings. *Cellulose* **2014,** *21* (6), 4497-4509.
49. Sjostrom, E., *Wood chemistry: fundamentals and applications*. Elsevier: **2013**.
50. Dumitriu, S., *Polysaccharides: structural diversity and functional versatility*. CRC press: **2004**.
51. Koshijima, T.; Watanabe, T., *Association between lignin and carbohydrates in wood and other plant tissues*. Springer Science & Business Media: **2013**.
52. MYu, B.; Capanema, E., A fraction of MWL with high concentration of lignin–carbohydrate linkages: isolation and analysis with 2D NMR spectroscopic techniques. *Holzforschung* **2007,** *61*, 1-7.
53. Li, J.; Henriksson, G.; Gellerstedt, G., Lignin depolymerization/repolymerization and its critical role for delignification of aspen wood by steam explosion. *Bioresource technology* **2007,** *98* (16), 3061-3068.
54. Xing, C.; Zhang, S.; Deng, J.; Riedl, B.; Cloutier, A., Medium-density fiberboard performance as affected by wood fiber acidity, bulk density, and size distribution. *Wood science and technology* **2006,** *40* (8), 637-646.
55. Das, K.; Ray, D.; Bandyopadhyay, N.; Sengupta, S., Study of the properties of microcrystalline cellulose particles from different renewable resources by XRD, FTIR, nanoindentation, TGA and SEM. *Journal of Polymers and the Environment* **2010,** *18* (3), 355-363.
56. Sarkanen, K. V.; Ludwig, C. H., *Liguins. Occurrence, formation, structure, and reactions*. New York.; Wiley-Interscience: **1971**.
57. Heitner, C.; Dimmel, D.; Schmidt, J., *Lignin and lignans: advances in chemistry*. CRC press: **2016**.
58. Leopold, B., Aromatic keto-and hydroxy-polyethers as lignin models. III. *Acta Chem. Scand* **1950,** *4*, 1523-1537.
59. Chan, F. D.; Nguyen, K. L.; Wallis, A. F., Contribution of lignin sub-structures to nitrobenzene oxidation products. *Journal of wood chemistry and technology* **1995,** *15* (3), 329-347.
60. Sturgeon, M. R.; Kim, S.; Lawrence, K.; Paton, R. S.; Chmely, S. C.; Nimlos, M.; Foust, T. D.; Beckham, G. T., A mechanistic investigation of acid-catalyzed cleavage of aryl-ether linkages: Implications for lignin depolymerization in acidic environments. *ACS Sustainable Chemistry & Engineering* **2013,** *2* (3), 472-485.

61. Lahive, C. W.; Deuss, P. J.; Lancefield, C. S.; Sun, Z.; Cordes, D. B.; Young, C. M.; Tran, F.; Slawin, A. M.; de Vries, J. G.; Kamer, P. C., Advanced model compounds for understanding acid-catalyzed lignin depolymerization: Identification of renewable aromatics and a lignin-derived solvent. *Journal of the American Chemical Society* **2016,** *138* (28), 8900-8911.
62. Wan, G.; Frazier, C. E., Lignin acidolysis predicts formaldehyde generation in pine wood. *ACS Sustainable Chemistry & Engineering* **2017,** *5* (6), 4830-4836.
63. Imai, T.; Yokoyama, T.; Matsumoto, Y., Revisiting the mechanism of β-O-4 bond cleavage during acidolysis of lignin IV: Dependence of acidolysis reaction on the type of acid. *Journal of wood science* **2011,** *57* (3), 219-225.
64. Yokoyama, T.; Matsumoto, Y., Revisiting the mechanism of β-O-4 bond cleavage during acidolysis of lignin. Part 1: Kinetics of the formation of enol ether from non-phenolic C6-C2 type model compounds. *Holzforschung* **2008,** *62* (2), 164-168.
65. Yasuda, S.; Adachi, K.; Terashima, N.; Ota, K., Chemical structures of sulfuric acid lignin, 8: Reactions of 1, 2-diaryl-1, 3-propanediol and pinoresinol with sulfuric acid. *Journal of the Japan Wood Research Society (Japan)* **1985**.
66. Myers, G. E., Mechanisms of formaldehyde release from bonded wood products. ACS Publications: **1986**, pp 87-106.
67. Meyer, B.; Andrews, B. K.; Reinhardt, R. M., *Formaldehyde release from wood products*. ACS Publications: **1986**.
68. Shuai, L.; Amiri, M. T.; Questell-Santiago, Y. M.; Héroguel, F.; Li, Y.; Kim, H.; Meilan, R.; Chapple, C.; Ralph, J.; Luterbacher, J. S., Formaldehyde stabilization facilitates lignin monomer production during biomass depolymerization. *Science* **2016,** *354* (6310), 329-333.
69. Shuai, L.; Amiri, M. T.; Luterbacher, J. S., The influence of interunit carbon–carbon linkages during lignin upgrading. *Current Opinion in Green and Sustainable Chemistry* **2016,** *2*, 59-63.
70. Dong, L.; Yu, Y.; Li, C.; So, S.; Tittel, F. K., Ppb-level formaldehyde detection using a CW room-temperature interband cascade laser and a miniature dense pattern multipass gas cell. *Optics Express* **2015,** *23* (15), 19821-19830.
71. Shimizu, K.; Sudo, K.; Ono, H.; Ishihara, M.; Fujii, T.; Hishiyama, S., Integrated process for total utilization of wood components by steam-explosion pretreatment. *Biomass and Bioenergy* **1998,** *14* (3), 195-203.
72. Li, J.; Gellerstedt, G., Improved lignin properties and reactivity by modifications in the autohydrolysis process of aspen wood. *Industrial Crops and Products* **2008,** *27* (2), 175-181.
73. Attack, D., On the characterisation of pressurized refiner mechanical pulps. *Svensk Papperstid* **1972,** *75* (3), 89-94.
74. Higgins, H.; Irvine, G.; Puri, V.; Wardrop, A., Conditions for obtaining optimum properties of radiata and slash pine thermomechanical and chemithermomechanical pulps. *Appita* **1978,** *32* (1), 22-33.
75. Chowdhury, S.; Frazier, C. E., Thermorheological complexity and fragility in plasticized lignocellulose. *Biomacromolecules* **2013,** *14* (4), 1166-1173.
76. Stokke, D. D.; Wu, Q.; Han, G., Consolidation Behavior of Lignocellulosic Materials. *Introduction to Wood and Natural Fiber Composites* **2013**, 85-127.
77. Winistorfer, P. M.; Moschler, W. W.; Wang, S.; DePaula, E.; Bledsoe, B. L., Fundamentals of vertical density profile formation in wood composites. Part I. In-situ density measurement of the consolidation process. *Wood and fiber science* **2007,** *32* (2), 209-219.
78. Wayman, M.; Lora, J., Aspen autohydrolysis: the effects of 2-naphthol and othe aromatic compounds. *Tappi Tech Assoc Pulp Paper Ind* **1978,** *61* (6), 55-57.

79. Chua, M. G.; Wayman, M., Characterization of autohydrolysis aspen (P. tremuloides) lignins. Part 1. Composition and molecular weight distribution of extracted autohydrolysis lignin. *Canadian Journal of Chemistry* **1979,** *57* (10), 1141-1149.
80. Robert, D.; Bardet, M.; Lapierre, C.; Gellerstedt, G., Structural changes in aspen lignin during steam explosion treatment. *Cellulose chemistry and technology* **1988,** *22* (2), 221-230.
81. Olsson, A.-M.; Bjurhager, I.; Gerber, L.; Sundberg, B.; Salmén, L., Ultra-structural organisation of cell wall polymers in normal and tension wood of aspen revealed by polarisation FTIR microspectroscopy. *Planta* **2011,** *233* (6), 1277-1286.
82. Chowdhury, S.; Madsen, L. A.; Frazier, C. E., Probing alignment and phase behavior in intact wood cell walls using 2H NMR spectroscopy. *Biomacromolecules* **2012,** *13* (4), 1043-1050.
83. Stevanic, J. S.; Salmén, L., Orientation of the wood polymers in the cell wall of spruce wood fibres. *Holzforschung* **2009,** *63* (5), 497-503.
84. Prime, R., *Thermal Characterization of Polymeric Materials (EA Turi, ed.), Chapter 6- Thermosets*. Academic Press: San Diego, **1997**.
85. Shuai, L.; Yang, Q.; Zhu, J.; Lu, F.; Weimer, P.; Ralph, J.; Pan, X., Comparative study of SPORL and dilute-acid pretreatments of spruce for cellulosic ethanol production. *Bioresource Technology* **2010,** *101* (9), 3106-3114.
86. Tokimatsu, T.; Umezawa, T.; Shimada, M., Synthesis of Four Diastereomeric Lignin Carbohydrate Complexes (LCC) Model Compounds Composed of a ß-O-4 Lignin Model Linked to Methyl ß-D-Glucoside. *Holzforschung-International Journal of the Biology, Chemistry, Physics and Technology of Wood* **1996,** *50* (2), 156-160.
87. Yuan, T.-Q.; Sun, S.-N.; Xu, F.; Sun, R.-C., Characterization of lignin structures and lignin–carbohydrate complex (LCC) linkages by quantitative 13C and 2D HSQC NMR spectroscopy. *Journal of agricultural and food chemistry* **2011,** *59* (19), 10604-10614.

Chapter 4 Thermosetting resin/fiber interactions impacted by thermomechanical refining energy

Mohammad Tasooji and Charles E. Frazier *

Sustainable Biomaterials, Virginia Tech, Cheatham Hall, RM 230 West Campus Drive, Blacksburg, Virginia 24061, United States

Macromolecules Innovation Institute, Virginia Tech, ICTAS II, 240 West Campus Drive, Blacksburg, Virginia 24061, United States

4.1. Abstract

As part of an industry/university cooperation, a North American medium density fiberboard (MDF) plant was the setting to study refining energy effects on fiber/amino resin interaction, using differential scanning calorimetry (DSC) and X-ray diffraction (XRD). All fiber types, refined and unrefined, caused only a slight increase in melamine-urea-formaldehyde (MUF) resin reactivity. Generally, all fiber types decreased the enthalpy of MUF cure, suggesting fiber absorption of small reactive species. But DSC did not reveal any dependency on fiber refining energy. According to XRD, all fiber types reduced crystallinity in cured MUF, more so with refined fiber, but independent of refining energy. The crystallinity in cured urea-formaldehyde resin was studied with one fiber type (highest refining energy); it caused a reduction in crystallinity that was cure temperature dependent. This suggests that resin crystallinity could vary through the thickness of an MDF panel, with possible effects on bond-line strength and formaldehyde emission (hydrolytic stability).

KEYWORDS: Thermomechanical refining, Medium density fiberboard, Amino resin cure behavior, Amino resin crystallinity,

4.2. Introduction

When cured in the presence of wood or wood fiber, the structure and properties of thermosetting resins are substantially different from when they are cured alone[1-12]. Such wood/resin interactions may be attributable to many effects, including fiber absorption of

water (or other solvents)[10], and also resin monomers, dimers, and trimers. Wood/fiber acidity and buffering capacity can interfere with resin catalysis[3, 10-11] , and specific fiber/resin secondary interactions could alter localized resin-network structures, perhaps even affecting the incidence of primary fiber/resin bonding. In fiber composites like medium density fiberboard (MDF), the potential for fiber/resin interactions is likely greater, and probably the most difficult to study because of variations in refining. For instance, in prior work we studied the influence of refining energy on Douglas fir (*Pseudotsuga menziesii*) fiber dimensions and acidity, surface area and porosity, surface and bulk chemistry, as well as crystallinity and rheology [13-14]. Many of these properties were affected by refining energy, but in a comparable effort, not using Douglas fir, Short and Lyon found that refining energy only affected fiber size and bulk density[15]. The discrepancy speaks to a practical challenge in MDF research: it is very difficult to relate pilot-scale refining (as for Short and Lyon[15]) to industrial practice, and critical aspects of processing vary substantially among industrial producers. In other words, wood fiber-based composites like MDF are the most technologically and scientifically complex wood-based composites. Consequently, this work represents an industry/university cooperation to determine whether and how fiber/resin interactions are affected by refining energy (kW•h/ton of fiber). The context for this study was an industrial MDF production facility processing Douglas fir; and the principal experimental variable was refining energy via changes in refiner-plate gap settings. This publication addresses how fiber refining energy affects amino resin cure and crystallinity.

4.3. Experimental

Materials

Douglas fir (*Pseudotsuga menziesii)* refined and unrefined samples were collected at Arauco's MDF production facility in Eugene, Oregon, U.S.A. Normal production at this facility uses Douglas fir particles (30% shavings, 70% sawdust) softened in a steam digester (0.77 MPa, 174°C, 3.5 min retention time). Steam digested material is sprayed with additives (urea and wax), then fed into a Sprout-Bauer SB150 thermomechanical refiner (0.77 MPa, 174°C, 1800 revolutions per min; disk configuration: spiral, 152 cm diameter). After passing through the

plant drying system, the fibers are resinated, formed and hot-pressed. For this research, additive inlet valves were closed and fiber was processed so as to clear additives from the system. Once clear of additives, and after the drying stage, fiber sampling occurred in an emergency fiber-dump section (a fire safety feature of the plant). Collected specimens had a moisture content of 5-6% (wet basis), and were identified as 188 and 349 corresponding to the refining energies used: 188 and 349 kW•h/ton. These refining energies (adjusted by changing the refiner-plate gap) are the practical range for production at this facility; the low and high refining energies produce "low" and "high" quality fiber as needed for commercial production. Unrefined control specimens (identified as DF; moisture content ~25%) were sampled from the production feedstock. All samples were collected in one day and sample preparation (below) started on the following day. Besides two different refining energies, all other production parameters were fixed. Fiber specimens were free of adhesive and additives.

Melamine-urea-formaldehyde (MUF, 65% solid content, F/U+M mole ratio=0.90, pH=8.0-8.8, 2% melamine based in liquid weight) and urea-formaldehyde (UF, 65% solid content, F:U mole ratio=0.95, pH=7.5-8.5) were industrial resins used in MDF production.

Fiber sample preparation

The unrefined sample (DF) was vacuum dried (0.10 mmHg, 25°C, overnight), ground by a Wiley mill, screened (18-80 mesh) and vacuum dried (0.10 mmHg, 25°C, overnight). Refined samples (188, 349) were not milled, but similarly screened and dried as described. All samples were then sealed/stored at room temperature.

Fiber acidity and buffering capacity

A Metrohm 905 titrando autotitrator was used. The pH probe (Syntrode with Pt 1000) was calibrated using Fisher Scientific buffer solutions (pH of 2, 4, 7 and 10). Vacuum dried, un-extracted sample (0.5 g) was placed in saline water (1mM NaCl, 300 mL) and stirred under N_2. Initial pH was measured after the suspension was equilibrated (10 min). Using separate samples acid and alkaline buffering capacities were respectively determined by adding NaOH (0.02 M) and HCl (0.02 M) until the suspension pH reached 10 or 3.

Preparation of resin/fiber mixtures

"Filtered mixtures" refer to resin/fiber mixtures, where fiber was removed by filtration, and the collected resin was analyzed in the absence of fiber. "Unfiltered mixtures" refer to resin/fiber mixtures, analyzed as mixtures of resin plus fiber. Filtered mixtures were only prepared with the MUF resin:

MUF (10 g) was added to fiber (0.5 g) in a vial, mixed using a glass rod, and vacuum was applied (50mBar, 45 min) opened to atmospheric pressure, and the contents were centrifuged (5000 rpm, 10 min), then filtered (Nylon syringe filter, 1 µm pore size) to collect the resin for analysis. Unfiltered mixtures (5 g of resin added to 0.5 g of fiber) were simply mixed with a glass rod without use of vacuum impregnation. Filtered mixtures and unfiltered mixtures are identified with resin/fiber designations such as MUF/DF (MUF resin and unrefined fiber), MUF/188 (MUF resin and fiber refined at 188kW•h/ton), and UF/349 (UF resin and fiber refined at 349 kW•h/ton). Neat resins (without fiber) were typically also subjected to filtration as a control treatment, and are referred to as "neat resin-filtered", otherwise they are identified as "neat resin-unfiltered."

Resin cure

A TA Instruments Discovery differential scanning calorimeter (DSC) was used with specimens in hermetic pans or high volume pans. Hermetic pans were used when greater accuracy was desired, as for low enthalpy curing events (melamine cure, defined below), and for precise determination of the onset of the major MUF resin curing event. For each of these cases, 2-5 mg of sample (neat resin-filtered; or filtered mixture) was sealed in a hermetic pan and analyzed (isothermal at 30°C for 5min, 30-120°C, 3°C/min). High volume pans were used to measure the total enthalpy of MUF cure, and the kinetics of this event: 25-30 mg of sample (neat resin-filtered; or filtered mixture) was sealed in a high volume pan and analyzed for enthalpy (isothermal at 30°C for 5min, 30-160°C, 3°C/min), or for kinetics (heat to 175°C, with heating rates of 2, 5, 8, 10 and 12°C/min). Activation energy calculations were conducted as described in ASTM E698-11 standard[16] (Appendix F). The DSC was calibrated for both hermetic and high volume pans using indium standard. TA instruments Trios v3.2.0 software was used for

data collection and calculations. Cure onset (major endotherm using hermetic pans) was defined as the temperature at which the extended baseline from melamine cure intersected the straight line defined by the leading edge of the major endotherm.

Resin crystallinity

A D8 Bruker XRD with a Cu Kα radiation source (λ = 0.154 nm) generated at 40 kV and 40 mA was used. 2theta scan was performed from 10 to 50° at a scan speed of 2.4 °/min, a 1 mm slit. Sample (~1 g, MUF filtered mixture, or MUF unfiltered mixture, or UF unfiltered mixture, or MUF neat resin-filtered or unfiltered, or UF neat resin-unfiltered) was spread on a petri dish, cured (UF neat resin-unfiltered or UF unfiltered mixture: 100°C, 5 h and 170°C, 10 min, for MUF neat resin-filtered or MUF filtered mixture, or MUF unfiltered mixture: 100°C, 5 h), cooled in a desiccator and ground using mortar and pestle. Ground sample was flattened on a quartz slide (1-2 mm thickness) to collect the diffraction profile. Bruker DIFRAC plus EVA software was used for data collection.

4.4. Results and discussion

Previously, we showed that increasing refining energy from 188 to 349 kW•h/ton, reduced fiber size, increased porosity and specific surface area, and also changed fiber surface chemistry[13]. Refining also caused changes in bulk fiber chemistry, with substantial polysaccharide degradation and increasing fiber acidity, more so at higher refining energy. Lignin acidolysis was also caused by refining, reducing β-O-4 linkages, increasing free phenols, and generating formaldehyde; but lignin repolymerization did not occur [14]. These refining effects are consequential and could be expected to alter fiber/resin interactions. When studying fiber/MUF resin interactions via differential scanning calorimetry (DSC), it was necessary to use both hermetic and high volume sample pans, Figure 4-1. When using hermetic pans (left axis of Figure 4-1), MUF resins exhibited two curing endotherms, a small event near 74°C (for convenience referred to as “melamine cure”) and a large event with onset near 100°C. Consequently, hermetic pans were used to measure the enthalpy of melamine cure, and the onset temperature of the major endotherm. In contrast, analysis with high volume pans (right

axis of Figure 4-1) did not resolve two endotherms, and this method was used to measure the total enthalpy of MUF cure, and the kinetics.

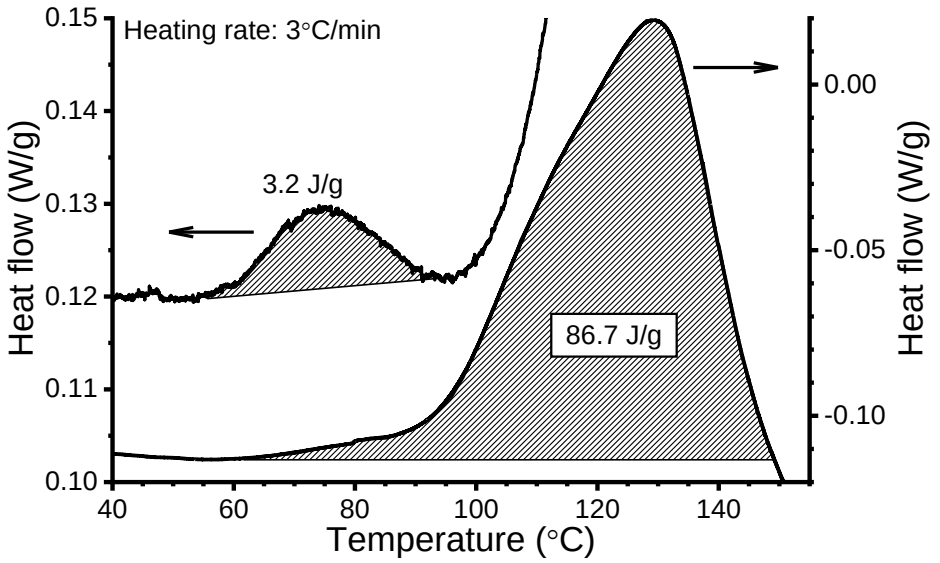

Figure 4-1. Example DSC thermograms for neat resin (MUF resin-filtered) using hermetic sample pans (left axis) and high volume pans (right axis); endotherm enthalpies indicated. Hermetic pans were used to measure the enthalpy of the minor endotherm (melamine cure, see text) and the onset of the major endotherm; high volume pans were used to measure the total enthalpy of cure, and well as the kinetics

Figure 4-2 summarizes the enthalpies and cure onset measured in MUF (neat resin-filtered) and in MUF filtered mixtures (fiber removed). Regarding the enthalpy of melamine cure, and relative to neat resin, the unrefined fiber (MUF/DF) had no significant impact, whereas the refined fibers did; but the enthalpy reductions were independent of refining energy (MUF/188, MUF/349). As for the total enthalpy, relative to neat resin all fiber types caused a reduction, but the effects of refining energy were unclear. Similarly for the cure onset (major endotherm using hermetic pans), all fiber types reduced the onset, but the effects of refining were not significant (statistical labels in Figure 4-2 using 95% confidence level). Decreases in resin cure enthalpy in the presence of wood have been reported for UF[10] and

phenol formaldehyde (PF)[17] resins; which is generally consistent with findings for all fiber types used here.

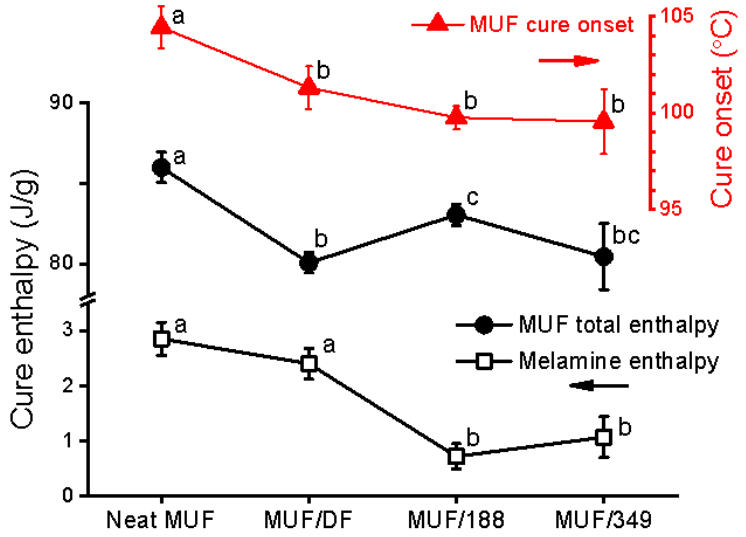

Figure 4-2. Cure enthalpies and onset temperatures for neat MUF resin-filtered, and for filtered mixtures (no fiber) using unrefined fiber (MUF/DF) and refined fiber (MUF/188, MUF/349). Error bars represent ± 1 standard deviation; n=3; lower case statistical labels according to 95% confidence.

Not shown is that none of the fiber types, refined or unrefined, affected cure kinetics; all measurements revealed an activation energy of about 102 kJ/mole, which is contrast to other similar reports [2, 4, 7-8]. According to the cure onset data, the addition of any fiber seems to have caused only a very slight increase in reactivity (which is not consistent with the literature [1, 3, 10-11]). This is unexpected since refining increased acidity (catalytic for MUF), and more so at the highest refining energy, Table 4-1. On the other hand, the acid catalytic effect may have been offset by the measured increase in alkaline buffering capacity (the resistance to added HCl), Table 4-1. Relative to the neat resin, the reductions in cure enthalpy imply a reduced degree of resin cure (a major reduction in enthalpy might suggest a fundamental change in resin character; but that did not happen- the activation energy of cure was unaffected by any fiber type). It is not clear how water absorption into fiber would reduce the enthalpy of cure. Instead, the absorption of very low molecular weight resin might alter the resin stoichiometry

and reduce the enthalpy of cure. Under this scenario the melamine enthalpy might be dominated by highly reactive, low molecular weight compounds, because refined samples exhibited an increase in sub-micron scale porosity [13] and the melamine enthalpy was the only cure parameter clearly affected by refining. Besides the absorption of water and/or low molecular weight resin into fiber, the reaction between lignin phenols and/or fiber extractives could affect resin cure [10]. Consequently, the higher free phenol levels in refined fiber (due to lignin acidolysis [18]) might also explain the changes in MUF cure observed here. Refining also increased the formaldehyde content of the fiber (measured at ~0.89 μmol/g fiber [14]), but the formaldehyde mole ratio (resin/fiber) in the DSC specimens was at least 180,000, suggesting that fiber formaldehyde would have no detectable impact on resin cure.

Table 4-1. Fiber pH, acid and alkaline buffering capacities of refined (188 and 349) and unrefined (DF) samples. Standard deviations in parentheses; n=10 for pH and 2 for buffering capacities.

Specimen	pH	Acid buffering capacity (mmol of NaOH/g sample)	Alkaline buffering capacity (mmol of NaOH/g sample)
DF	6.01 (0.01)	0.42 (0.00)	0.77 (0.00)
188	5.84 (0.01)	0.45 (0.00)	0.79 (0.00)
349	5.80 (0.01)	0.44 (0.00)	0.80 (0.00)

The amino resins used to manufacture MDF exhibit crystallinity in the cured state, and fiber/resin interactions might be expected to affect this important property. Once cured, MUF neat resin-filtered exhibited a major X-ray diffraction (XRD) peak at 2θ=22.75° with less pronounced peaks at 25°, 32°, and 42°, similar to what has been reported for UF [9, 19-21]. The MUF used here contained only 2% melamine (on total wet resin mass), so XRD similarity to that published for UF is reasonable. In UF resins, crystallinity in the cured state is promoted by lower F:U mole ratios [5, 20-25], which are recently the overwhelming industrial trend to reduce formaldehyde emissions. Qualitatively relative to neat MUF, Figure 4-3 shows that 2θ peaks at 22.75° and 25° were reduced in intensity for MUF/DF, and more so for MUF/188 and MUF/349.

Furthermore, the peaks at 2θ =32° and 42° were substantially reduced in both refined samples (MUF/188 and MUF/349). Note that these were MUF filtered mixtures, and no wood fiber was present during XRD.

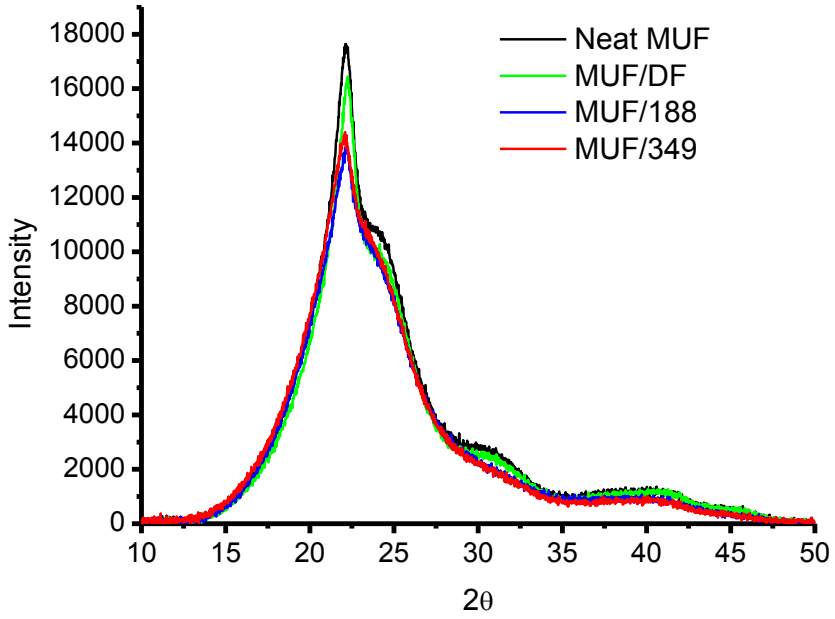

Figure 4-3. XRD 2θ scans of cured resin specimens: neat MUF resin-filtered, and MUF filtered mixtures (no fiber) using unrefined fiber (MUF/DF) and refined fiber (MUF/188, MUF/349). One measurement of three is shown.

In Figure 4-4, the XRD of MUF/349-unfiltered mixture is compared to MUF/349-filtered mixture (respectively scanned with and without fiber present). When fiber was present during XRD, cellulose I peaks were detectable near 2θ = 15° and 34°, and the major peak at 2θ = 23° was buried within the major MUF signal. Otherwise, the MUF signals were quite similar for the respective specimens where MUF/349-unfiltered mixture exhibited reduced intensity at 2θ = 22.75° and 25°. The crystallinity reductions shown in Figures 4-3 and 4-4 might have arisen from fiber absorption effects mentioned previously, but specific secondary interactions with fiber surfaces could also play a role. Previously we showed that 188 fiber surfaces were more hydrophobic than unrefined fiber (DF), and that the greater damage imposed upon 349 fiber

may have exposed a greater number of high energy surface sites [13]. Whatever the true cause, it is apparent that fiber can reduce resin crystallinity and that the effect appears to have a dependence on refining energy. These results are consistent with other reports [5-6, 9] however Pizzi reported that UF resins became completely amorphous when cured in the presence of wood [26].

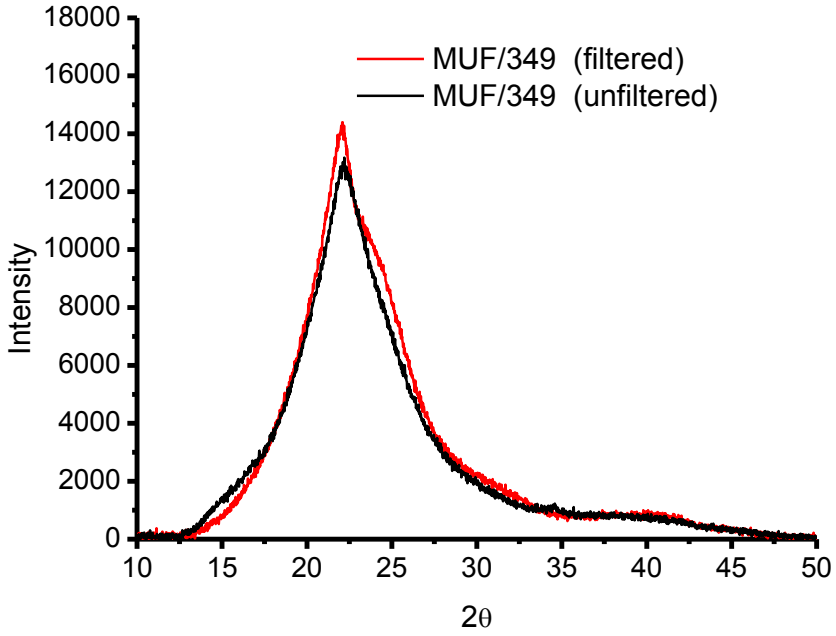

Figure 4-4. XRD 2θ scans of cured resins: MUF/349-filtered (no fiber) and MUF/349-unfiltered (with fiber present). One measurement of three is shown.

Figure 4-5 shows XRD scans for neat UF resin-unfiltered, and for UF/349 unfiltered mixture prepared with two different curing conditions: 1) at 170°C for 10 min, and 2) 100°C for 5 hours. The brief 170°C condition simulates hot-press exposure for MDF panel face layers (contacting the platen), whereas the prolonged 100°C condition simulates the central core layer (never as hot as the face layer) that remains hot for long periods after removal from the hot-press. Under both cure conditions, 349 fiber caused a reduction in UF resin crystallinity, and in the case of the 170°C condition it appeared as if the lattice spacings were also changed. Perhaps most notable is that the respective curing conditions resulted in substantially different degrees of crystallinity, suggesting that bondline properties will vary through the thickness of

an MDF panel, as suspected. We might also predict that MDF panel face layers will exhibit greater formaldehyde emission since the reduced crystallinity should allow greater access for moisture and resin hydrolysis. These results are generally consistent with prior reports [24]. It should be noted that for both specimens cured at 170°C, an unknown peak occurred at 2θ~27.5°. It is known that resin crystallinity can affect adhesive strength[9] and resin formaldehyde emission[19]. Effects such as low cross-link density[27], high brittleness[28], or high residual stress[29] can also reduce adhesion strength. Increasing the F/U mole ratio will increase crosslink density[27] and decrease crystallinity [21]. Under these scenarios, one could argue that increasing crystallinity could have positive or negative effects on adhesion strength and formaldehyde emissions[9 19-20], but a more detailed study would be required to determine this.

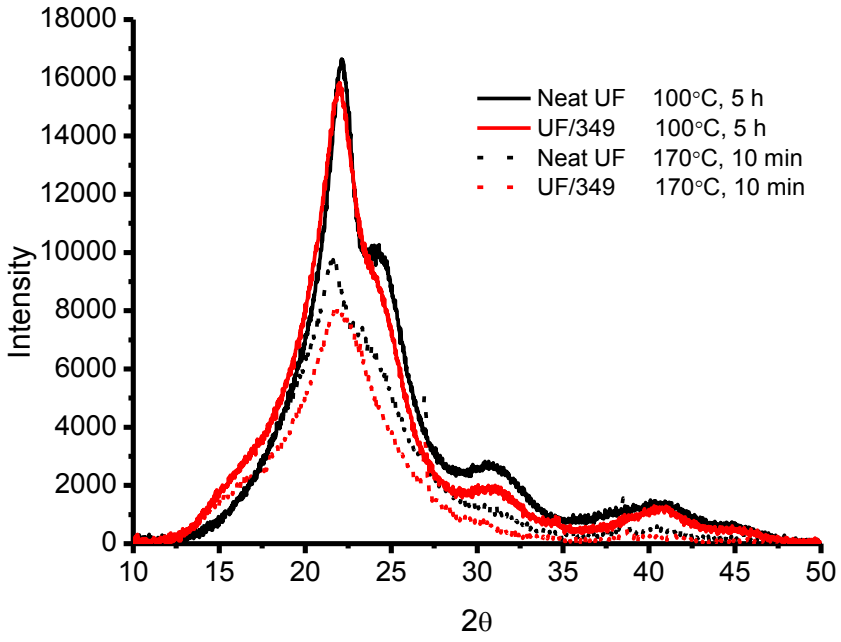

Figure 4-5. XRD 2θ scans of neat UF resin-unfiltered and UF/349 unfiltered mixture cured at 100°C, 5h and 170°C, 10 min. One measurement of two is shown.

4.5. Summary and conclusions

A North American medium density fiberboard (MDF) plant was the setting to study refining energy effects on fiber/amino resin interaction, using differential scanning calorimetry

(DSC) and X-ray diffraction (XRD). All fiber types, refined and unrefined, caused only a slight increase in melamine-urea-formaldehyde (MUF) resin reactivity. Generally, all fiber types decreased the enthalpy of MUF cure, suggesting fiber absorption of small reactive species. But DSC did not reveal any dependency on fiber refining energy. According to XRD, all fiber types reduced crystallinity in cured MUF, more so with refined fiber, but independent of refining energy. The crystallinity in cured urea-formaldehyde resin was studied with one fiber type (highest refining energy); it caused a crystallinity decrease that was cure temperature dependent. This suggests that resin crystallinity could vary through the thickness of an MDF panel, with possible effects on bond-line strength and formaldehyde emission (hydrolytic stability).

Acknowledgement

This project was supported by the Wood-Based Composites center, a National Science Foundation Industry/University Cooperative Research Center (Awards IIP-1035009 and IIP 1624536). Funding for this work was provided in part by the Virginia Agricultural Experiment Station and the McIntire Stennis Program of the National Institute of Food and Agriculture, U.S. Department of Agriculture. Special thanks are extended to the many collaborators at Arauco for providing samples and insight.

4.6. References

1. Gao, Z.; Wang, X. M.; Wan, H.; Liu, Y., Curing characteristics of urea–formaldehyde resin in the presence of various amounts of wood extracts and catalysts. *Journal of Applied Polymer Science* **2008,** *107* (3), 1555-1562.
2. He, G.; Yan, N., Effect of wood on the curing behavior of commercial phenolic resin systems. *Journal of applied polymer science* **2005,** *95* (2), 185-192.
3. Johns, W. E.; Niazi, K. A., Effect of pH and buffering capacity of wood on the gelation time of urea-formaldehyde resin. *Wood and fiber science* **2007,** *12* (4), 255-263.
4. Lee, Y.-K.; Kim, H.-J., Relationship between curing activation energy and free formaldehyde content in urea-formaldehyde resins. *Journal of Adhesion Science and Technology* **2013,** *27* (5-6), 598-609.
5. Levendis, D.; Pizzi, A.; Ferg, E., The correlation of strength and formaldehyde emission with the crystalline/amorphous structure of UF resins. *Holzforschung-International Journal of the Biology, Chemistry, Physics and Technology of Wood* **1992,** *46* (3), 263-269.
6. Nuryawan, A.; Singh, A. P.; Park, B.-D.; Causin, V., Micro-Morphological Features of Cured Urea-Formaldehyde Adhesives Detected by Transmission Electron Microscopy. *The Journal of Adhesion* **2016,** *92* (2), 121-134.
7. Pizzi, A.; Mtsweni, B.; Parsons, W., Wood-induced catalytic activation of PF adhesives autopolymerization vs. PF/wood covalent bonding. *Journal of applied polymer science* **1994,** *52* (13), 1847-1856.
8. Pizzi, A.; Panamgama, L., Diffusion hindrance vs. wood-induced catalytic activation of MUF adhesive polycondensation. *Journal of applied polymer science* **1995,** *58* (1), 109-115.
9. Singh, A. P.; Causin, V.; Nuryawan, A.; Park, B.-D., Morphological, chemical and crystalline features of urea–formaldehyde resin cured in contact with wood. *European Polymer Journal* **2014,** *56*, 185-193.
10. Xing, C.; Deng, J.; Zhang, S.; Riedl, B.; Cloutier, A., Differential scanning calorimetry characterization of urea–formaldehyde resin curing behavior as affected by less desirable wood material and catalyst content. *Journal of Applied Polymer Science* **2005,** *98* (5), 2027-2032.
11. Xing, C.; Zhang, S.; Deng, J., Effect of wood acidity and catalyst on UF resin gel time. *Holzforschung* **2004,** *58* (4), 408-412.
12. Schmidt, R. G.; Frazier, C. E., 13 C CP/MAS NMR as a direct probe of the wood-phenol formaldehyde adhesive bondline. *Wood and fiber science* **2007,** *30* (3), 250-258.
13. Tasooji, M.; Frazier, C. E., Physical, surface and rheological characterization of thermomechanical wood fiber. *Bioresource technology; submitted for publication* **2018**.
14. Tasooji, M.; Frazier, C. E., Lignin acidolysis without repolymerization during thermomechanical refining of Douglas fir wood. *ACS Sustainable Chemistry & Engineering; submitted for publication* **2018**.
15. Short, P. H.; Lyon, D. E., Pressure-refined fiber from low-grade southern hardwoods. *Wood and Fiber Science* **2007,** *10* (2), 82-94.
16. International, A., E698-11 Standard Test Method for Arrhenius Kinetic Constants for Thermally Unstable Materials Using Differential Scanning Calorimetry and the Flynn/Wall/Ozawa Method1. West Conshohocken, PA, **2011**.
17. He, G.; Riedl, B., Curing kinetics of phenol formaldehyde resin and wood-resin interactions in the presence of wood substrates. *Wood Science and Technology* **2004,** *38* (1), 69-81.
18. Lahive, C. W.; Deuss, P. J.; Lancefield, C. S.; Sun, Z.; Cordes, D. B.; Young, C. M.; Tran, F.; Slawin, A. M.; de Vries, J. G.; Kamer, P. C., Advanced model compounds for understanding acid-catalyzed lignin depolymerization: Identification of renewable aromatics and a lignin-derived solvent. *Journal of the American Chemical Society* **2016,** *138* (28), 8900-8911.

19. Park, B.-D.; Jeong, H.-W., Hydrolytic stability and crystallinity of cured urea–formaldehyde resin adhesives with different formaldehyde/urea mole ratios. *International Journal of Adhesion and Adhesives* **2011,** *31* (6), 524-529.
20. Park, B.-D.; Causin, V., Crystallinity and domain size of cured urea–formaldehyde resin adhesives with different formaldehyde/urea mole ratios. *European Polymer Journal* **2013,** *49* (2), 532-537.
21. Stuligross, J.; Koutsky, J. A., A morphological study of urea-formaldehyde resins. *The Journal of Adhesion* **1985,** *18* (4), 281-299.
22. Pratt, T. J.; Johns, W. E.; Rammon, R. M.; Plagemann, W. L., A novel concept on the structure of cured urea-formaldehyde resin. *The Journal of Adhesion* **1985,** *17* (4), 275-295.
23. Ferg, E.; Pizzi, A.; Levendis, D., 13C NMR analysis method for urea–formaldehyde resin strength and formaldehyde emission. *Journal of Applied Polymer Science* **1993,** *50* (5), 907-915.
24. Nuryawan, A.; Singh, A. P.; Zanetti, M.; Park, B.-D.; Causin, V., Insights into the development of crystallinity in liquid urea-formaldehyde resins. *International Journal of Adhesion and Adhesives* **2017,** *72*, 62-69.
25. Park, B.-D.; Frihart, C. R.; Yu, Y.; Singh, A. P., Hardness evaluation of cured urea–formaldehyde resins with different formaldehyde/urea mole ratios using nanoindentation method. *European Polymer Journal* **2013,** *49* (10), 3089-3094.
26. Pizzi, A., A molecular mechanics approach to the adhesion of urea-formaldehyde resins to cellulose. Part 1. Crystalline Cellulose I. *Journal of Adhesion Science and Technology* **1990,** *4* (1), 573-588.
27. Park, B. D.; Kim, J. W., Dynamic mechanical analysis of urea–formaldehyde resin adhesives with different formaldehyde-to-urea molar ratios. *Journal of applied polymer science* **2008,** *108* (3), 2045-2051.
28. Bolton, A.; Irle, M., Physical Aspects of Wood Adhesive Bond Formation with Formaldehyde Based Adhesives Part I. The Effect of Curing Conditions on the Physical Properties of Urea Formaldehyde Films. Walter de Gruyter, Berlin/New York: **1987**.
29. van Houts, J.; Bhattacharyya, D.; Jayaraman, K., Determination of residual stresses in medium density fibreboard. *Holzforschung* **2000,** *54* (2), 176-182.

Chapter 5 Conclusions and future work

Several analytical/synthetic and characterization tools were used to study the effect of refining energy on wood fiber physical and chemical characteristics; also the interaction between wood fibers and amino resins was investigated. These analyses were conducted to determine aspects of fiber quality that might impact MDF properties or process control efficiency, specific to a single industrial facility.

In Chapter 2 various physical properties of Douglas fir fibers were studied as well as the fiber surface chemistry; also a novel rheological method was developed for studying fiber compaction and densification. The highest refining energy produced smaller fiber dimensions, and increased fiber bulk density. Highest refining energy also increased the porosity and surface area of the fibers. Thermoporosimetry revealed increases in sub-micron scale porosity while (MIP) revealed porosity on a higher dimensional scale. BET gas adsorption and MIP were used for measuring the surface area. Inverse gas chromatography revealed changes in fiber surface chemistry. The lowest refining energy produced surfaces dominated by the effects of lignin and extractives. In contrast, the highest refining energy produced substantially more fiber damage and this perhaps resulted in more cellulose exposure, uncovering higher energy active sites. The rheological method appeared to reveal a mechano-sorptive effect and related aspects of fiber densification.

Chapter 3 focused on the effect of refining on fiber bulk chemistry and lignin chemistry was studied in detail. Refining caused substantial polysaccharide degradation and increased fiber acidity, more so at the highest energy. A corresponding crystallinity increase was observed, but with no dependence on refining energy. Lignin acidolysis was detected using nitrobenzene oxidation, conductometric titration of free phenols, and determination of formaldehyde. It was revealed that C3 cleavage was the dominant pathway in lignin acidolysis. Both dynamic mechanical analysis and thermogravimetric analysis showed that lignin condensation reactions did not occur during lignin acidolysis. This was a very interesting finding since it is well known that both repolymerization and depolymerization occur simultaneously during lignin acidolysis. 2D NMR HSQC showed that the reaction of benzyl cations with non-

lignin nucleophiles (carbohyrates) might be the reason for not observing lignin repolymerization.

Chapters 2 and 3 revealed changes in fiber physical and chemical characteristics because of refining. In Chapter 4 the interaction between fibers/resin was studied. It was found that the onset of cure for melamine portion of MUF was detectable. It was revealed that both unrefined and refined samples had effect on resin cure. Refining reduced the onset and enthalpy of MUF cure however no big difference was observed between two refining energies. Refining was shown to have no effect on the curing activation energy. The crystallinity of MUF resin was studied in two ways, 1) MUF was in contact with fiber then filtered and cured, and 2) MUF was in contact with fiber and cured without filtration. In both cases, cured neat MUF had higher crystallinity compared to cured MUF that was in contact with both unrefined and refined samples and in both cases refining reduced the MUF crystallinity more. In other words, both filtered and unfiltered MUF resins which were in contact with wood/fiber showed similar crystallinity results. Finally it was revealed that UF cured at higher temperature and shorter time had lower crystallinity than UF cured at lower temperature and longer time. The effect of fiber on UF crystallinity was similar to that on MUF.

The fiber characteristics measurements conducted in this research can lead to practical findings. For example wood formaldehyde measurement does suggest that on-line formaldehyde monitoring might be useful for real-time process control in all type of biomass processing. However it is not known how cleavage pathways in lignin acidolysis affect fiber properties; this topic will require much more research. Also it was found that repolymerization did not occur during lignin acidolysis which might suggest that lignin repolymerization and depolymerization reactions could be manipulated during refining and hot-pressing, which can be very practical for industrial applications.

Appendix A Thermoporosimetry

The relationship between pore diameter and freezing bound water depressed melting point temperature is described by the following Gibbs-Thomson equation [1]:

1) $$D = \frac{-4T_0\gamma_{ls}\cos\theta}{(T_0 - T_m)\rho H_f}$$

D is the average pore diameter, T_0 is the melting temperature of bulk water, T_m is the freezing bound water depressed melting point temperature, θ is the contact angle between ice and pore wall, γ_{ls} is the surface energy of ice/water interface, ρ is the water density, and H_f is the specific melting enthalpy of water.

Using differential scanning calorimetry, depressed melting point temperatures were set arbitrarily in an isothermal step scan procedure, Figure B-1. From each step the amount of melting freezing bound water was measured. First step (-30 to -20°C) was used for measuring the sensible heat (applied heat that was not used for melting the bound water) and it was assumed that no melting occurred at the first step.

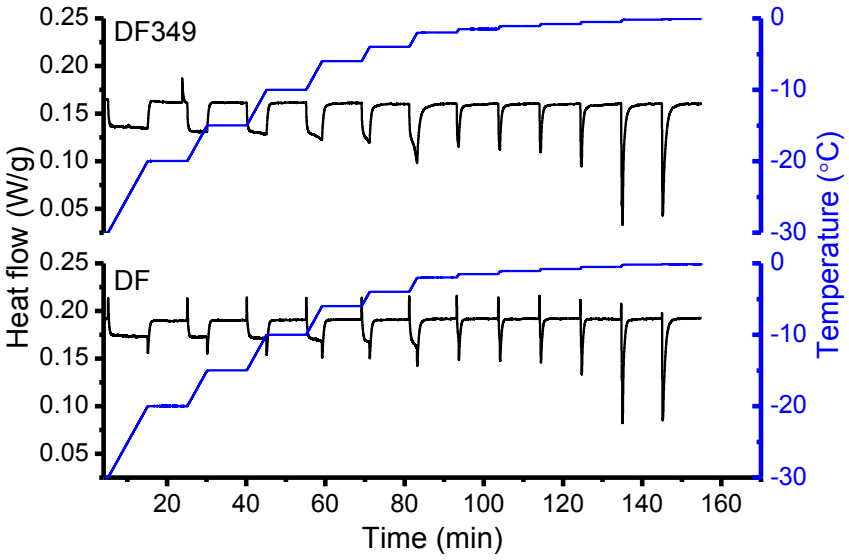

Figure 0-1. Example of isothermal step scan procedure used in differential scanning calorimetry. Top: DF349; bottom: DF. (DF has less porosity than DF349)

References

1. Park, S.; Venditti, R. A.; Jameel, H.; Pawlak, J. J., Changes in pore size distribution during the drying of cellulose fibers as measured by differential scanning calorimetry. *Carbohydrate polymers* **2006,** *66* (1), 97-103.

Appendix B BET gas adsorption

Specific surface area measurement

For measuring the specific surface area of vacuum dried and freeze dried samples Kr gas was used and for solvent-exchanged dried samples N_2 gas was used. The isotherm plots for vacuum dried sample using N_2 and Kr is shown in Figure C-1. As can be seen the shape of N_2 isotherm was not reasonable therefore Kr was used for measuring specific surface area of vacuum dried and freeze dried samples. Kr due to its lower vapor pressure than N_2 gas is more sensitive for measuring samples with low surface area.

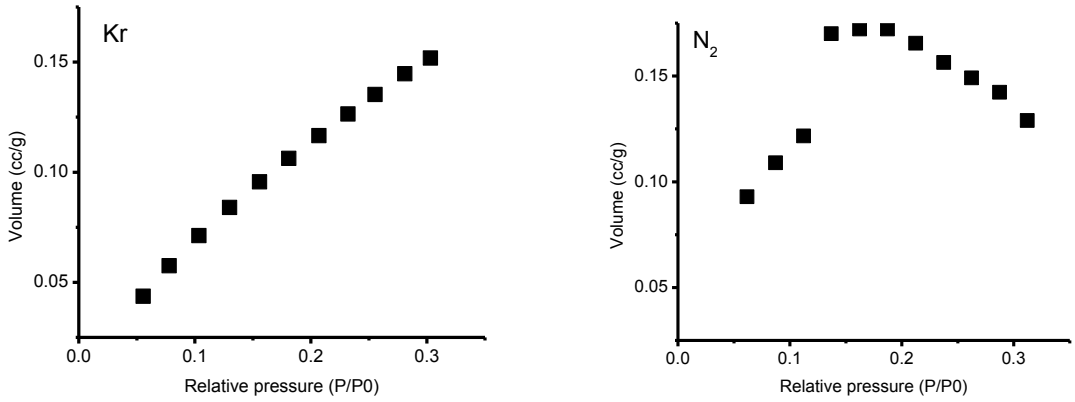

Figure 0-1. Kr (left) and N2 (right) isotherm plots for vacuum dried fiber

Following BET equation and plot were used for calculating specific surface area of the samples. The slope and intercept of the plot was used for calculating W_m which was used for specific surface area calculation as shown below.

$$\frac{1}{W\left(\left(\frac{p_0}{p}\right)-1\right)} = \frac{1}{W_m C} + \frac{C-1}{W_m C}\left(\frac{p}{p_0}\right)$$

Where:

P: Gas equilibrium pressure

P0: Gas saturation pressure

W: Weight of adsorbed Gas

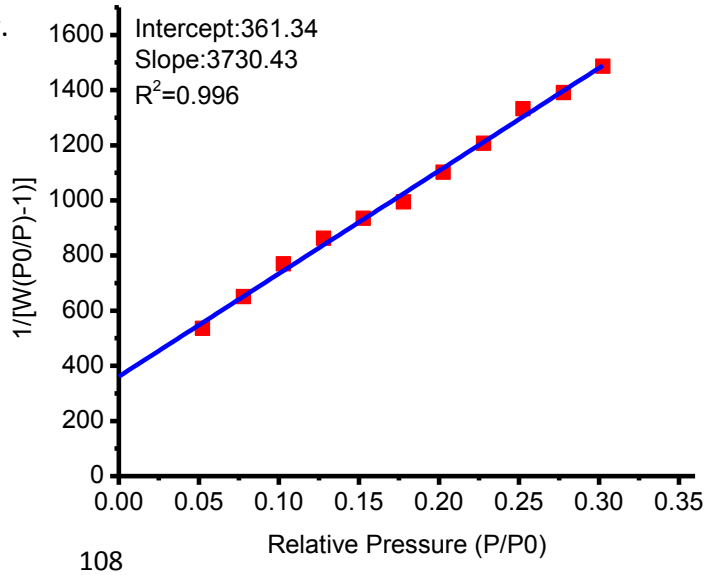

Wm: Weight of monolayer adsorbed Gas

C: BET constant

$$\mathbf{W_m} = \frac{1}{Slope + Intercept}$$

$$\textbf{Total surface area} = \frac{\mathbf{Wm.N.Acs}}{\mathbf{M}}$$

$$\textbf{Specific surface area: } \frac{\textbf{Total surface area}}{\boldsymbol{Fiber\ mass}}$$

Where:

N=Avogadro's number

M=Molecular weight of gas

Acs: Gas Cross-sectional area

The effect of drying method on specific surface area is shown below (Figure C-2). Specific surface area of solvent-exchange dried samples was significantly higher than freeze-dried and vacuum dried samples. Freeze dried samples also had higher surface area compare to vacuum dried samples. Surface tension effects in solvent-exchange drying prevented void collapse, as it has been state in the literature[1-3]. Scanning electron microscope images of solvent-exchange dried sample versus vacuum dried are shown in Figure C-3.

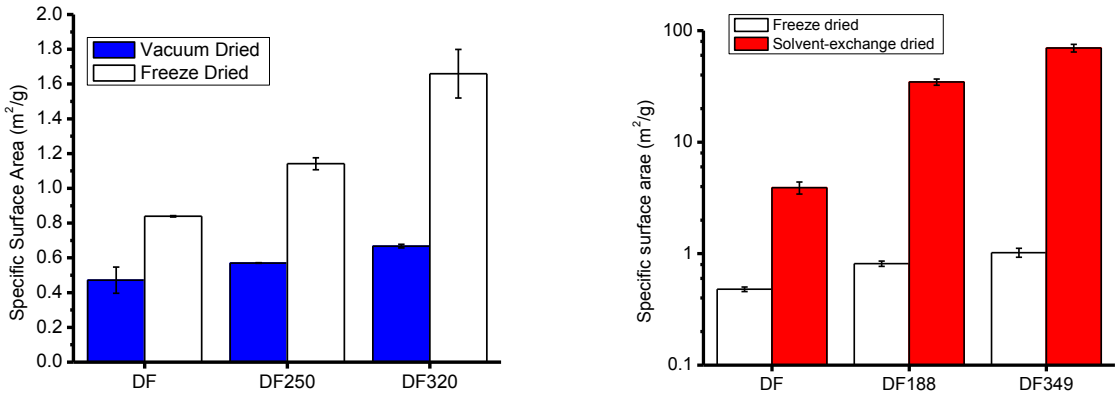

Figure 0-2. Left: specific surface area of vacuum dried and freeze dried unrefined (DF) and refined (DF250 and DF320, refined at 250 and 320 kW•h/ton respectively); right: specific surface area of freeze dried and solvent-exchange dried unrefined (DF) and refined (DF188 and DF349, refined at 188 and 349 kW•h/ton respectively)

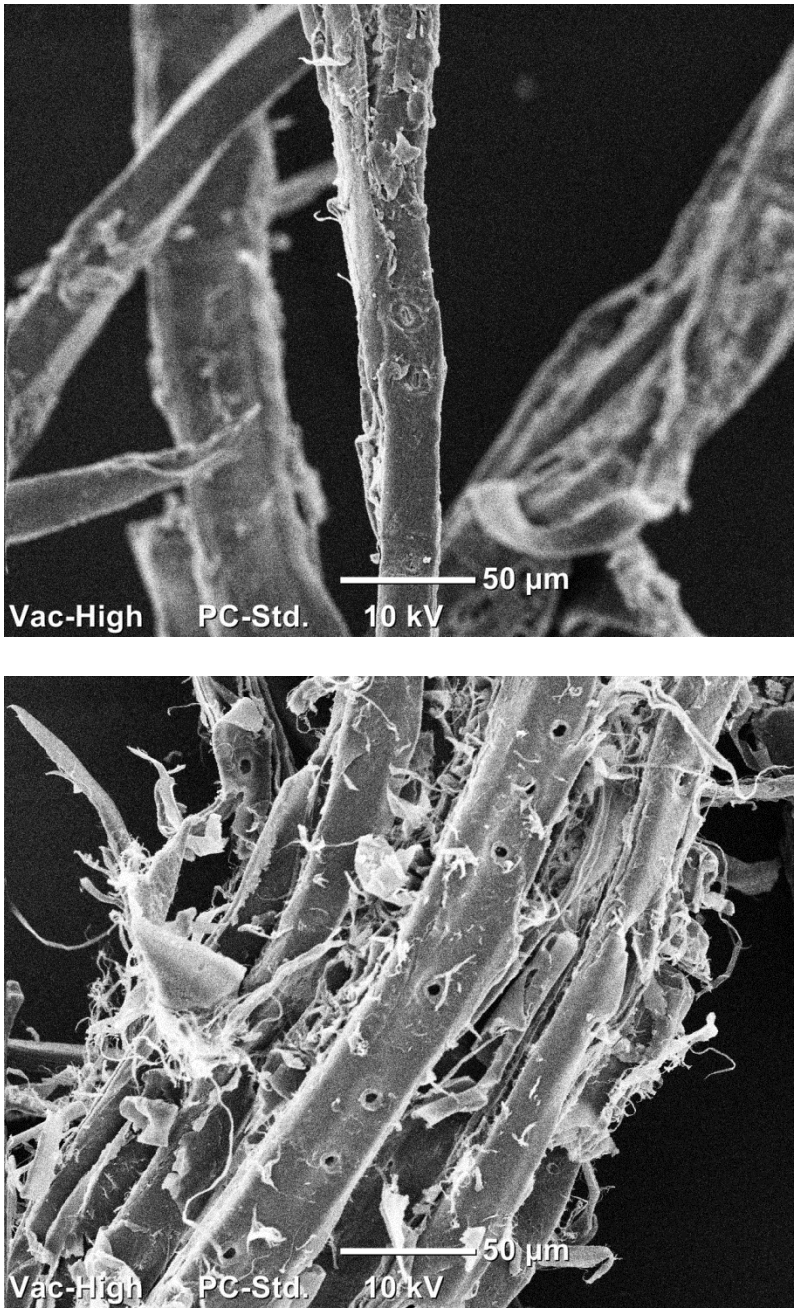

Figure 0-3. Scanning electron microscope of vacuum dried (top) and solvent-exchange dried Douglas fir fibers

References

1. Comstock, G., Longitudinal permeability of wood to gases and nonswelling liquids. *Forest products journal* **1967,** *17* (10), 41-46.
2. Hart, C.; Thomas, R., Mechanism of bordered pit aspiration as caused by capillarity. *Forest Products Journal* **1967,** *17* (11), 61-68.
3. Petty, J.; Puritch, G., The effects of drying on the structure and permeability of the wood of Abies grandis. *Wood Science and Technology* **1970,** *4* (2), 140-154.

Appendix C Conductometric titration

Conductometric titration was used for determining the amount of weak acids and phenols. Weak acids were titrated with sodium bicarbonate (0.1 M) and phenols were determined by difference after titrating separate specimens with sodium hydroxide (0.1 M). An example of conductometric titration graph used for determining weak acids and phenols is shown below.

Conductometric titration consists of 3 phases:

1) The conductivity of the suspension decreases due to neutralization of excess acid groups (excess acid was added to protonate all the weak acids and phenols) 2) All the excess acid groups are already neutralized and neutralization of weak acids and phenols start in this phase. 3) All the weak acids and phenols are already neutralized and by adding excess titrant the conductivity increases.

The following equation was used for calculating the amount of total weak acids and phenols:

$$\text{Weak acid+phenols (mmol/g dry sample)} = \frac{C \times V}{Dry\ sample\ mass}$$

Where C is titrant concentration and V is the volume of titrant consumed in titration phase 2.

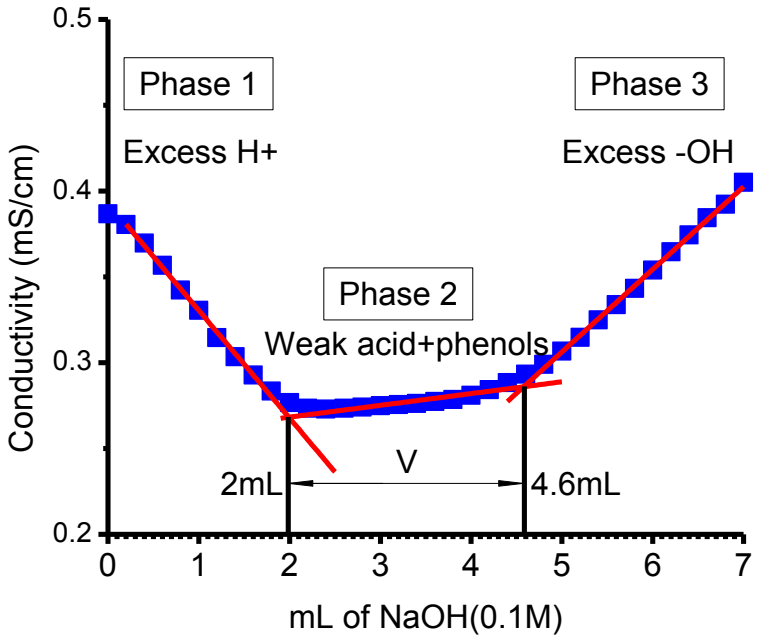

Figure 0-1. Example of conductometric titration for determining weak acids and phenols

Appendix D Nitrobenzene oxidation reaction

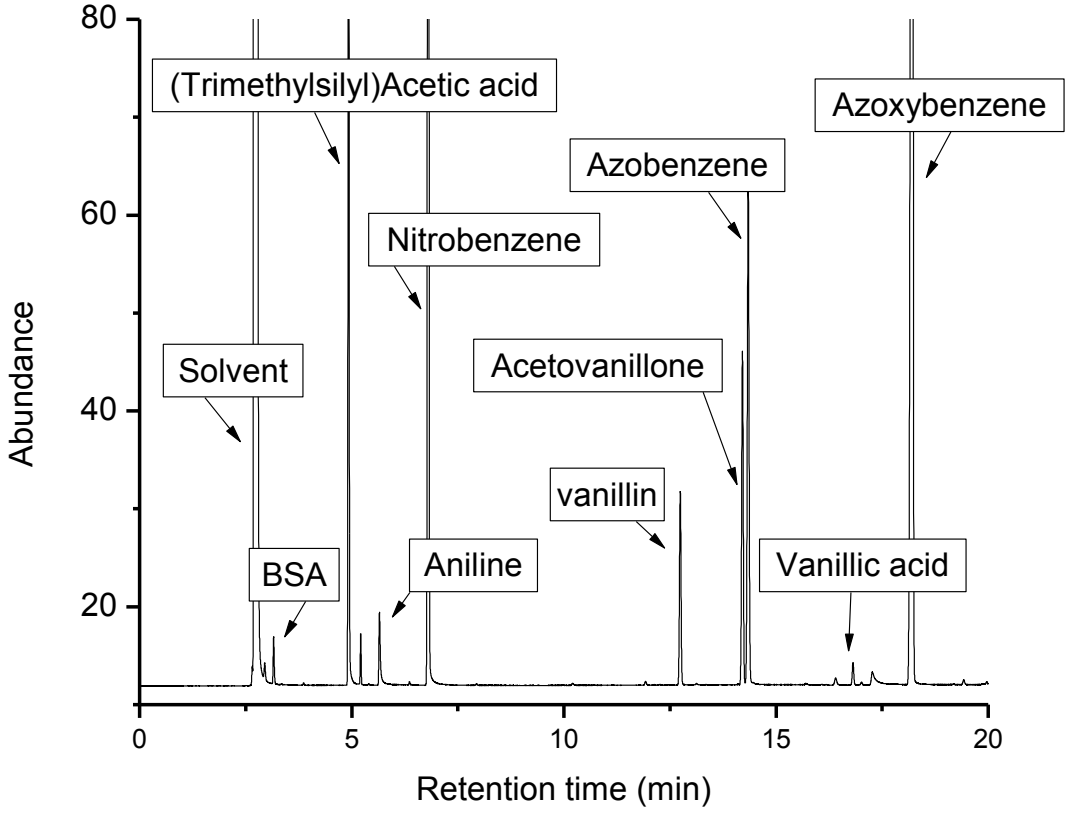

Figure 0-1. Example of nitrobenzene oxidation reaction chromatogram with peaks labeled. Sample was derivatized with BSA : N,O-bis (trimethylsilyl)acetamide.

Appendix E 2DNMR HSQC

It starts on the next page.

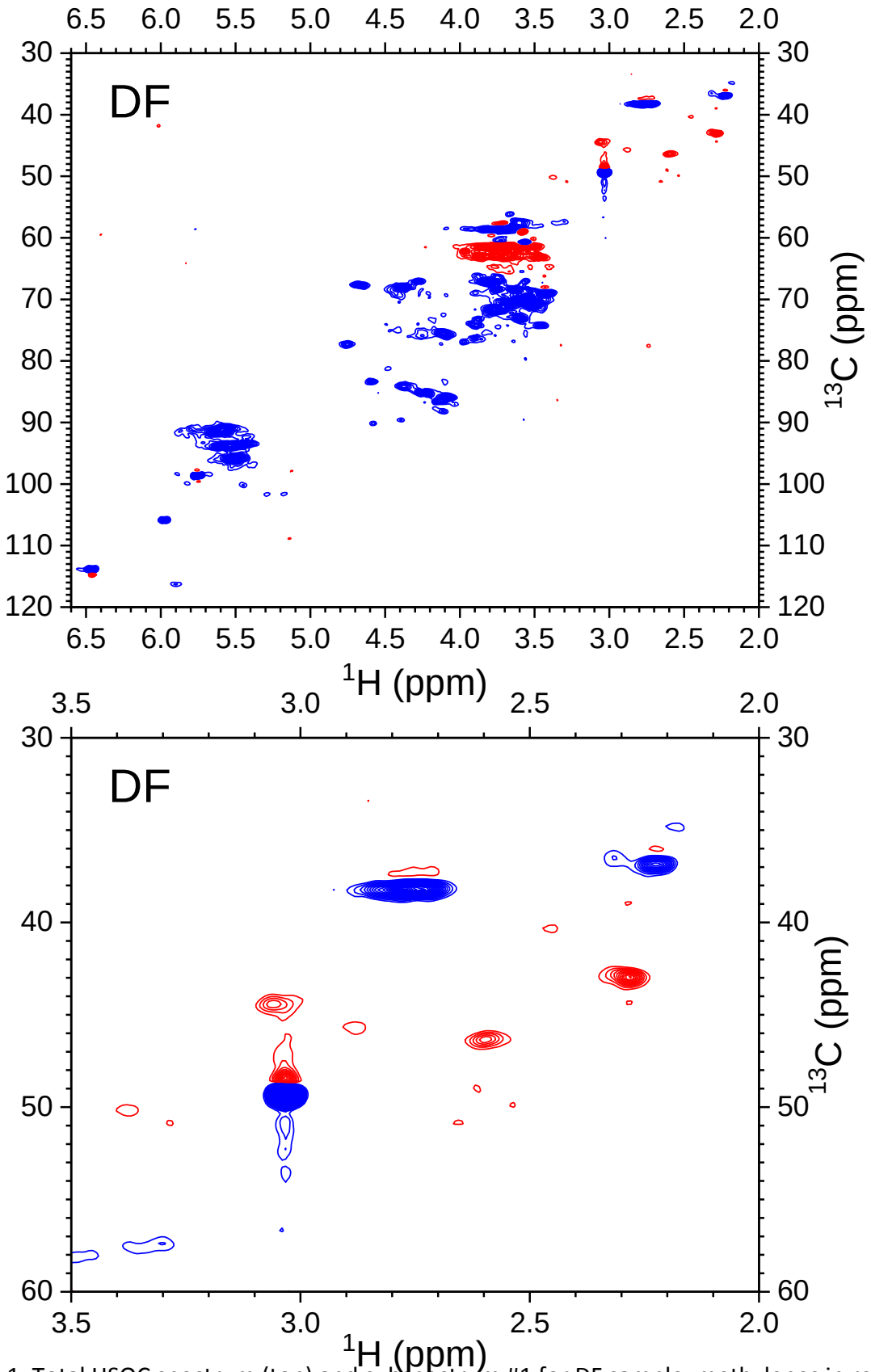

Figure 0-1. Total HSQC spectrum (top) and subspectrum #1 for DF sample; methylenes in red.

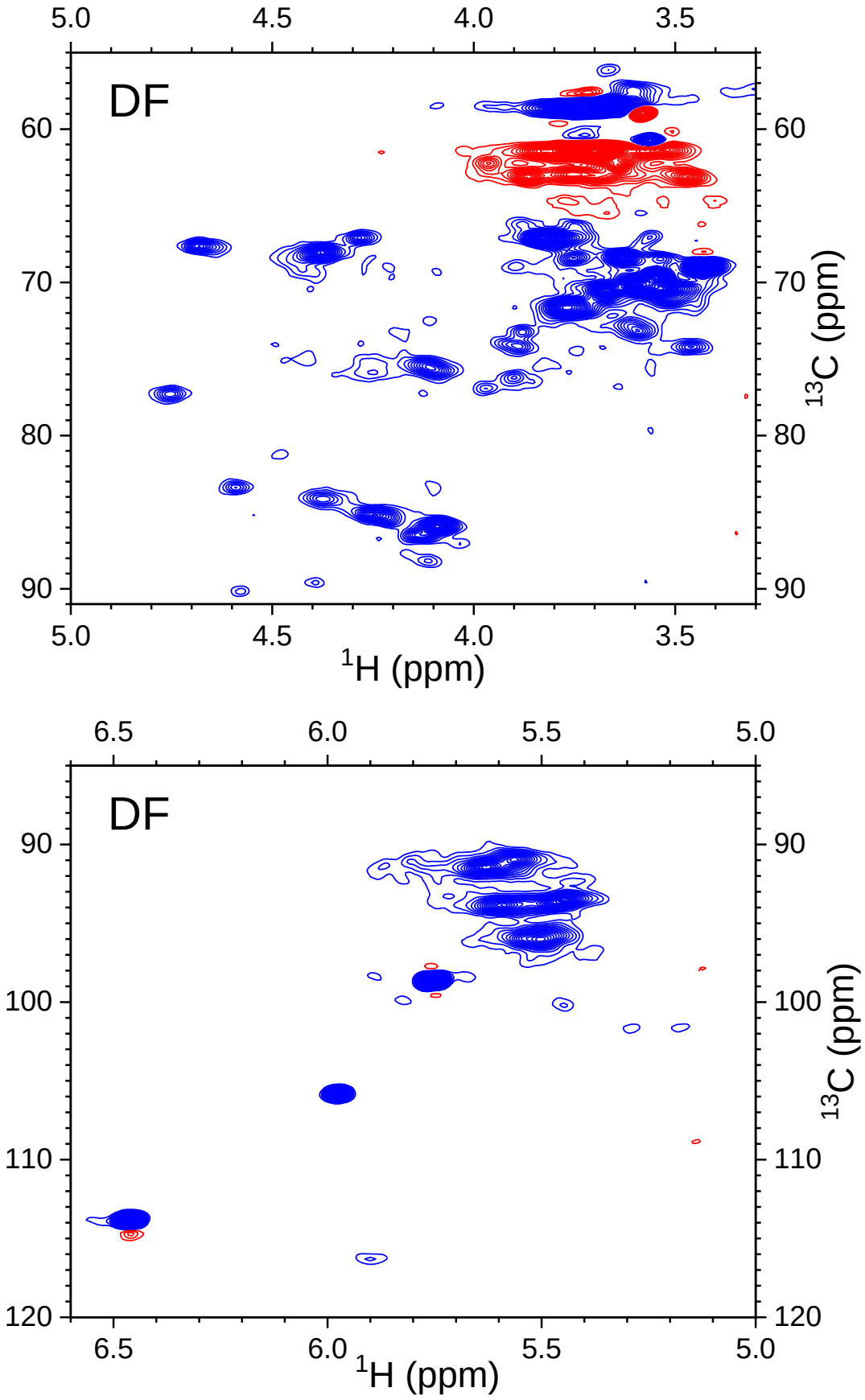

Figure 0-2. Figure 0 1. HSQC subspectrum #2 (top) and #3 for DF sample; methylenes in red.

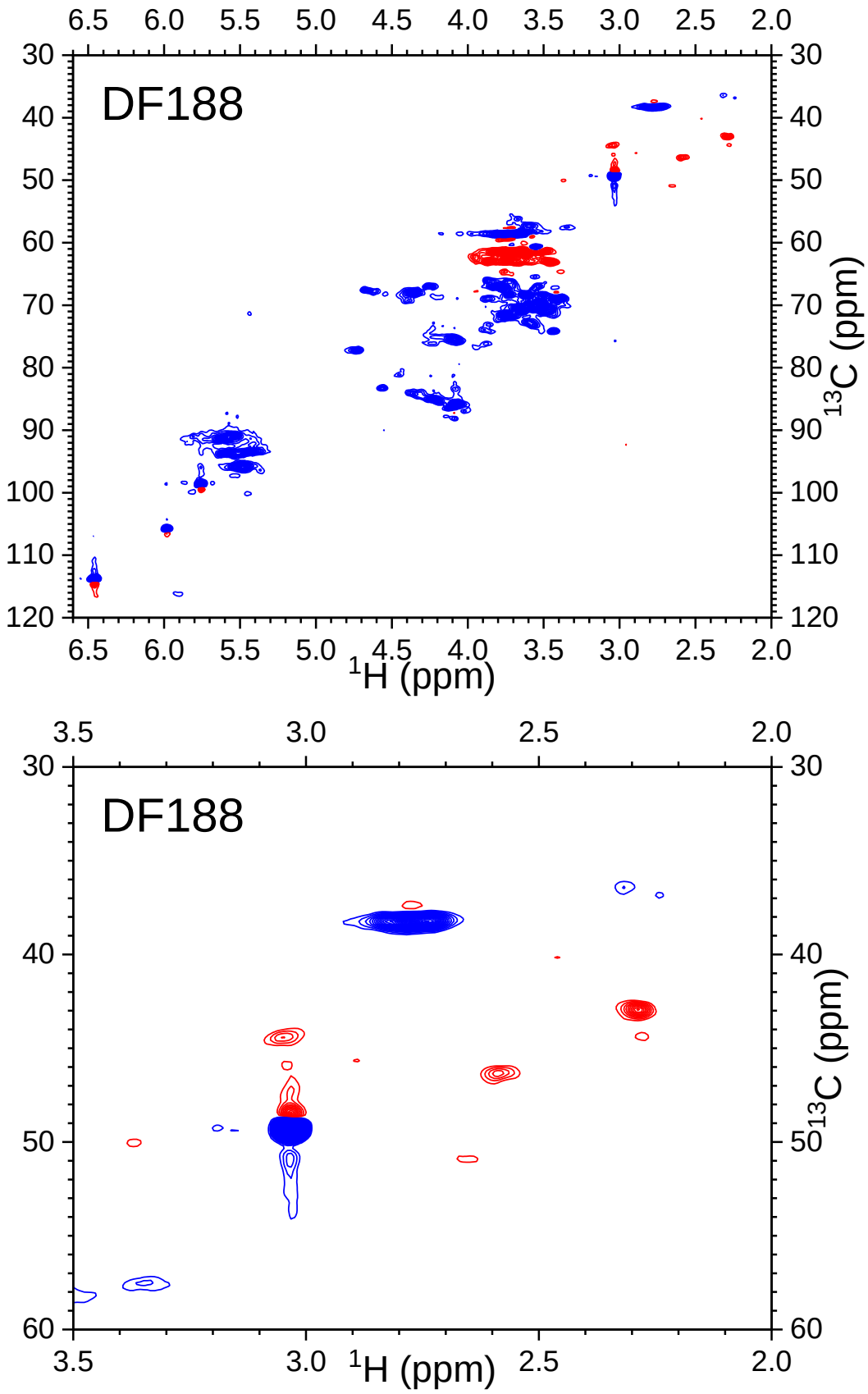

Figure 0-3. Total HSQC spectrum (top) and subspectrum #1 for DF188 sample; methylenes in red.

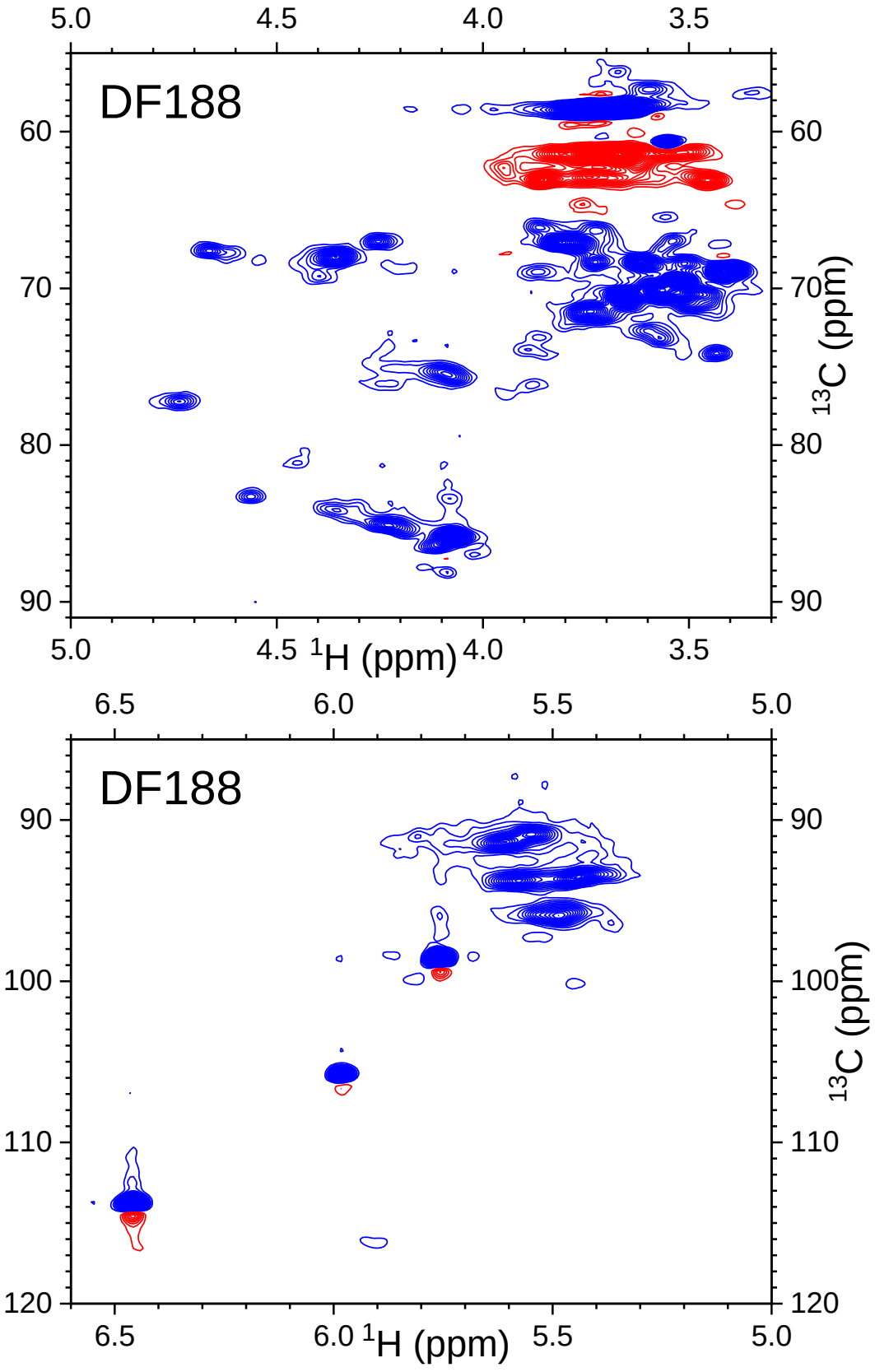

Figure 0-4. HSQC subspectrum #2 (top) and subspectrum #3 for DF188 sample; methylenes in red.

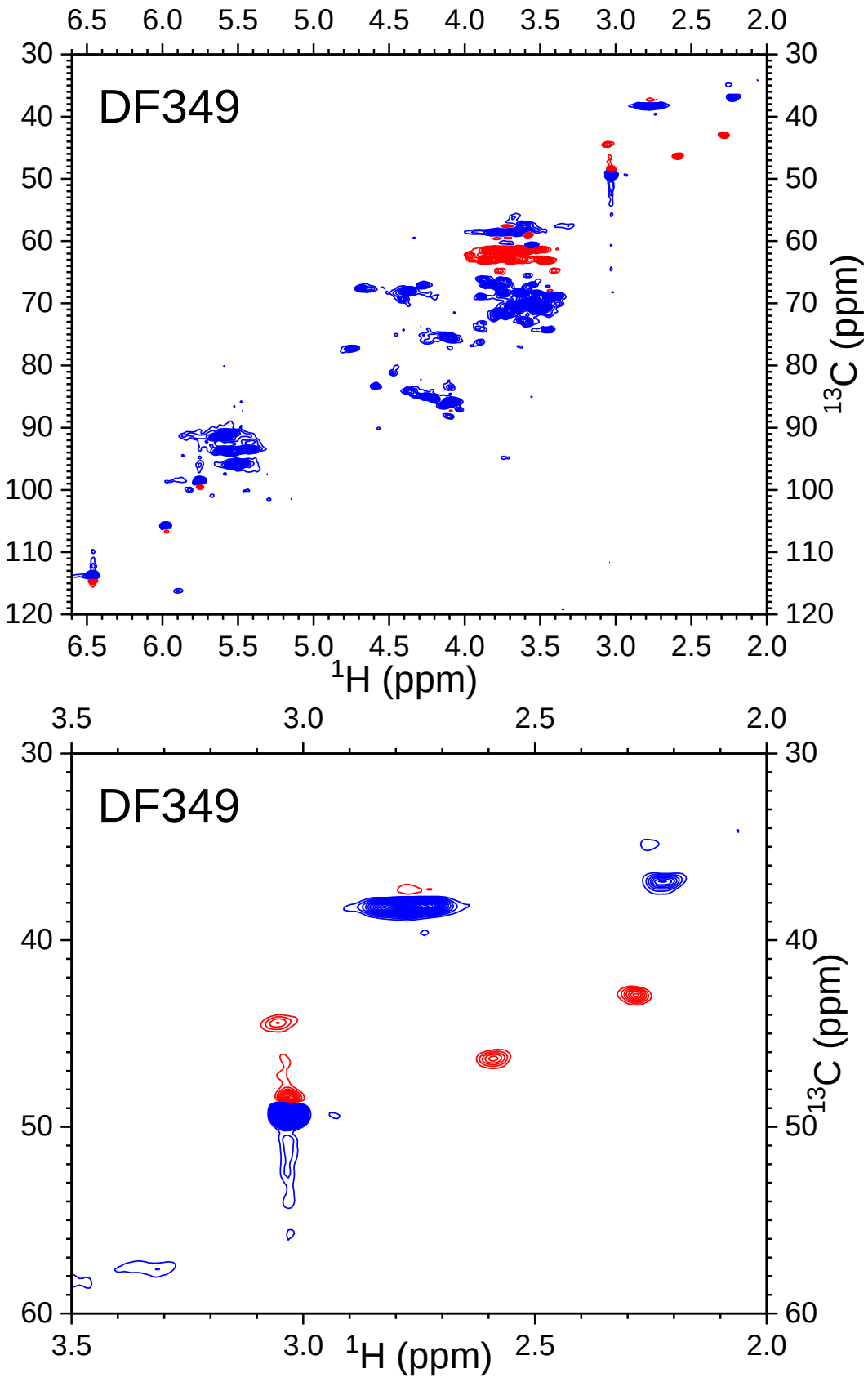

Figure 0-5. Total HSQC spectrum (top) and subspectrum #1 for DF349 sample; methylenes in red.

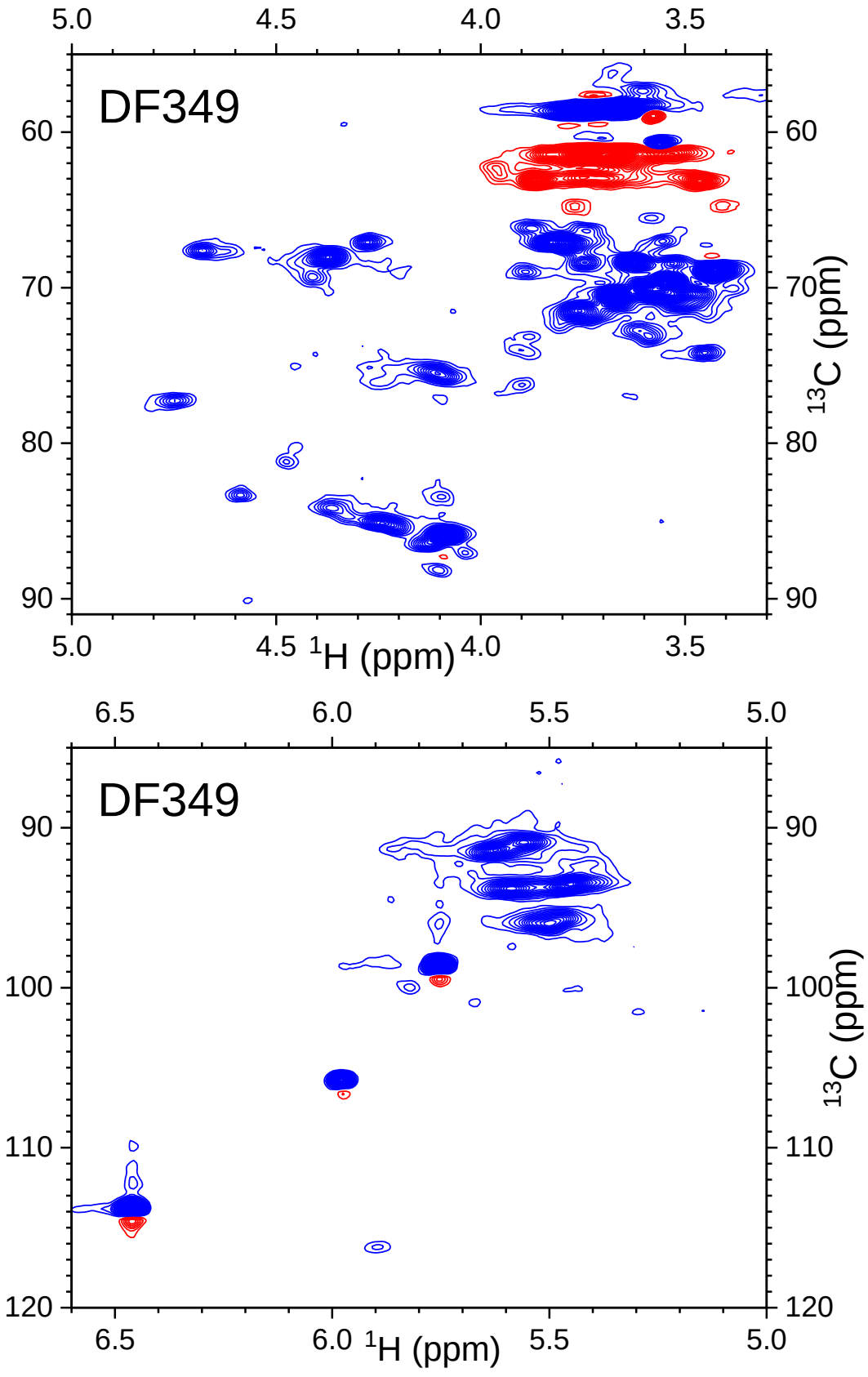

Figure 0-6. HSQC subspectrum #2 (top) and subspectrum #3 for DF349 sample; methylenes in red.

Appendix F MUF kinetic study (activation energy)

Sample was analyzed using DSC (heat to 175°C, at heating rates of 2, 5, 8, 10 and 12°C/min). From DSC results (Figure 1) the curing peak temperatures were used and based on the following Kissinger equation[1], the activation energy was obtained from the plotting of $-\ln\left(\frac{\beta}{T_p{}^2}\right)$ against 1/T (Figure G-2).

$$-\ln\left(\frac{\beta}{T_p{}^2}\right) = \frac{E}{RT_p} - \ln\left(\frac{K_0 R}{E}\right)$$

β= heating rate (K/s), T_p= peak temp (K), E=activation energy (J/mol), R= gas constant (8.314 J/mol.K) and K_0= frequency factor (1/s).

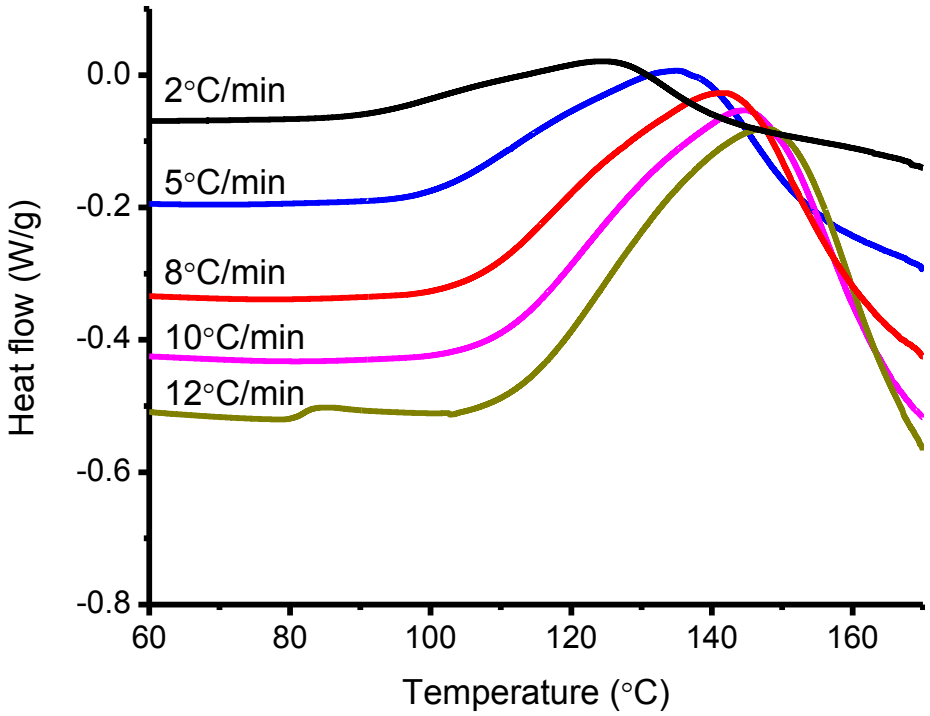

Figure 0-1. Example of curing peak temperatures obtained from different heating rates. Sample: neat MUF

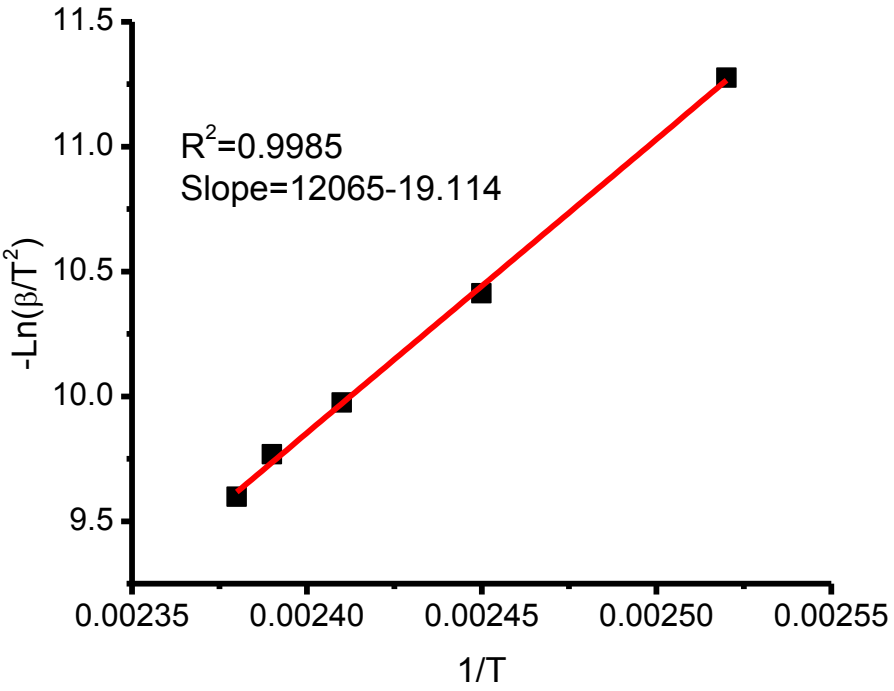

Figure 0-2. Example of $-\ln\left(\frac{\beta}{T_p{}^2}\right)$ against 1/T plot, the slope was used for calculating the activation energy. Sample: neat MUF

References

1. International, A., E698-11 Standard Test Method for Arrhenius Kinetic Constants for Thermally Unstable Materials Using Differential Scanning Calorimetry and the Flynn/Wall/Ozawa Method1. West Conshohocken, PA, **2011**.

Appendix G Aging effect on MDF fibers

During the early days of this study Douglas fir fibers refined under conditions shown in Table H-1 were used and the aging effect on fiber water chemistry (pH, weak acids, phenols, acid buffering capacity, alkaline buffering capacity) was studied over two-month period. Aging effect was observed even when samples were stored at -80°C.

Sample preparation

The unrefined samples (DF1 and DF2) were vacuum dried (0.10 mmHg, 25°C, overnight), ground by a Wiley mill, screened (18-80 mesh) and vacuum dried (0.10 mmHg, 25°C, overnight). Refined samples (DF250 and DF320) were not milled, but similarly screened and dried as described. Samples were either sealed/stored in deep freeze (-80°C) or at room temperature and were called Cold and RT respectively.

Table 0-1. Samples specifications

Douglas fir specimens	Refining energy (kW•h/ton)	Digester pressure	Year sample received
Unrefined (DF1)	-	-	2015
Refined (DF320)	320	0.74	
Unrefined (DF2)	-	-	2016
Refined (DF250)	250	0.82	

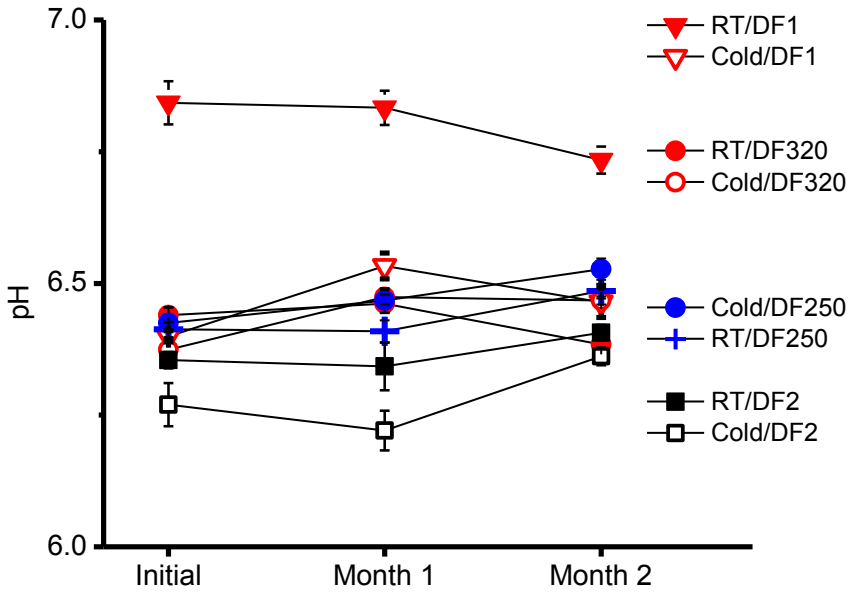

Figure 0-1. Aging effect on fiber pH. RT: stored at room temperature, Cold: Stored at -80°C

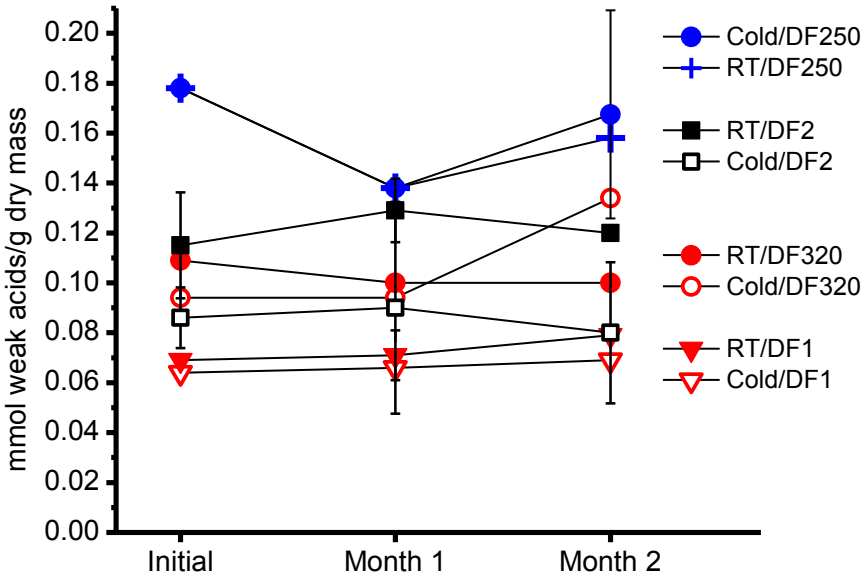

Figure 0-2 Aging effect on fiber weak acids. RT: stored at room temperature, Cold: Stored at -80°C

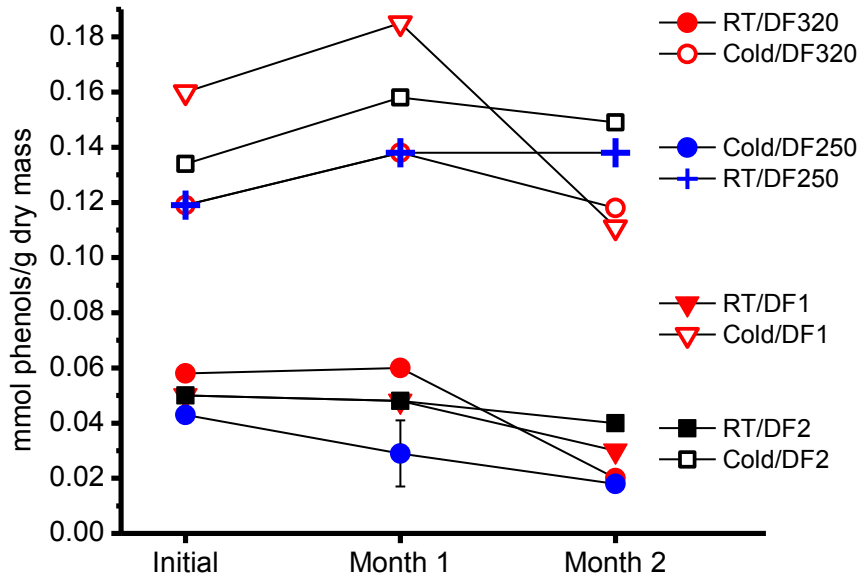

Figure 0-3. Aging effect on fiber phenols. RT: stored at room temperature, Cold: Stored at -80°C

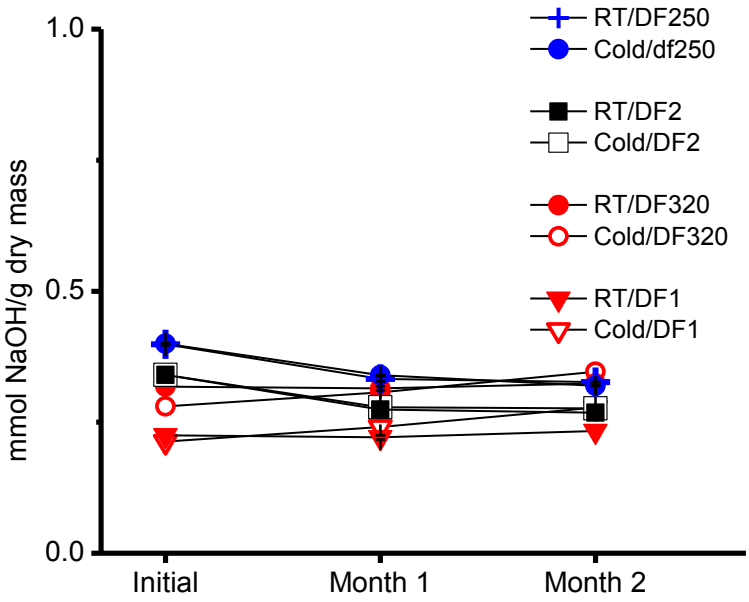

Figure 0-4 Aging effect on fiber acid buffering capacity. RT: stored at room temperature, Cold: Stored at -80°C

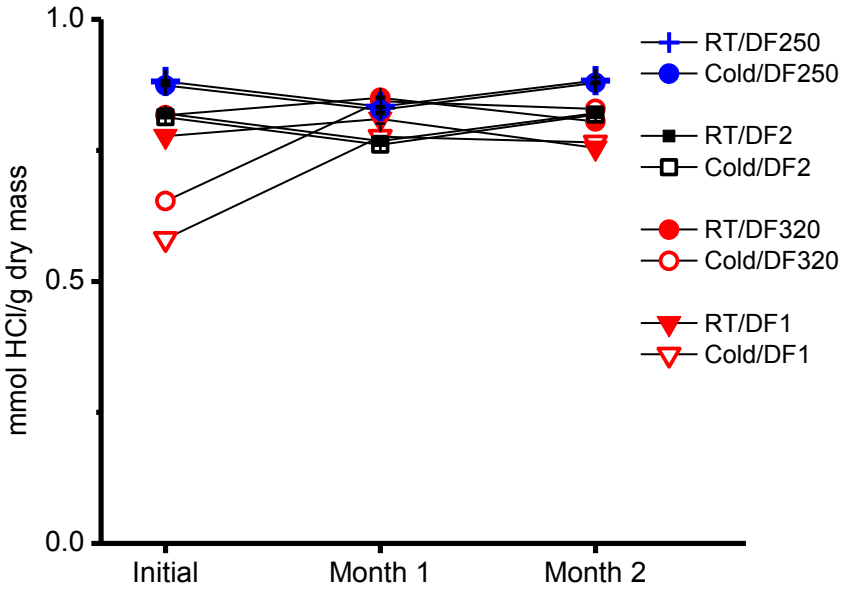

Figure 0-5. Aging effect on fiber alkaline buffering capacity. RT: stored at room temperature, Cold: Stored at -80°C

Appendix H Biogenic formaldehyde: Content and heat generation in the wood of three tree species

Attribution

Following this page is a collaborative publication (Tasooji, M., Wan, G., Lewis, G., Wise, H., Frazier, C.E. 2016. Biogenic formaldehyde: Content and heat generation in the wood of three tree species. ACS Sustainable Chemistry & Engineering. 5 (5), 4243-4248) where Virginia pine formaldehyde measurements were conducted by Mohammad Tasooji and Heather Wise, respectively 40% and 10% of the total publication effort, and noting that Tassoji supervised Wise in the effort. Guigui Wan and George Lewis completed all yellow-poplar and Radiata pine work (approximately 50% of the total publication effort).

ACS Sustainable Chemistry & Engineering

Research Article

pubs.acs.org/journal/ascecg

Biogenic Formaldehyde: Content and Heat Generation in the Wood of Three Tree Species

Mohammad Tasooji, Guigui Wan, George Lewis, Heather Wise, and Charles E. Frazier*

Sustainable Biomaterials, Virginia Tech, 310 West Campus Drive, Cheatham Hall, RM 230, Blacksburg, Virginia 24061, United States
Macromolecules Innovation Institute, 1075 Life Science Circle, Suite 110 (0201), Blacksburg, Virginia 24061, United States

Supporting Information

ABSTRACT: Global trends in allowable formaldehyde (CH_2O) emissions from nonstructural wood-based composites require a renewed consideration of biogenic CH_2O from wood. Increment cores from living Virginia pine (*Pinus virginiana*), yellow-poplar (*Liriodendron tulipifera*), and radiata pine (*P. radiata*) trees were used to measure CH_2O and CH_2O generation due to heating (200 °C, 10 min). Significant variations within and between trees of the same species were observed. Tissue types (juvenile/mature, heartwood/sapwood) sometimes correlated to higher CH_2O contents and greater heat-generation potential; however, this did not always depend upon species. Heating increased CH_2O levels 3−60-fold. Heating with high moisture levels generated more CH_2O than that generated from dry specimens. Radiata pine generated extraordinarily high CH_2O levels when heated, far exceeding the other species. It was suggested that pine extractives might catalyze CH_2O generation, perhaps in lignin. Regarding wood-based composites, findings suggested that compliance with emissions regulations may be complicated by CH_2O generated in the hot press. If we could reveal the precise mechanisms of CH_2O generation in wood, we could perhaps manipulate these mechanisms for beneficial purposes.

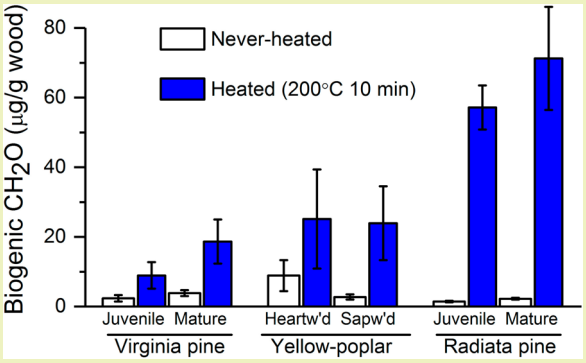

KEYWORDS: *Lignocellulose, Wood composites, Lignin, Emissions, Regulations*

INTRODUCTION

This work addresses biogenic formaldehyde (CH_2O) generated by wood during the manufacture of nonstructural wood-based composites from which CH_2O emissions are regulated. Global trends have shown steady reductions in allowable CH_2O emissions from these products. The regulation target has been anthropogenic CH_2O released from hydrolytically unstable amino resins. However, current regulations restrict allowable emissions to such low levels that biogenic CH_2O may affect regulation compliance. It is well-known that wood contains biogenic CH_2O and that heating generates much greater quantities.[1−6] The latest emissions regulations have been met with new amino resin technologies. Nevertheless, there are persistent anecdotal reports of complications attributed to biogenic CH_2O. As part of an industry/university cooperation, we seek a more thorough accounting of all CH_2O sources in wood-based composites, both anthropogenic and biogenic. Biogenic CH_2O from wood has been documented for at least 39 years, but relatively little data is available, and none addresses CH_2O levels in living trees.[4,7,8] Our goal is to document the occurrence of biogenic CH_2O in the living tree and simulate its generation during composite manufacture. Here, industrial drying is omitted, and emphasis is placed on hot-press simulation using 10 min, 200 °C treatments. To conduct large scale, nondestructive sampling of living trees, a simple milligram-scale water extraction was developed and shown to recover ∼94% of the extractable CH_2O.[9] Specimen heat treatments and CH_2O determinations are conveniently conducted in a single glass vessel, so nearly all CH_2O is retained and quantified. For our purposes, this new procedure is preferable to the perforator method that exposes 100 g specimens to boiling toluene.[10] Because wood possesses abundant hydroxyl groups, CH_2O exists in a complex equilibrium that includes sorbed CH_2O (methylene glycol), covalently bonded hemiformal (hemiacetal), and covalently bonded formal (acetal).[9,11,12] Among these compounds, all except formal are free forms that are readily extractable with water at room temperature. All free CH_2O that is readily extractable is capable of gaseous emission.[9,11] However, the rate of emission is strongly dependent upon the wood moisture content. Dry wood retains CH_2O, and water-saturated wood rapidly releases it, suggesting that hemiformals play a key role.[11]

The tree species studied were Virginia pine, yellow-poplar, and radiata pine. While commercially insignificant, Virginia pine was studied because of its availability and similarity to the commercially important southern pines. Yellow-poplar is commercially important in the eastern United States, and radiata pine is commercially valued on a global scale.

Received: January 21, 2017
Revised: March 17, 2017
Published: March 28, 2017

DOI: 10.1021/acssuschemeng.7b00240
ACS Sustainable Chem. Eng. 2017, 5, 4243−4248

Table 1. Tree Specimen Information[a]

	Virginia pine	yellow-poplar	radiata pine
age (years)	60−85	30−40	19−28
no. of trees	8	5	2

	Virginia pine		yellow-poplar		radiata pine	
tissue type	mature	juvenile	sapwood	heartwood	mature	juvenile
MC (%)	81.7 (11.4)	29.3 (12.4)	72.5 (0.8)	128.3 (10.9)	~130[b]	~40[b]
EC (%)	3.5 (1.0)	7.3 (0.5)	3.4 (1.1)	4.3 (0.9)	1.1 (0.2)	2.3 (0.6)

[a]Moisture content (MC) at harvest and extractives content (EC) based on dry wood mass. MC and EC for yellow-poplar and radiata pine averaged over all trees listed. MC for Virginia pine was averaged over trees 1−6, and EC was averaged over trees 5 and 6. Standard deviations are in parentheses. [b]MC was not available and was estimated by collaborators according to other measurements.

Ultimately, the desire is to determine how biogenic CH_2O affects emissions from composite products.

MATERIALS AND METHODS

In Blacksburg, Virginia, United States, increment cores were sampled from eight living Virginia pine (*Pinus virginiana*) and five yellow-poplar (*Liriodendron tulipifera*) trees; from a commercial plantation near Concepcion, Chile, two Radiata pine (*P. radiata*) trees were sampled. The increment cores were razor cut to 1 mm thick disks. Details of the sampling are described in the Supporting Information. All trees were healthy except Virginia pine tree 8, which had large sections of dead branches in the crown.

Extractives content was measured using 95% ethanol (NREL/TP-510-42910: Determination of Extractives in Biomass.)

Specimen Preparation. Specimens are identified with respect to drying history (never-dried or dried) and thermal treatment (never-heated or heated). Never-dried specimens: freshly cut disks were sealed in screw-capped vials and placed in a second container (purged with N_2) and stored at −18 or −80 °C. Dried specimens: wood disks were placed in a desiccator and dried by cycling between vacuum (0.15 mmHg) and dry N_2 three times and then stored over P_2O_5 (or molecular sieves) and N_2 for at least 48 h until a constant weight was reached. Heated specimens: 200 °C, 10 min as detailed below. Never-heated specimens: no heat exposure. Within each tree, 1−3 cores were used for never-dried measurements, while another 3−5 cores were used for dried measurements. Within each core, 2−4 CH_2O measurements were conducted.

CH_2O Measurements. The CH_2O determination was described previously: wood samples (never-heated: 30−60 mg; heated: 5−10 mg, dry mass) were sealed in a 50 mL serum bottle.[9] All samples were subjected to either heat treatment (200 °C, 10 min) or no heating. After cooling to room temperature, water (15 or 20 mL) was charged via syringe, and the specimen/bottle set at room temperature for 1 h with occasional shaking. After 1 h, 4 mL of the CH_2O solution was sampled and analyzed by fluorimetric acetylacetone detection. Measured CH_2O was reported as μg/g dry wood. Simple pairwise statistical comparisons were conducted, but data normality was not verified.

RESULTS AND DISCUSSION

Table 1 summarizes tree specimen information. Wood specimens are discussed with respect to drying history (never-dried or dried) and thermal treatment (never-heated or heated). Notable was the variability within individual cores and between cores within the same tree as related to CH_2O content and generation potential. Typical results from a randomly selected Virginia pine tree are presented in the Supporting Information. Sometimes, there was significant variability within individual cores, but on average, there was no significant difference between cores. In other cases, there was little variability within individual cores with or without significant differences between cores. In other words, the CH_2O content and its generation potential were nonuniform within the tissues studied. Because subsample groupings were based upon tissue maturity (cm scale), the heterogeneity within and between cores could be related to anatomical variations that were not randomized during tree core sectioning (mm scale). For instance, the occurrence of resin canals is expected to vary among tree core sections, whereas earlywood/latewood effects (if they occur) would undergo randomization with perhaps no detectable impact. Consequently, the within and between core variability observed may be associated with the heterogeneous distribution of extractives/resin canals. If wood extractives play a role in CH_2O generation, they must be considered as a potential source because they might interact with wood to suppress or promote CH_2O. For instance, condensed tannins are used in resin formulations as formaldehyde scavengers.[2,13−15] Likewise, CH_2O generation in lignocellulose is acid catalyzed,[16] and so acidic wood extractives will likely play a catalytic role.

Figure 1 shows tissue maturity effects in never-dried/never-heated Virginia pine for trees 3−8. CH_2O levels ranged from

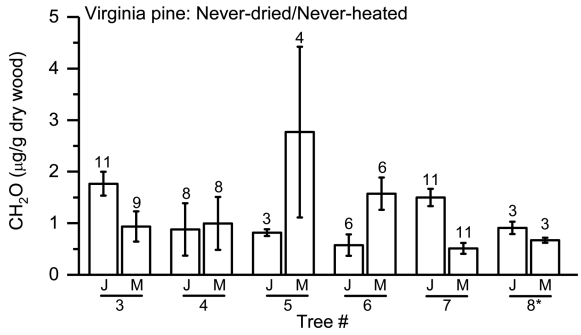

Figure 1. Average CH_2O content in never-dried/never-heated Virginia pine, trees 3−8, by tissue type (J, juvenile; M, mature). Numbers above columns indicate total number of measurements. *Tree 8 was diseased. Error bars = ±1 standard deviation.

about 1−5 μg/g of dry wood, comparable to findings of others using the perforator extraction on pine specimens.[1,4] Tree 8 was diseased, but its CH_2O content was not unusual. Among trees 3−7, it appeared as if tissue maturity effects were effectively random with no sensible pattern. Using *P. sylvestris*, Weigl et al. found that juvenile wood contained less CH_2O than mature wood.[4] Similarly, Dix and Raffael showed that particleboard made with *P. sylvestris* heartwood generally emitted less CH_2O than the corresponding sapwood.[17]

In a comparison of never-dried/never-heated to never-dried/heated Virginia pine specimens, Figure 2 demonstrates the well-known impact of heating on CH_2O generation,[18−20] and in this case, tissue maturity effects became clear. Heating increased the

DOI: 10.1021/acssuschemeng.7b00240
ACS Sustainable Chem. Eng. 2017, 5, 4243−4248

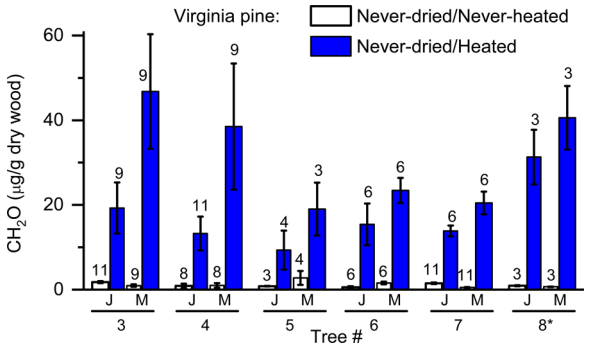

Figure 2. CH_2O generation by comparison of never-dried/never-heated and never-dried/heated Virginia pine specimens as a function of tree and tissue type (J, juvenile; M, mature). Numbers above columns indicate total number of measurements. *Tree 8 was diseased. Error bars = ±1 standard deviation.

CH_2O content by a factor of 9−34 in juvenile wood and by a factor of 7−61 in mature wood. Upon heating, the mature tissue always exhibited higher CH_2O content, and the generation potential (factor increase) was greater in mature tissue for trees 3, 4, 7, and 8. The true CH_2O generation potential requires correction for levels found in never-dried/never-heated specimens, but that was not applied to Figure 2, and the correction had little impact on the factor increase. Mature Virginia pine contained less extractives and more water than juvenile wood (Table 1). For trees 3, 4, 7, and 8, perhaps the greater moisture content in the mature tissue explains the greater CH_2O generation potential, but both tissue types were likely above the fiber saturation point. Again, the variability within and between trees was notable, and the diseased tree 8 appeared normal in comparison to the healthy trees. If the behavior shown in Figure 2 is applicable to commercially significant southern pines like *P. taeda*, it is apparent that CH_2O generation during composite hot-pressing could be highly variable. The potential impact on panel emissions seems obvious, but the precise relationship between CH_2O generation and actual product emissions is currently unknown (discussed later).

As in Virginia pine, yellow-poplar trees exhibited a similar degree of variability within and between trees (Figure 3). However, in never-dried/never-heated yellow-poplar, the heartwood always exhibited CH_2O content higher than that

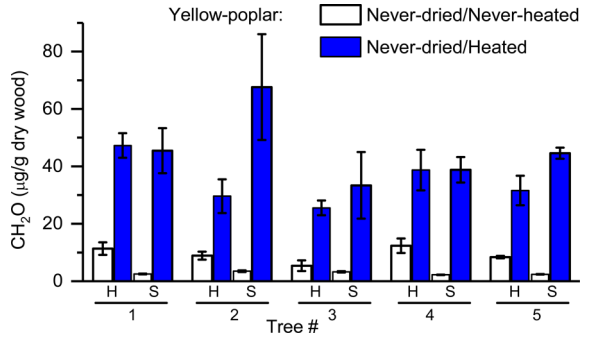

Figure 3. Average CH_2O content (never-dried/never-heated) and CH_2O generation potential (never-dried/heated) in yellow-poplar. Heartwood (H) and sapwood (S) specimens were respectively randomized among 4−8 cores from the same tree. Error bars = ±1 standard deviation.

of sapwood. The extractives content in the respective tissues was about the same, but the composition was known to differ, and the heartwood had higher moisture (Table 1). Upon heating, the CH_2O generation was greater for the sapwood (increasing by a factor of 10−19), whereas in heartwood, the CH_2O content increased by a factor of 3−5. The lower CH_2O generation of yellow-poplar heartwood might be due to CH_2O reaction with aporphine alkaloids occurring in the heartwood at levels of about 1%; only trace quantities appear in the sapwood.[21,22]

A general species comparison was conducted by pooling all yellow-poplar data and comparing it to Virginia pine data pooled over trees 3−8, Figure 4. Considering never-dried/never-heated specimens, it was determined that living yellow-poplar trees contained more CH_2O than living Virginia pine. This suggests that CH_2O emissions in the drying stage might be greater when processing yellow-poplar as compared to southern pine. Yellow-poplar wood appeared to generate more CH_2O when heated (never-dried/heated). CH_2O generated in yellow-poplar heartwood was significantly greater than that generated in Virginia pine juvenile wood ($p \ll 0.01$); but when yellow-poplar sapwood is compared to Virginia pine mature wood, the difference was less significant ($p = 0.11$).

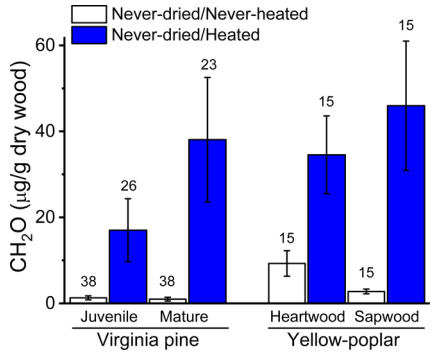

Figure 4. Average CH_2O content (never-dried/never-heated) and CH_2O generation potential (never-dried/heated) for Virginia pine trees 3−8 and all yellow-poplar trees 1−5 (respective tissue types randomized among cores from the same tree). Numbers above columns indicate total number of measurements. Error bars = ±1 standard deviation.

When Virginia pine was analyzed, it was observed that room temperature drying was often associated with higher wood CH_2O levels. This was surprising given that no specimen heating occurred. Meyer and Boehme made similar observations after drying pine, spruce, and Douglas fir at 30 °C; drying resulted in increased CH_2O emission.[1] When drying resulted in greater emissions, Meyer and Boehme suggested that CH_2O generation must have occurred even after their specimens were dried.[1] This hypothesis cannot be refuted, but it seems questionable because over short periods elevated temperatures are required to form biogenic CH_2O (data not shown). In any case, we became suspicious that room temperature drying in the presence of P_2O_5 might lead to catalytic effects from phosphoric acid contamination. We confirmed that specimen drying with P_2O_5 leads to higher CH_2O levels (see the Supporting Information), and we concluded that P_2O_5 should never be used to dry wood that is intended for chemical study. The remaining discussion only features specimens dried with molecular sieves, and it was found that drying resulted in higher CH_2O levels in Virginia pine wood but not yellow-poplar wood

DOI: 10.1021/acssuschemeng.7b00240
ACS Sustainable Chem. Eng. 2017, 5, 4243−4248

(Figure 5). This result is similar to that of Meyer and Boehme but only in that the behavior of softwoods and hardwood is

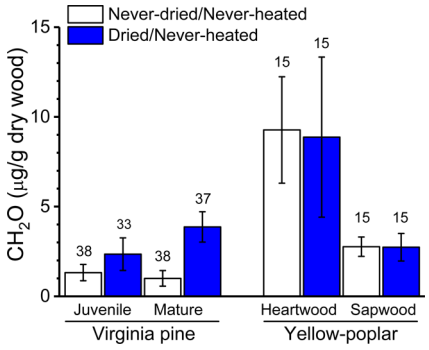

Figure 5. Effect of drying (molecular sieves) on CH_2O content in never-heated Virginia pine (trees 5−8) and yellow-poplar (trees 1−5). Numbers above columns indicate total number of measurements from 4−5 trees with 1−8 cores per tree. Error bars = ±1 standard deviation.

very different. Meyer and Boehme found that drying caused a significant reduction of CH_2O content in oak.[1] Initial consideration might suggest that drying (without heating) would result in a CH_2O content reduction. However, if hemiformals dominate the equilibria in wood, then CH_2O retention would increase as drying proceeds. Regarding the effects of drying on hardwoods, the discrepancy with Meyer and Boehme might be explained by the different drying conditions employed. In this work, vacuum drying to a moisture content of less than 1% was employed, whereas Meyer and Boehme dried specimens to 7−9% moisture. If these observations are explained by the moisture dependent hemiformal equilibrium, then one could conceive relatively simple methods to reduce CH_2O content in wood, where increasing moisture promotes CH_2O release.[11] Nevertheless, it is perplexing and currently inexplicable that CH_2O content is higher in softwoods after drying.

When heated at 200 °C for 10 min, wet wood generated significantly more CH_2O (Figure 6). Because acids catalyze

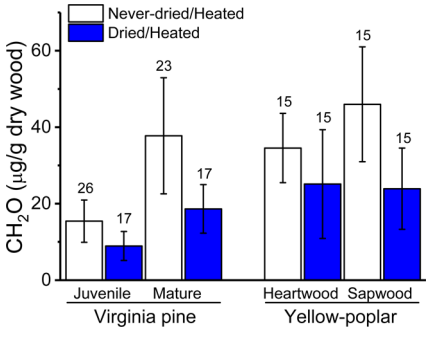

Figure 6. Effect of moisture content on heat generation of CH_2O: Virginia pine (trees 5−7) vs yellow-poplar (trees 1−5). Numbers above columns represent number of measurements. Error bars = ±1 standard deviation.

CH_2O generation,[16] it is reasonable to conclude that naturally occurring wood acids would be less active when wood is very dry. Furthermore, heating at higher moisture contents is expected to hydrolyze wood esters and release more acids that catalyze a corresponding increase in CH_2O generation.

Radiata pine specimens were received after room temperature, vacuum drying, and the comparison to Virginia pine and yellow-poplar is shown in Figure 7. When heated, the CH_2O

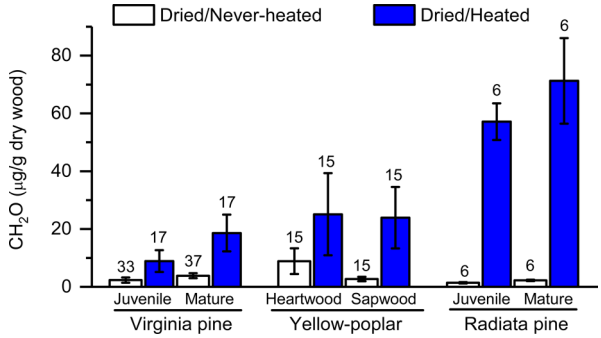

Figure 7. Species effect on CH_2O content and generation from molecular sieve-dried specimens. Numbers above columns indicate number of measurements. Virginia pine, trees 5−7; yellow-poplar, trees 1−5; radiata pine, 2 trees. Error bars = ±1 standard deviation.

content in dry radiata pine increased by a factor of 32−40, whereas the increases for Virginia pine and yellow-poplar were by factors of 4−5 and 3−9, respectively. The extraordinary CH_2O generation in radiata pine suggests that compliance to emissions regulations could be troublesome for radiata-based composites, noting that all CH_2O determined in this work is capable of gaseous emission. As mentioned, the precise relationship between biogenic CH_2O levels and actual composite emissions is currently unknown. However, a direct relationship seems reasonable, as demonstrated by Birkeland et al.,[5] who measured significant biogenic emissions from panels bonded with no-added CH_2O adhesives. Birkeland et al.[5] demonstrated that biogenic emissions dissipated 12−20 days after hot pressing (storage at 50% relative humidity, 23 °C). Consequently, special measures might be required to meet emissions regulations in radiata-based composites (verified from personal communication with industry representatives). Note that both pines exhibit tissue maturity effects. Mature wood in Virginia pine generates significantly more CH_2O than juvenile wood ($p \ll 0.01$), but the effect is less significant in radiata pine ($p = 0.07$).

Compared to Virginia pine, what could explain the extraordinary CH_2O generation in radiata pine? Among the structural wood polymers, the available literature indicates that lignin generates much more CH_2O than the polysaccharides,[2] consistent with our findings.[16] It seems unlikely that lignin effects would explain the differences observed in Virginia and radiata pine. Consequently, a plausible hypothesis might involve differences in the extractives. Three scenarios should be considered: (1) that extractives directly generate CH_2O, (2) that extractives react with CH_2O, or (3) that extractives catalyze CH_2O generation, perhaps in lignin. The first scenario is known to occur, and strong evidence exists for the second.[2] Schäfer and Roffael's results suggest a catalytic role for extractives,[2] but they did not discuss this topic. When heated (150 °C, 3 h), unextracted pine generated CH_2O at 288 μg/g dry wood, and extracted pine generated 167 μg/g dry wood, a 42% reduction caused by extractives removal (4% extractives).[2] Using pure specimens, they also demonstrated that pine fatty acids and the resin acid, abietic acid, directly generate CH_2O when heated similarly, but abietic acid was far more productive, generating CH_2O at 179 μg/g abietic acid.[2] Using these

DOI: 10.1021/acssuschemeng.7b00240
ACS Sustainable Chem. Eng. 2017, 5, 4243−4248

numbers and assuming direct CH_2O generation by abietic acid, if this pine wood contained 4% extractives in the form of pure abietic acid, removal should cause only a 3% reduction in CH_2O generated by heating. In other words, Schäfer and Roffael's data suggests that pine extractives could be acting as catalysts, indirectly generating much more CH_2O than is directly generated from their thermal decomposition. The catalytic role of pine extractives in CH_2O generation by wood is a plausible hypothesis that must be verified. It is also plausible that every combination of scenarios 1, 2, and 3 mentioned above could affect CH_2O generation by wood (and implicit to scenario 1 is that lignocellulose could catalyze CH_2O generation by the extractives). Perhaps this explains some of the findings in this work, where influential parameters such as tissue type and moisture content appeared to be highly complex and variable within and between tree species. Hopefully future studies will reveal the precise mechanisms of biogenic CH_2O generation. Perhaps we could manipulate those mechanisms to reduce CH_2O emissions in wood composites or even use biogenic CH_2O to improve composite performance regardless of the adhesive technology.

CONCLUSIONS

As is well-known, wood naturally contains CH_2O and generates much more when heated at 200 °C for 10 min. This study documented these effects in increment cores sampled from living Virginia pine, yellow-poplar, and radiata pine trees. Significant variations within and between trees of the same species were observed, as expected. Besides this normal variation, other influential parameters appeared to be complex and highly varied. For instance, tissue types (juvenile/mature, heartwood/sapwood) sometimes correlated to higher CH_2O content and greater heat-generation potential; however, this did not always depend upon tree species. When heated, wet wood (near or above fiber saturation) generated more CH_2O than did dry wood, consistent with an acid catalyzed mechanism. Heating increased CH_2O levels anywhere from 3 to 60 times that measured in unheated wood, depending upon tissue type, moisture content, and species. Most remarkable was that radiata pine generated extraordinarily high CH_2O levels when heated, far exceeding that in Virginia pine and yellow-poplar. It was hypothesized that the remarkable behavior of radiata pine might be related to extractives effects. It was suggested that pine extractives might catalyze CH_2O generation, perhaps in lignin. When the manufacture of wood-based composites is considered, the findings suggest that compliance with CH_2O emissions regulations can be complicated by biogenic CH_2O generated in the hot press. The precise relationship between biogenic CH_2O levels and actual composite emissions is currently unknown. However, it is known that all CH_2O measured here is capable of gaseous emission, and higher moisture levels promote emission. If we could reveal the precise mechanisms of CH_2O generation in wood, we could perhaps manipulate these mechanisms for beneficial purposes.

ASSOCIATED CONTENT

Supporting Information

The Supporting Information is available free of charge on the ACS Publications website at DOI: 10.1021/acssuschemeng.7b00240.

Experimental details about tree increment core sampling and more detailed results that demonstrate (1) typical within (and between) tree increment core variability in CH_2O content and generation and (2) the effects of using P_2O_5 as a specimen drying agent (PDF)

AUTHOR INFORMATION

Corresponding Author

*E-mail: cfrazier@vt.edu; Phone: +1 540 231 8318.

ORCID

Charles E. Frazier: 0000-0002-5733-4744

Notes

The authors declare no competing financial interest.

ACKNOWLEDGMENTS

This project was supported by the Wood-Based Composites Center, a National Science Foundation Industry/University Cooperative Research Center (Award 1035009). Partial funding was also supplied by the Virginia Agricultural Experiment Station and the McIntire Stennis Program of the National Institute of Food and Agriculture, United States Department of Agriculture. Special thanks go to collaborators at Arauco for sampling, drying, and shipping radiata pine specimens.

REFERENCES

(1) Meyer, B.; Boehme, C. Formaldehyde emission from solid wood. *For. Prod. J.* **1997**, *47* (5), 45.

(2) Schäfer, M.; Roffael, E. On the formaldehyde release of wood. *Holz Roh Werkst* **2000**, *58* (4), 259−264.

(3) Roffael, E. Volatile organic compounds and formaldehyde in nature, wood and wood based panels. *Holz Roh Werkst* **2006**, *64* (2), 144−149.

(4) Weigl, M.; Wimmer, R.; Sykacek, E.; Steinwender, M. Wood-borne formaldehyde varying with species, wood grade, and cambial age. *For. Prod. J.* **2009**, *59* (1/2), 88.

(5) Birkeland, M. J.; Lorenz, L.; Wescott, J. M.; Frihart, C. R. Determination of native (wood derived) formaldehyde by the desiccator method in particleboards generated during panel production. *Holzforschung* **2010**, *64* (4), 429−433.

(6) Salem, M. Z. M.; Bohm, M. Understanding of formaldehyde emissions from solid wood: an overview. *BioResources* **2013**, *8* (3), 4775−4790.

(7) Martinez, E.; Belanche, M. I. Influence of veneer wood species on plywood formaldehyde emission and content. *Holz Roh Werkst* **2000**, *58* (1−2), 31−34.

(8) Bohm, M.; Salem, M. Z. M.; Srba, J. Formaldehyde emission monitoring from a variety of solid wood, plywood, blockboard and flooring products manufactured for building and furnishing materials. *J. Hazard. Mater.* **2012**, *221*, 68−79.

(9) Tasooji, M.; Frazier, C. E. Simple milligram-scale extraction of formaldehyde from wood. *ACS Sustainable Chem. Eng.* **2016**, *4* (9), 5041−5045.

(10) ISO. *Wood-based panels: Determination of formaldehyde release, Part 5: Extraction method (called the perforator method)*; ISO: Geneva, 2015.

(11) Myers, G. E. Mechanisms of formaldehyde release from bonded wood products. In *Formaldehyde release from wood products*, ACS Symposium Series 316; Andrews, B. A., Meyer, B., Reinhardt, R. M., Eds.; American Chemical Society: Washington, DC, 1986 pp 87−106.

(12) Aydin, I.; Colakoglu, G.; Colak, S.; Demirkir, C. Effects of moisture content on formaldehyde emission and mechanical properties of plywood. *Build Environ* **2006**, *41* (10), 1311−1316.

(13) Hashida, K.; Ohara, S.; Makino, R. Improvement of formaldehyde-scavenging ability of condensed tannins by ammonia treatment. *Holzforschung* **2006**, *60* (2), 178−183.

DOI: 10.1021/acssuschemeng.7b00240
ACS Sustainable Chem. Eng. 2017, 5, 4243−4248

(14) Hoong, Y. B.; Paridah, M. T.; Loh, Y. F.; Jalaluddin, H.; Chuah, L. A. A new source of natural adhesive: Acacia mangium bark extracts co-polymerized with phenol-formaldehyde (PF) for bonding Mempisang (Annonaceae spp.) veneers. *Int. J. Adhes. Adhes.* **2011**, *31* (3), 164−167.
(15) Navarrete, P.; Pizzi, A.; Tapin-Lingua, S.; Benjelloun-Mlayah, B.; Pasch, H.; Rode, K.; Delmotte, L.; Rigolet, S. Low formaldehyde emitting biobased wood adhesives manufactured from mixtures of tannin and glyoxylated lignin. *J. Adhes Sci. Technol.* **2012**, *26* (10−11), 1667−1684.
(16) Wan, G.; Frazier, C. E. Lignin acidolysis predicts formaldehyde generation in pine wood. *ACS Sustain Chem. Eng.*, manuscript ID: sc-2017-00264x, 2017.
(17) Dix, B.; Roffael, E. Influence of heartwood and the age of tree on the properties of particleboards from pine (Pinus sylvestris). 2. Physical-technical properties and formaldehyde release of particleboards made from sap- and heartwood of pine. *Holz Roh Werkst* **1997**, *55* (2), 103−109.
(18) Marutzky, R.; Roffael, E. Über die abspaltung von formaldehyd bei der thermischen behandlung von holzspänen. Teil I: modellversuche. *Holzforschung* **1977**, *31* (1), 8−12.
(19) Jiang, T.; Gardner, D. J.; Baumann, M. G. Volatile organic compound emission arising from the hot-pressing of mixed-hardwood particleboard. *For. Prod. J.* **2002**, *52* (11/12), 66.
(20) McDonald, A. G.; Gifford, J. S.; Steward, D.; Dare, P. H.; Riley, S.; Simpson, I. Air emission from timber drying: high temperature drying and re-drying of CCA treated timber. *Holz Roh Werkst* **2004**, *62* (4), 291−302.
(21) Chen, C. L.; Chang, H. M.; Cowling, E. B. Aporphine alkaloids and lignans in heartwood of Liriodendron-tulipifera. *Phytochemistry* **1976**, *15* (4), 547−550.
(22) Chen, C. L.; Chang, H. M.; Cowling, E. B.; Hsu, C. Y. H.; Gates, R. P. Aporphine alkaloids and lignans formed in response to injury of sapwood in Liriodendron-tulipifera. *Phytochemistry* **1976**, *15* (7), 1161−1167.

DOI: 10.1021/acssuschemeng.7b00240
ACS Sustainable Chem. Eng. 2017, 5, 4243−4248

Supporting Information for:

Biogenic formaldehyde: Content and heat generation in the wood of three tree species

Authors: Mohammad Tasooji, Guigui Wan, George Lewis, Heather Wise, Charles E. Frazier

Macromolecular Science & Engineering, Sustainable Biomaterials

Virginia Tech, Blacksburg VA 24061, U.S.A

Pages: 4 including the cover

Figures: 2

Tables: 0

Materials and methods

Virginia pine (*Pinus virginiana*) trees from a wooded region east of Blacksburg, VA, U.S.A. (Nellies Cave area), were sampled as follows: increment cores (5 mm dia.) sampled ~1.4 m above ground, from 8 trees, 6-8 cores per tree from a 100 cm^2 area; sealed in plastic straws (trees 1-6) or Pyrex glass tubes (trees 7-8), and subsequently razor cut into ~1 mm thick disks; juvenile (first 10-15 rings) and mature (last 40-70 rings) tissue was isolated and stored frozen (-18˚C for trees 1-6; -80˚C for trees 7-8). Among the 8 Virginia pines, all appeared healthy except tree 8 which had large sections of dead branches in the crown.

Yellow-poplar (*Liriodendron tulipifera*) trees were isolated specimens growing on the Virginia Tech campus and sampled as follows: increment cores (5 mm dia.) sampled ~1.4 m above ground from 5 healthy trees, 4-8 cores per tree from a 100 cm^2 area, sealed in Pyrex glass tubes, and razor cut into ~1 mm thick disks; heartwood and sapwood were separated based on color. Within each tree, all heartwood and sapwood sections were randomized respectively, and separately stored at -80˚C.

Radiata pine (*Pinus radiata*) trees were sampled from a commercial plantation in Chile. Tree 1 was sampled from a stock having 587 trees/ha (silvicultural management pruned and thinned), at UTM coordinate location 18 H, 664859.83 m E, 5913603.16 m S. Tree 2 was sampled from a stock having 933 trees/ha, at UTM coordinate location 18 H, 664847.41 m E, 5913502.29 m S. Sampling occurred as follows: increment cores (10 mm dia.) sampled 1.2-1.6 m above ground in a vertical line with 8 cm separation, 6 cores per tree, vacuum dried at 17˚C for one week, sealed in plastic tubes, shipped from Chile, and received four days later. Upon arrival, juvenile (first 10 rings) and mature (last 9-18 rings) tissue was separated, and cut into ~1 mm thick disks. Within

each tree, all juvenile and mature sections were randomized respectively, and separately stored at -80˚C.

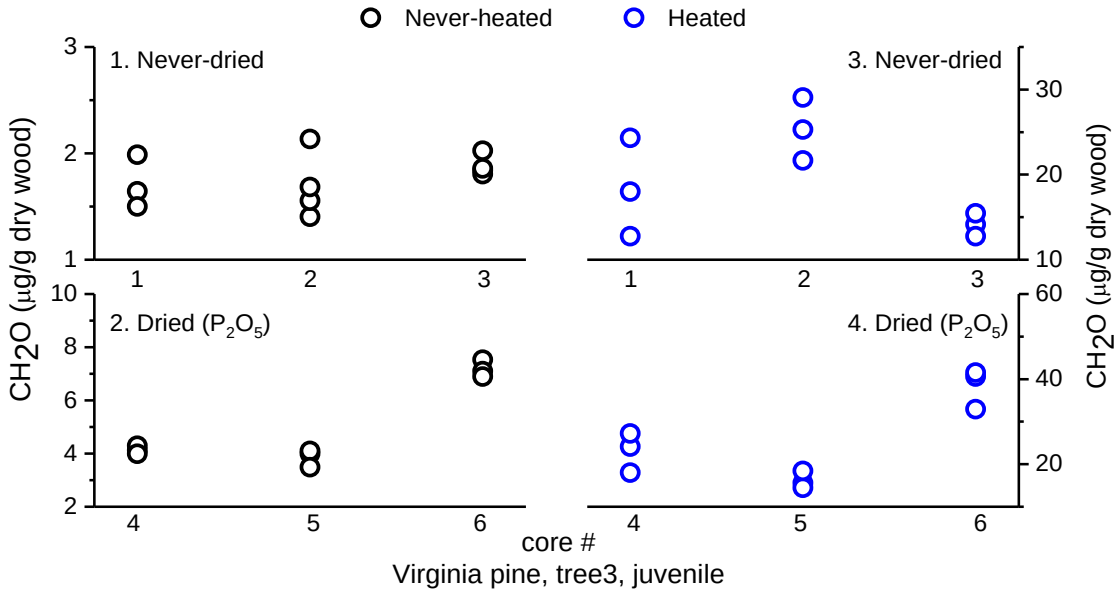

Figure S1. Typical within core, and between core, variability in CH_2O content, and in CH_2O generation, among cores from the same tree (Virginia pine tree 3, juvenile tissue), under different drying and thermal treatments as indicated. Note ordinate scales vary.

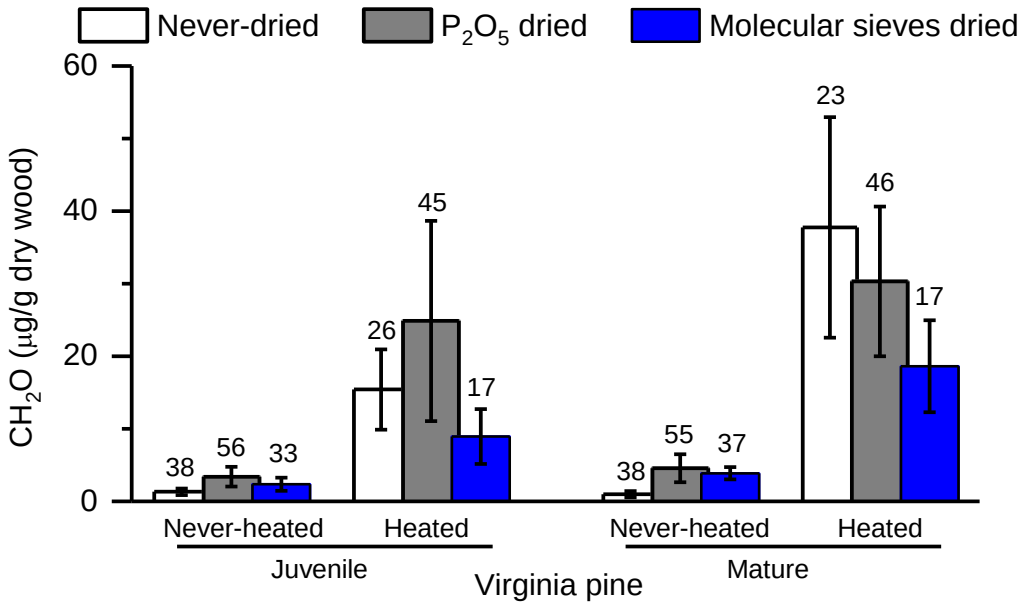

Figure S2. Effect of drying agent (P_2O_5 vs. molecular sieves) on CH_2O content and CH_2O generation in Virginia pine. Never-dried specimens: trees 3-7; P_2O_5 dried specimens: trees 1-4; molecular sieves dried specimens: trees 5-7. Numbers above columns indicate total number of measurements. Error bars = ±1 standard deviation. In the absence of heating, on average it was found that drying always caused an increase in CH_2O content in juvenile and mature Virginia pine; but this increase was significantly less when drying with molecular sieves as compared to P_2O_5. This suggests that phosphoric acid contamination could catalyze CH_2O formation.